



University  
of Glasgow

Syed, Abeer (2013) *Microsystems for parasite enrichment*. PhD thesis.

<http://theses.gla.ac.uk/4353/>

Copyright and moral rights for this thesis are retained by the author

A copy can be downloaded for personal non-commercial research or study

This thesis cannot be reproduced or quoted extensively from without first obtaining permission in writing from the Author

The content must not be changed in any way or sold commercially in any format or medium without the formal permission of the Author

When referring to this work, full bibliographic details including the author, title, awarding institution and date of the thesis must be given

# **Microsystems for Parasite Enrichment**

Abeer Syed

Submitted in fulfilment of the requirements for the  
Degree of PhD

School of Engineering  
College of Science and Engineering  
University of Glasgow

June 2013

## Abstract

The aim of this project was to develop a lab-on-chip platform upon which activities in engineering and parasitology can be brought together to create new low cost diagnostic technologies for Human African Trypanosomiasis, a disease also known as sleeping sickness, for use in resource-poor environments like Sub-Saharan Africa.

Filtration and separation of particles is essential for many biochemical and analytical assays. This work describes the development of novel techniques to enhance the separation/enrichment of parasites from whole blood. Techniques like chemotaxis, inertial microfluidics and density based separation were used to achieve the separation/enrichment.

This thesis describes (i) development of an assay to confirm the chemotaxis of *Trypanosoma brucei* towards higher concentrations of glucose, (ii) designing, fabrication and use of inertial microfluidic device for continuous sorting of trypanosomes from blood cells, (iii) density based separation of trypanosomes from whole blood using a two phase Dextran-Ficoll system, and (iv) density based enrichment of trypanosomes using surface acoustic waves.

This work represents an important step towards improving the detection of trypanosomes in blood for which microscopy is still considered to be the gold standard.

## Publications

“Chemotaxis in *Trypanosoma brucei*.” **Abeer Syed**, Jonathan M. Cooper and Michael P. Barrett. (Submitted)

“Enrichment of Reticulocytes from Whole Blood using Aqueous Multiphase Systems of Polymers.” Ashok A. Kumar, Caeul Lim, Yovany Moreno, Charles R. Mace, **Abeer Syed**, Daria Van Tyne, Dyann F. Wirth, Manoj T. Duraisingh, and George M. Whitesides. (Submitted)

“Rapid Ultrasonic Isopycnic Separations of Cells for Diagnostics.” Yannik Bourquin, **Abeer Syed**, Julien Reboud, Lisa Ranford-Cartwright, Michael P. Barrett and Jonathan M. Cooper. (Submitted)

## Conferences

“Microfluidic Separation of *Trypanosoma brucei* from Blood Cells.” **Abeer Syed**, Christian Witte, Steven Neale, Mike Barrett and Jon Cooper. EMBL Microfluidics 2012, 25 -27 July 2012, Heidelberg, Germany.

“Rapid Ultrasonic Isopycnic Separation of Trypanosomes for Diagnostics.” **Abeer Syed**, Yannik Bourquin, Julien Reboud, Mike Barrett and Jon Cooper. Gordon Research Conference on Microfluidics, Physics & Chemistry of, 09 - 14 June, 2013, Lucca (Barga), Italy.

# Table of Contents

Publications .....	iii
List of Figures .....	vii
List of Tables.....	xii
Acknowledgements.....	xiii
Author's Declaration.....	xiv
Abbreviations .....	xv
List of Symbols.....	xvii
1. Introduction.....	1
1.1 Human African trypanosomiasis .....	1
1.2 <i>Trypanosoma brucei</i> .....	2
1.3 Current Diagnostics.....	6
1.4 The Challenge .....	7
1.5 A Fresh Approach .....	7
1.6 Motivation.....	10
1.7 Introduction to Thesis.....	11
2. Chemotaxis in <i>Trypanosoma brucei</i> .....	12
2.1 Introduction.....	12
2.2 Background .....	13
2.3 Experimental Details .....	14
2.3.1 Cultivation of trypanosomes.....	14
2.3.2 Dialysis .....	14
2.3.3 Chemotaxis assay .....	14
2.3.4 Data Analysis .....	16
2.3.5 Diffusion of Glucose in the Capillary Tube .....	16
2.3.6 Simulation .....	16
2.4 Results and Discussion .....	18
2.5 Conclusion.....	22
3. Pinched Flow Fractionation .....	23
3.1 Introduction.....	23
3.2 Background .....	27
3.3 Experimental Details .....	28
3.3.1 Microfabrication and Soft Lithography .....	28
3.3.2 Device Fabrication.....	30
3.3.3 Cultivation of trypanosomes.....	30
3.4 Results and Discussion .....	32

3.5 Conclusion.....	35
4. Dean Flow .....	36
4.1 Introduction.....	36
4.2 Background .....	38
4.3 Experimental Details .....	40
4.4 Results and Discussion .....	41
4.5 Conclusion.....	45
5. Inertial Microfluidics.....	46
5.1 Introduction.....	46
5.2 Background .....	50
5.3 Experimental Details .....	50
5.3.1 Device Design.....	50
5.3.2 Device Characterization .....	53
5.3.3 Cultivation of Trypanosomes .....	53
5.4 Results and Discussion .....	54
5.5 Conclusion.....	58
6. Density Based Separation of Whole Blood and Enrichment of Trypanosomes.....	59
6.1 Introduction.....	59
6.2 Background .....	61
6.3 Experimental Details .....	62
6.3.1 Reagents .....	62
6.3.2 Formation and Analysis of Aqueous Two-Phase Systems .....	63
6.3.3 Separation of Blood .....	63
6.3.4 Extraction of Fractions of Cells after Separation .....	63
6.3.5 Density Based Enrichment of Trypanosomes .....	64
6.3.6 Selection of ATPSs.....	65
6.3.7 Separations Using Small Steps in Density .....	66
6.3.8 Filtration of Particles Based on Density Using ATPSs .....	67
6.3.9 Analysis of the Components of Blood.....	68
6.3.10 Analysis of <i>Trypanosoma</i> Enrichment.....	70
6.4 Results and Discussion .....	71
6.4.1 Separation of Whole Blood .....	71
6.4.2 Enrichment of Trypanosomes .....	75
6.5 Conclusion.....	77
7. Rapid Ultrasonic Isopycnic Separation of Trypanosomes .....	79
7.1 Introduction.....	79
7.1.1 Diagnosis of Sleeping Sickness .....	79

7.2 Background .....	81
7.3 Materials and Methods .....	82
7.3.1 Device Fabrication .....	82
7.3.2 Density Solutions.....	85
7.3.3 <i>Trypanosoma cyclops</i> preparation .....	85
7.3.4 <i>Trypanosoma</i> Enrichment .....	86
7.4 Results and Discussion .....	86
7.5 Conclusion .....	89
8. Conclusions.....	90
9. References .....	94
10. Appendices .....	104
10.1 HM1 - 9 Medium Recipe .....	104
10.2 Carter's Balances Salt Solution (CBSS) Recipe.....	105
10.3 Cunninghams Medium Recipe.....	105

## List of Figures

- Figure 1.1: Progression of sleeping sickness in humans. (Figure adapted from Wiser, 1999) 2
- Figure 1.2: The schematic representation of the life cycle of *Trypanosoma brucei*. (Figure reproduced from CDC, 2012) 3
- Figure 1.3: Geographic distribution of *T. b. gambiense* and *T. b. rhodesiense*. *T. b. gambiense* is endemic in Western and Central Africa whereas, *T. b. rhodesiense* is endemic in Eastern and Southern Africa (Visser, 2012). 4
- Figure 1.4: (A) Fixed thin blood smear of *Trypanosoma brucei brucei* (WT 427). This picture was taken using an oil immersion objective (100X). (B) Scanning electron microscope (SEM) picture of *Trypanosoma cyclops* and a red blood cell (Figure reproduced from Holm et al., 2011). 5
- Figure 1.5: Fixed thin blood smear illustrating the physical differences between trypanosomes and red blood cells. The picture was taken using an oil immersion objective (100X). 9
- Figure 2.1: Schematic representation of the experimental setup. 15
- Figure 2.2: Simulation of the glucose gradient in the capillary tube at t=3600 seconds. The scale bar represents the concentration of the glucose in mM. 17
- Figure 2.3: Concentration gradient profile of glucose along the length of the capillary tube from t=10 - t=60 minutes. 18
- Figure 2.4: Attraction coefficients of test compounds including whole blood and plasma. Error bars indicate the standard error of the mean (n=5). The results have been normalized against the control. [\* statistically significant p-values]. 19
- Figure 2.5: Growth curve of *T. brucei*. Parasites were grown in HMI-9 supplemented with 10% dialysed FBS and glucose (red), fructose (blue), glycerol (magenta) and galactose (green) as energy source and without an energy source (black). 20
- Figure 2.6: Attraction coefficient of dialysed plasma with different D-glucose concentrations. 100  $\mu$ L of dialysed serum was added to each sample unless stated otherwise. The control neither had serum nor any glucose. The results have been normalized against the control. Error bars indicate the standard error of the mean (n=5). [\* statistically significant p-values] 21
- Figure 2.7: Attraction coefficient of various dilutions of whole blood (black) and plasma (blue). The dilutions were made in CBSS. The control (CBSS) does not contain any blood or plasma. Error bars indicate the standard error of the mean (n=3). 22
- Figure 3.1: Principle of pinched flow fractionation. Schematic diagram showing particle behaviour in pinched and broadened segments. 26
- Figure 3.2: Schematic of the soft lithography process used to fabricate microfluidic devices. SU-8 3050 is dispensed on to a silicon wafer. Photolithography was used to define the structure of the device. The master was developed and PDMS mixed in a ratio of 10:1 is poured onto a finished master and baked for 45 minutes at 90 °C. The cured PDMS device was peeled from the master and oxygen plasma treated at 100 W for 2 minutes before being bonded to a glass slide. 29

Figure 3.3: SEM of the PFF device for separation of 10.14 and 24.99  $\mu\text{m}$  beads. Length and width of inlet channels is 1 mm and 150  $\mu\text{m}$  respectively (A). The pinched segment is 100  $\mu\text{m}$  wide and 750  $\mu\text{m}$  long, the broadened segment is 1mm long and 1.5 mm wide (B). The length and width of outlets is 1mm and 300  $\mu\text{m}$  respectively. The picture was taken using Hitachi S-4700 operating at 5kV. 31

Figure 3.4: SEM of the PFF device. Length and width of inlet channels are 500  $\mu\text{m}$  and 50  $\mu\text{m}$  respectively. The pinched segment is 15  $\mu\text{m}$  wide and 150  $\mu\text{m}$  long, the broadened segment is 750  $\mu\text{m}$  long and 250  $\mu\text{m}$  wide. The length and width of outlets is 750  $\mu\text{m}$  and 50  $\mu\text{m}$  respectively. The picture was taken using Hitachi S-4700 operating at 5kV. 32

Figure 3.5: Separation performance of 10  $\mu\text{m}$  and 25  $\mu\text{m}$  beads. The width of the pinched segment was 100  $\mu\text{m}$  and a boundary angle of 180°. The beads were counted by haemocytometry in samples taken from outlets after separation. The data are means of 3 replicates and the error bars are standard deviation. The initial concentration of 10  $\mu\text{m}$  and 25  $\mu\text{m}$  beads was  $1.3 \times 10^6$  and  $3.6 \times 10^6 \text{ mL}^{-1}$  respectively. 33

Figure 3.6: Separation performance of 3  $\mu\text{m}$  and 10  $\mu\text{m}$  beads. The width of the pinched segment was 20  $\mu\text{m}$  and the boundary angle was 90°. The beads were counted by haemocytometry in samples taken from outlets after separation. The data are means of 3 replicates and the error bars are standard deviation. . The initial concentration of 10  $\mu\text{m}$  and 3  $\mu\text{m}$  beads was  $5 \times 10^5$  and  $7.5 \times 10^5 \text{ mL}^{-1}$  respectively. 34

Figure 3.7: Separation performance of trypanosomes and red blood cells. The width of the pinched segment was 20  $\mu\text{m}$  and the boundary angle was 90°. The cells were counted by haemocytometry in samples taken from outlets after separation. The flow rates used were kept at  $5 \mu\text{L min}^{-1}$  for the particle stream and  $30 \mu\text{L min}^{-1}$  for the buffer stream. The data are means of 3 replicates and the error bars are standard deviation. The initial concentration of RBCs and trypanosomes was  $2.7 \times 10^7$  and  $1 \times 10^6 \text{ mL}^{-1}$  respectively. 35

Figure 4.1: Schematic of size based separation of beads in spiral microchannels. Under the influence of counter acting lift forces and Dean Drag, the particles equilibrate according to the size along the inner wall of the spiral microchannel (where  $F_{LW}$  is inertial lift force exerted by channel wall,  $F_{LS}$  is the shear lift force and  $F_D$  is the Dean drag force). 38

Figure 4.2: SEM image of the 5 loop spiral device. The design consists of two inlets and two outlets. The sample was introduced through the inner inlet. The spiral microchannel is 500  $\mu\text{m}$  wide and 40  $\mu\text{m}$  high. The picture was taken using Hitachi S-4700 operating at 5kV. 41

Figure 4.3: (A) Schematic of the 5-loop spiral with two inlets and two outlets. The device was fabricated in PDMS using soft lithography. (B) Picture of the first loop of the spiral with 5  $\mu\text{m}$  and 10  $\mu\text{m}$  polystyrene beads. (C) Picture of the 5<sup>th</sup> loop of the spiral. The 10  $\mu\text{m}$  beads are focussed along the inner wall whereas  $\mu\text{m}$  beads are focussed towards the centre of the channel. (D) Picture of the separation at the outlet. 42

Figure 4.4: Distribution of 5  $\mu\text{m}$  and 10  $\mu\text{m}$  particles in the inner (outlet 1) and outer (outlet 2) outlets of the spiral device. The separation was achieved at a flow rate of  $15 \mu\text{L min}^{-1}$  and  $De = 0.06$ . The error bars represent the standard deviation ( $n = 3$ ). The initial concentration of 5  $\mu\text{m}$  and 10  $\mu\text{m}$  beads was  $5.2 \times 10^6$  and  $2.2 \times 10^5 \text{ mL}^{-1}$  respectively. 43

Figure 4.5: (A) Picture of 1<sup>st</sup> loop of the device with unsorted whole blood. (B) Picture of the 5<sup>th</sup> loop. The blood cells focus along the inner wall whereas the plasma is focussed along the out wall. (C) Picture of the outlet showing separation of blood cells and plasma into inner and out outlets respectively. Pictures were cleaned digitally using GIMP to remove dust and adjust orientation. 44

Figure 4.6: Distribution of blood cells and plasma in the inner and outer outlets of the spiral device. The blood cells were collected mainly from the inner outlet (outlet 1) whereas the plasma was collected from the outer outlet (outlet 2). The separation was achieved at a flow rate of 15  $\mu\text{L min}^{-1}$  and  $De = 0.06$ . The error bars represent the standard deviation ( $n = 3$ ). Control is the input (50X diluted blood with a concentration of  $1.2 \times 10^8 \text{ cells mL}^{-1}$ ) and cells collected from outlets are the output. 44

Figure 5.1: Inertial migration of particles in a square microchannel for  $Re < 100$  (A) and  $Re \geq 500$  (B). 47

Figure 5.2: Schematic of a rectangular microchannel showing the equilibration of the particles. The particles are randomly distributed at the inlet and align along the channel walls as they reach the outlet. 49

Figure 5.3: Schematic of the inertial microfluidic device for separating trypanosomes from infected blood. The device has one inlet and two outlets. The channel has 75 alternating pinched and expanded units. The length of each unit is 100  $\mu\text{m}$  and the width of the expanded units is 60  $\mu\text{m}$ . The total length of the channel is 1.5 cm. 51

Figure 5.4: SEM of the channel outlets. The device has one central outlet for collection of trypanosomes and two outer outlets for the collection of blood cells. Each outlet is 100  $\mu\text{m}$  wide. The picture was taken using Hitachi S-4700 operating at 5kV. 52

Figure 5.5: SEM of the expansion-contraction regions of the channel. The expansion regions are 100  $\mu\text{m}$  long and 90  $\mu\text{m}$  wide. The contraction regions are 100  $\mu\text{m}$  long and 30  $\mu\text{m}$  wide. The height of the channel is 50  $\mu\text{m}$ . The picture was taken using Hitachi S-4700 operating at 5kV. 53

Figure 5.6: Picture of the experimental setup showing the microscope, syringe pump and the microfluidic device. 54

Figure 5.7: Picture of the PDMS microchannel. The length and height of each unit is 100 and 50  $\mu\text{m}$  respectively. 55

Figure 5.8: Pictures of *Trypanosoma cyclops* spiked blood in various flow conditions inside the microfluidic device. (A) No flow (B) 100  $\mu\text{L min}^{-1}$  (C) 200  $\mu\text{L min}^{-1}$  (D) 300  $\mu\text{L min}^{-1}$ , and (E) 400  $\mu\text{L min}^{-1}$ . These pictures have been extracted from videos. A, B, C and D are the pictures of broadened segment that leads to the outlets and E is the picture of the broadened segments with the three outlets. 56

Figure 5.9: The enrichment effect of inertial microfluidics on *Trypanosoma cyclops* spiked blood. The blood was injected in to the device at a flow rate of 400  $\mu\text{L min}^{-1}$ . Trypanosomes were mainly collected at the outlet 1 and the red blood cells at outlet 2. The error bars represent the standard deviation ( $n = 3$ ). The initial concentration of RBCs and trypanosomes was  $2.13 \times 10^7$  and  $1 \times 10^5 \text{ mL}^{-1}$  respectively. 58

Figure 6.1: Procedure to recover cellular components after separation by ATPS. Each image depicts a single step in the protocol to isolate 500- $\mu\text{L}$  fractions of cells from the interfaces of an ATPS by pipette: the boundary between the plasma and the top phase is removed first, followed by the interface between phases, the remaining supernatant,

and, finally, the pellet. Some cell loss occurs due to non-quantitative isolation of fractions and some non-specific binding. 64

Figure 6.2: An image of Dextran-Ficoll ATPS ( $\rho_{top} = 1.0783 \text{ g cm}^{-3}$ ,  $\rho_{bottom} = 1.0806 \text{ g cm}^{-3}$ ; 21% (w/v) Ficoll and 21% (w/v) Dextran) separating three density standard beads with a density difference between each bead of  $0.0020 \text{ g cm}^{-3}$ . 67

Figure 6.3: Density-based filtration of particles using an ATPS. The density step produced by a poly(ethylene glycol)-Ficoll ATPS ( $\rho_{top} = 1.025 \text{ g cm}^{-3}$ ,  $\rho_{bottom} = 1.074 \text{ g cm}^{-3}$ ; 15% (w/v) poly(ethylene glycol) and 20% (w/v) Ficoll) selectively filters particles of equivalent size ( $d = 2.8 \mu\text{m}$ ) based on their differences in density. Around 250000 particles were added to a microhaematocrit tube containing the ATPS. After centrifugation, the density step produced by the ATPS filtered solutions containing: (A) superparamagnetic microspheres only (Dynabeads (Dy);  $\rho = 1.14 \text{ g cm}^{-3}$ ), (B) polystyrene only (PS;  $\rho = 1.05 \text{ g cm}^{-3}$ ), and (C) a mixture of Dynabeads and polystyrene (Dy/PS). 69

Figure 6.4: Morphology of cells after separation using an ATPS. Representative micrographs of red blood cells, polymorphonuclear cells, and mononuclear cells before and after centrifugation in an ATPS demonstrate no significant morphological change as a result density-based separation. 70

Figure 6.5: Morphology of trypanosomes before (*T. brucei*) and after (*T. cyclops*) separation using an ATPS. Representative brightfield micrographs before and after centrifugation in an ATPS demonstrate no significant morphological change. 71

Figure 6.6: Enrichment and concentration of cells by density from 1 mL of whole blood. 3 mL of the Dextran-Ficoll ATPS ( $\rho_{top} = 1.076 \text{ g cm}^{-3}$ ,  $\rho_{bottom} = 1.080 \text{ g cm}^{-3}$ ; 20.5% (w/v) Ficoll and 20.5% (w/v) Dextran) was used to separate the cellular components of human blood based on density. After 100 minutes of centrifugation at 2000 g, the top and bottom phase of the ATPS are intact and separate different isolates of blood (Fractionated Blood). The contents of each isolate were examined; the protein content of the plasma fraction was evaluated with a Bradford assay and cellular contents were evaluated for morphology using optical microscopy (Isolates). A mixture of cells was present in each fraction; micrographs depict the cell types that were most prevalent. 73

Figure 6.7: Enrichment and concentration of cells by density from 10  $\mu\text{L}$  of whole blood. The ATPS was Dextran-Ficoll ( $\rho_{top} = 1.076 \text{ g cm}^{-3}$ ,  $\rho_{bottom} = 1.080 \text{ g cm}^{-3}$ ; 20.5% (w/v) Ficoll and 20.5% (w/v) Dextran). Leukocytes (i.e., mononuclear cells and polymorphonuclear cells) and platelets segregated into two bands—one at the top of the ATPS and one at the liquid/liquid interface of the ATPS. Each band contained a mix of all three types of cells. Erythrocytes and leukocytes sedimented below the ATPS. Micrographs depict the types of cells that were most prevalent in each band (Isolates). 75

Figure 6.8: Enrichment and concentration of cells by density from 1 mL of spiked blood. 3 mL of the Dextran-Ficoll ATPS ( $\rho_{top} = 1.076 \text{ g cm}^{-3}$ ,  $\rho_{bottom} = 1.082 \text{ g cm}^{-3}$ ) was used for separation. 76

Figure 7.1: (A) Picture of the SAW device comprising a slanted finger interdigitated electrode (SFIDT) on  $\text{LiNbO}_3$ . The surface acoustic wave (SAW) is generated at a defined position asymmetrically with respect to the drop of blood, only a fraction of which will lie in the acoustic pathway, thereby inducing a rotational motion within the drop. The scale bar is 3 mm; (B) Pictures of the concentration of red blood cells before and (C)

after actuation with SAW. Red blood cells (RBCs) are concentrated in the middle of the drop, while trypanosomes are enriched at the periphery. 83

Figure 7.2: Schematic representation of the flow pattern in infected blood droplet. The SAW induced streaming in the drop and a secondary flow brings the particles at the centre of the drop. The two lower schematics show the forces acting on the RBCs and trypanosomes for different value of  $\rho_f$ . When  $\rho_{\text{try}} \leq \rho_f < \rho_{\text{RBC}}$ , the resultant force  $F_{\text{res}}$  is strong enough to lift the trypanosomes but not the RBCs. 84

Figure 7.3: The concentration effect of SAW microseparation on *Trypanosoma cyclops* suspended in Histodenz as a function of the density of the solution for a frequency of 10.9 MHz and power of 2 W. Control indicates the parasitaemia in the sample used prior to SAW microseparation. Parasitaemias were determined by haemocytometry in samples taken from the periphery of the droplet following SAW microseparation. The data are means of 3 replicates and the error bars are standard errors of the mean deviations. Statistically significant enrichment is marked with \* (99%). 87

Figure 7.4: The fold enrichment achieved following SAW microseparation of samples containing trypanosomes at parasitaemia from 0.0023% to  $4.32 \times 10^{-5}\%$  in Histodenz at 15% ( $\rho=1.08326 \text{ g cm}^{-3}$ ), input frequency of 10.9 MHz and power of 2 W. The data are means of 3 replicates and the error bars are standard errors of the mean deviations. 88

Figure 7.5: Enrichment of *Trypanosoma cyclops* suspended in 15% Histodenz as a function of the initial parasitaemia for a frequency of 8.8 MHz and input power of 1 W on a disposable superstrate. Parasitaemias were determined by haemocytometry in samples taken from the periphery of the droplet following SAW microseparation. The data are means of 3 replicates and the error bars are standard errors of the mean deviations. 88

## List of Tables

Table 1.1: Common microfluidic continuous separation methods.	8
Table 2.1: Concentration gradient of glucose inside the capillary tube at various time points.	16
Table 2.2: List of input data for material balance. At the inlet the concentration of glucose was set to 0.1 M and the boundary condition for outlet was set to convective flux. The simulation was solved for time dependent diffusion.	17
Table 5.1: List of Reynolds numbers and particles Reynolds numbers associated with different flow rates.	57
Table 6.1: Average distribution of sub-populations of the cellular components of blood that are enriched at the interface and boundaries of an ATPS. Blood was analyzed from five different individuals. Whole blood (1 mL) was centrifuged over a Dextran-Ficoll ATPS ( $\rho_{\text{top}} = 1.076 \text{ g cm}^{-3}$ , $\rho_{\text{bottom}} = 1.080 \text{ g cm}^{-3}$ ; 20.5% (w/v) Ficoll and 20.5% (w/v) Dextran). The components of blood separated into four fractions: (i) above the ATPS (plasma), (ii) at the boundary between the plasma and the ATPS (boundary), (iii) at the liquid/liquid interface of the ATPS (interface), and (iv) below the ATPS (bottom). The plasma fraction contained less than $150 \text{ cells } \mu\text{L}^{-1}$ . A haematology analyzer counted cells from the bottom three fractions (“boundary”, “interface”, and “bottom”).	73
Table 6.2: Average distribution of trypanosomes and blood cells at the interface and boundaries of ATPS. The blood separated into four fractions: (i) above the ATPS (plasma), (ii) at the boundary between the plasma and the ATPS (top layer), (iii) at the liquid/liquid interface of the ATPS (interface), and (iv) below the interface (bottom layer).	77

## Acknowledgements

First and foremost, I would like to thank Prof. Jon Cooper, my PhD supervisor, for giving me this opportunity to work with his group and for his guidance and support during this work. I would also like to thank Prof. Mike Barrett, my co-supervisor, for his steady guidance and useful discussions throughout this work. I would also like to extend my sincere gratitude towards the Darwin Trust of Edinburgh for funding my PhD research.

I am grateful to the members of Prof. Cooper's and Prof. Barrett's groups especially Dr. Norbert Kluake, for teaching me everything I know about microfabrication, Dr. Federica Giordani for helping me with Trypanosoma cultures, Dr. Pui Ee Wong for providing mice blood and Dr. Rab Wilson for listening to all my ideas (good and bad) and everything else. I would also like to thank Dr. Julien Reboud for his help throughout my PhD and going through the initial drafts of my thesis.

I would like to express my gratitude to Prof. George Whitesides for letting me work in his group at Harvard University. I would like to thank his group members especially T. J. Martin and A. A. Kumar for making my stay there enjoyable and extremely fruitful. The work conducted at Harvard was funded by the Bill and Melinda Gates foundation and my visit to Harvard was made possible by the grants from Royal Society of Edinburgh's J. M. Lessells scholarship and Mac Robertson scholarship.

My particular thanks go to my friends and colleagues Chiara, Yannyk, and Christian for all those countless discussions and their help and support. To Jay and Vanita for making my stay in Glasgow enjoyable, for all the great food and good times we had together. To Shatakshi, my friend and fellow PhD student, for listening to me whine for hours about my unsuccessful experiments.

Last, but not the least, I would like to thank my family for believing in me and for all their support and encouragement throughout these three years. Abu, badi-mummy, mummy and Nabil this is for you. I hope that the rest of my family doesn't read the previous line.

## **Author's Declaration**

The work presented in this thesis was conducted by the author and has not previously been submitted for a degree or diploma at this university or any other institution.

## Abbreviations

ATPS	Aqueous Two-Phase Systems
CATT	Card Agglutination Test for Trypanosomiasis
CBSS	Carter's Balanced Salt Solution
<i>E. coli</i>	<i>Escherichia coli</i>
EDTA	Ethylenediaminetetraacetic acid
FBS	Fetal Bovine Serum
HAT	Human African Trypanosomiasis
HepB	Hepatitis B
HepC	Hepatitis C
HIV	Human Immunodeficiency Virus
HMI - 9	Hirumi's Modified Iscoves Medium
HTLV	Human T-lymphotropic Virus
IDT	Interdigitated Transducer
IPA	Isopropyl Alcohol
KCl	Potassium Chloride
KH <sub>2</sub> PO <sub>4</sub>	Monopotassium Phosphate
LiNbO <sub>3</sub>	Lithium Niobate
mAECT	Mini Anion Exchange Centrifugation Technique
MCH	Mean Corpuscular Haemoglobin
MCV	Mean Corpuscular Volume
MHCT	Microhaematocrit Centrifugation Technique
MNCs	Mononuclear cells (lymphocytes and monocytes)
NaCl	Sodium Chloride

Na <sub>2</sub> HPO <sub>4</sub> •7H <sub>2</sub> O	Sodium Monohydrogen Phosphate heptahydrate
PBS	Phosphate Buffered Saline
PDMS	Polydimethylsiloxane
PEG	Polyethylene Glycol
PFF	Pinched Flow Fractionation
Plts	Platelets
PMNs	Polymorphonuclear Cells (PMNs) (basophils, eosinophils, neutrophils)
PTFE	Polytetrafluoroethylene
QBC	Quantitative Buffy Coat
RBC	Red Blood Cells
RCF	Relative Centrifugal Force
RO	Reverse Osmosis
SAW	Surface Acoustic Waves
SEM	Scanning Electron Microscope
SFIDT	Slanted Finger Interdigitated Transducer
<i>T. brucei</i>	<i>Trypanosoma brucei</i>
<i>T. cyclops</i>	<i>Trypanosoma cyclops</i>
WBC	White Blood Cells

## List of Symbols

$AR$	Aspect ratio
$C_0$	Concentration
$C_L$	Lift coefficient
$\Delta C$	Difference between particle positions
$D$	Diffusion coefficient
$De$	Dean number
$D_h$	Hydraulic diameter
$D_p$	Particle diameter
$\rho$	Density
$\delta_{ts}$	Time scaling factor
$f$	Body force
$F_B$	Buoyancy
$F_D$	Drag force
$F_g$	Force due to gravity
$F_L$	Lift force
$F_{LS}$	Shear lift forces
$F_{LW}$	Wall effect forces
$F_{res}$	Resultant force
$g$	Acceleration due to gravity
$G$	Average shear rate
$h$	Microchannel height
$l$	Length
$L_C$	Characteristic dimension length
$m$	mass
$Mr$	Molecular weight
$p$	Pressure
$r$	Radius
$R$	Reaction rate
$R_c$	Radius of curvature of the spiral
$Re$	Reynolds number
$Re_p$	Particle Reynolds number
$u$	Velocity

$U_D$	Dean velocity
$U_F$	Fluid velocity
$\mu$	Dynamic viscosity
$w$	Microchannel width
$w_b$	Width of broadened segment
$w_p$	Width of pinched segment
$w/v$	Weight/volume

## Chapter 1 - Introduction

### 1.1 Human African trypanosomiasis

Human African Trypanosomiasis (HAT) or sleeping sickness is a vector-borne parasitic disease transmitted to humans by the *Glossina* spp., commonly known as the tsetse fly (Barrett et al., 2003; 2007). Presently, 60 million people are at risk of the sleeping sickness according to WHO estimates (WHO, 2002). At the end of the twentieth century an estimated 500,000 people were infected over 37 countries, mostly in the sub-Saharan Africa where the lack of health facilities and infrastructure contribute to the prevalence, morbidity and mortality of the disease. Although the disease threatens dozens of countries in the Sub-Saharan Africa, only a few are under surveillance, and even fewer have access to basic health care. In some areas vector control interventions are implemented as well (WHO, 2012). The number of reported cases has declined in recent years and the WHO has called for elimination of sleeping sickness. Improved diagnostics will be central to such a programme (WHO, 2010).

Parasitic protozoa from the order Kinetoplastida include *Trypanosoma brucei*, which are the causative agents of both sleeping sickness in humans and Nagana in cattle. Both wild and domestic animals have been found to carry the infection caused by this subspecies (Barrett et al. 2007). Another species, *Trypanosoma cruzi* is the causative agent of Chagas' disease or the American Trypanosomiasis; the parasite causing the acute infection is different from the ones that cause the disease in Africa. Poor people, living in the rural and underdeveloped areas are the worst hit by sleeping sickness (Barrett et al., 2003; 2007). Rural areas favour the insect as the population in these areas depends mainly on farming, fishing and animal husbandry. Moreover, the lack of political resource and medical infrastructure aggravates the problem as there is no health care and the populations are displaced regularly, involuntarily helping the disease to spread (WHO, 2012).

In HAT, the trypanosomes initially infect and multiply in the blood, lymph nodes and the subcutaneous tissues, causing chancres, intermittent fever and lymphadenopathy (Figure 1.1). The second stage involves the trypanosomes crossing the blood-brain barrier to invade the central nervous system. Once the

blood-brain barrier is crossed, the patients undergo severe mood swings and develop serious sleep disturbances. If left untreated, HAT is fatal in 100% of people. Although chemotherapy is available for both stages of the diseases, the existing procedures and drugs are far from ideal for curing the diseases (Barrett et al. 2003).

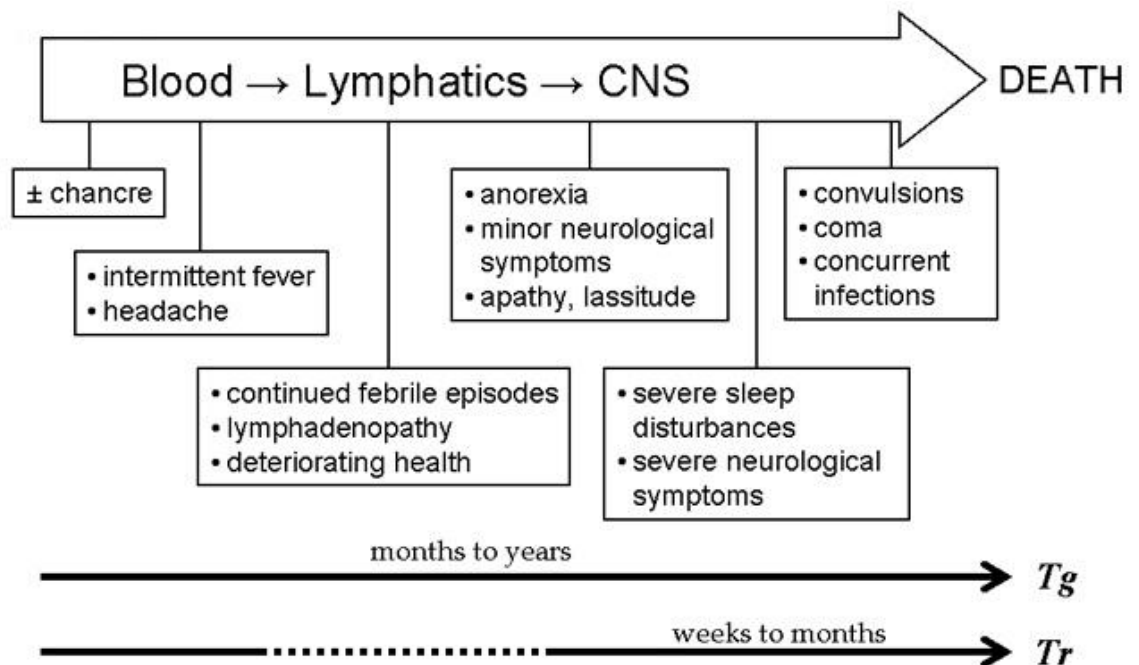


Figure 1.1: Progression of sleeping sickness in humans. (Figure adapted from Wiser, 1999)

## 1.2 *Trypanosoma brucei*

Trypanosomes are unicellular flagellates 20-30  $\mu\text{m}$  long. A single flagellum emerges from the posterior end, runs along the undulating cell membrane and extends beyond the anterior end of the parasite. Trypanosomes are extracellular parasites that multiply by binary fission. They are injected as metacyclic trypomastigotes that later transform into bloodstream trypomastigotes. When the tsetse fly ingests a meal containing stumpy form trypomastigotes from the infected humans, these cells are transformed into the procyclic trypomastigotes in the midgut of these flies. Stumpy forms are an intermediate in terms of biochemical physiology between slender bloodstream forms and procyclic forms.

Further, the procyclic trypomastigotes have to transform into epimastigotes forms and later metacyclic trypomastigotes. The transformation from the epimastigote to metacyclic trypomastigotes takes place in the salivary glands of the tsetse fly (Figure 1.2). The metacyclic trypomastigotes are infectious and cause sleeping sickness when injected into the humans by the tsetse fly thus completing the life cycle of the trypanosome (Barrett et al., 2003; Chappuis et al., 2005).

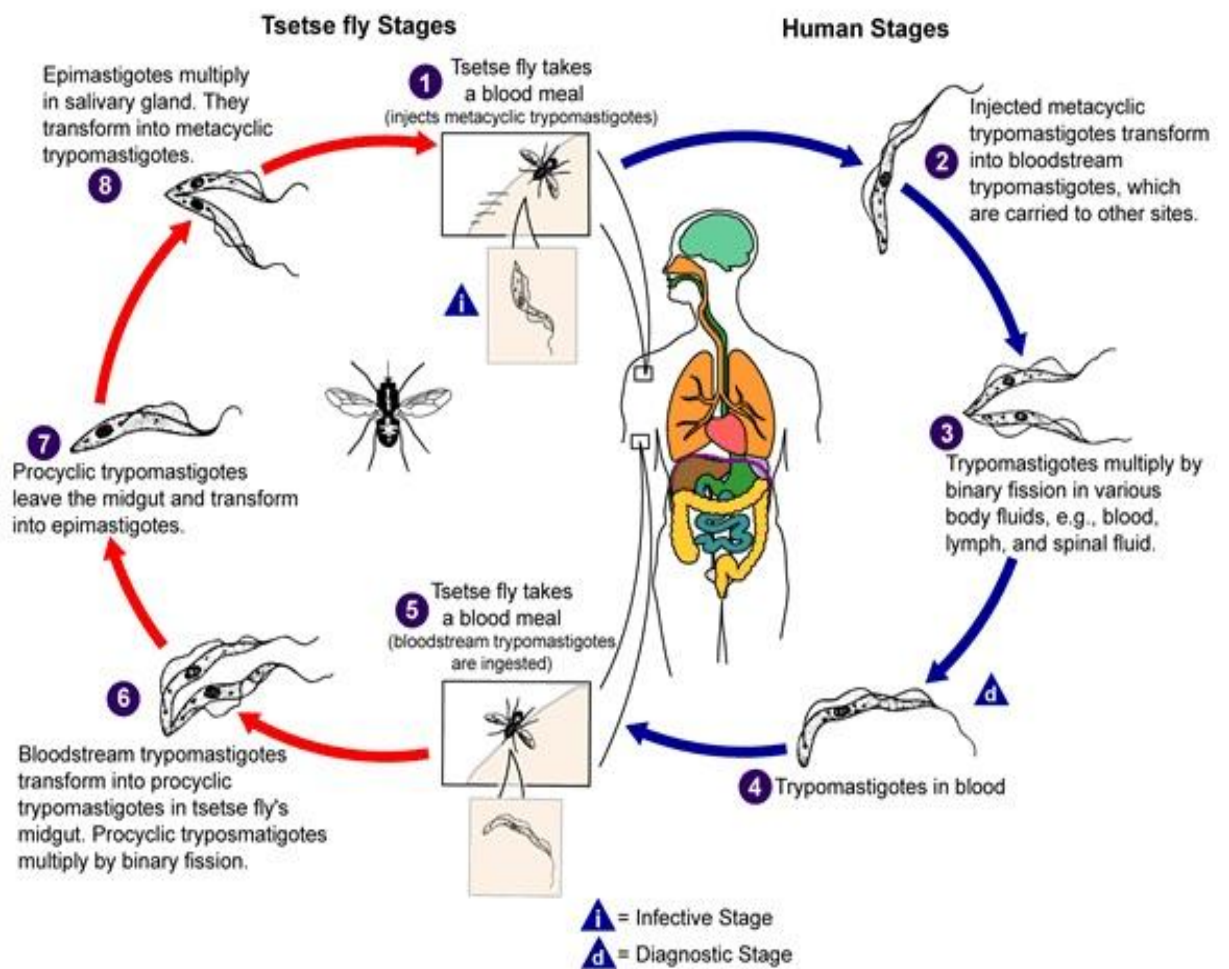


Figure 1.2: The schematic representation of the life cycle of *Trypanosoma brucei*. (Figure reproduced from CDC, 2012)

*Trypanosoma brucei gambiense* (*T. b. gambiense*) and *Trypanosoma brucei rhodesiense* (*T. b. rhodesiense*) are responsible for sleeping sickness in West and East Africa respectively (Figure 1.3). *T. b. gambiense* is the most common form

of the acute infection with more than 90% of the reported cases. This type of sickness can be fatal because one may be infected for a prolonged period of time without any major signs or symptoms of the disease.

At the same time, *T. b. rhodesiense* develops rapidly and the signs are visible in the first few weeks of infection and may result in death of the patient if treatment is not carried out. Less than 10% of the reported cases are *T. b. rhodesiense*. Although the species can hardly be differentiated morphologically, the epidemiological characteristics of both parasites are completely different. There are considerable differences at the host-parasite interface level, which have disrupted most efforts to use the information gained about one species to help in control of the other (Barrett et al. 2003).

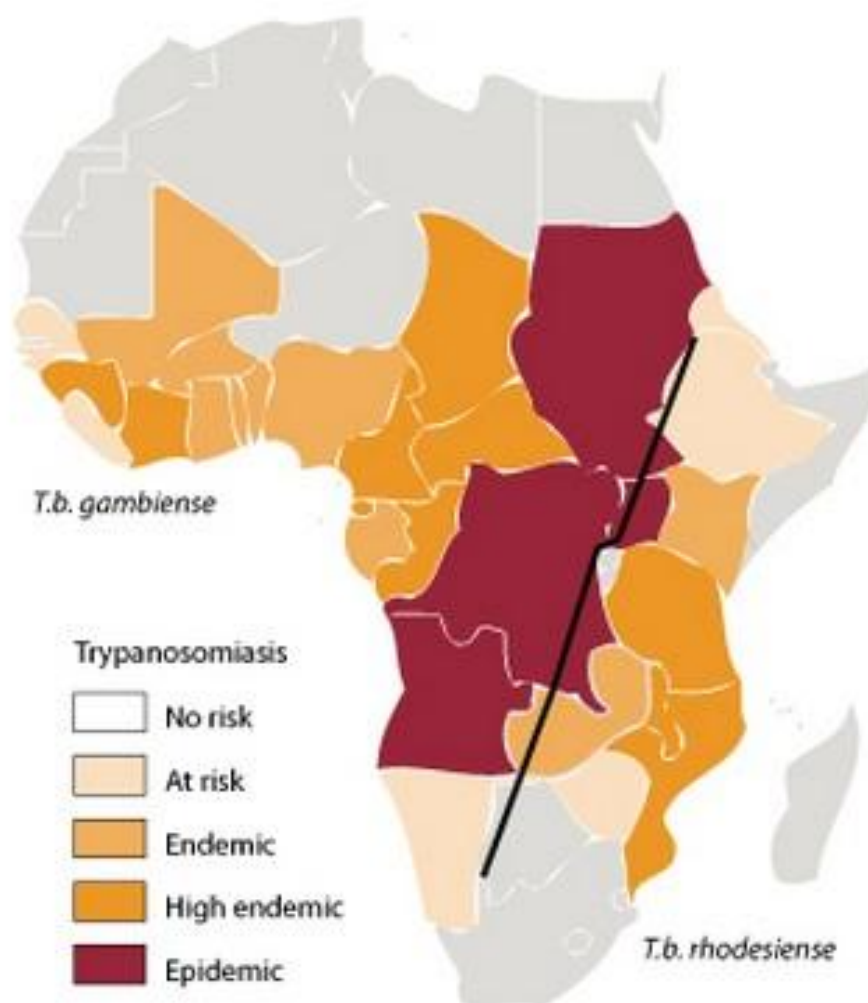


Figure 1.3: Geographic distribution of *T. b. gambiense* and *T. b. rhodesiense*. *T. b. gambiense* is endemic in Western and Central Africa whereas, *T. b. rhodesiense* is endemic in Eastern and Southern Africa (Visser, 2012).

For the purpose of experimentation, *Trypanosoma brucei brucei* (Figure 1.4a) and *Trypanosoma cyclops* (Figure 1.4b) were used as surrogates for *T. brucei gambiense* and *T. brucei rhodesiense* due to regulatory safety rules, but are still useful to demonstrate the separation techniques developed in this thesis.

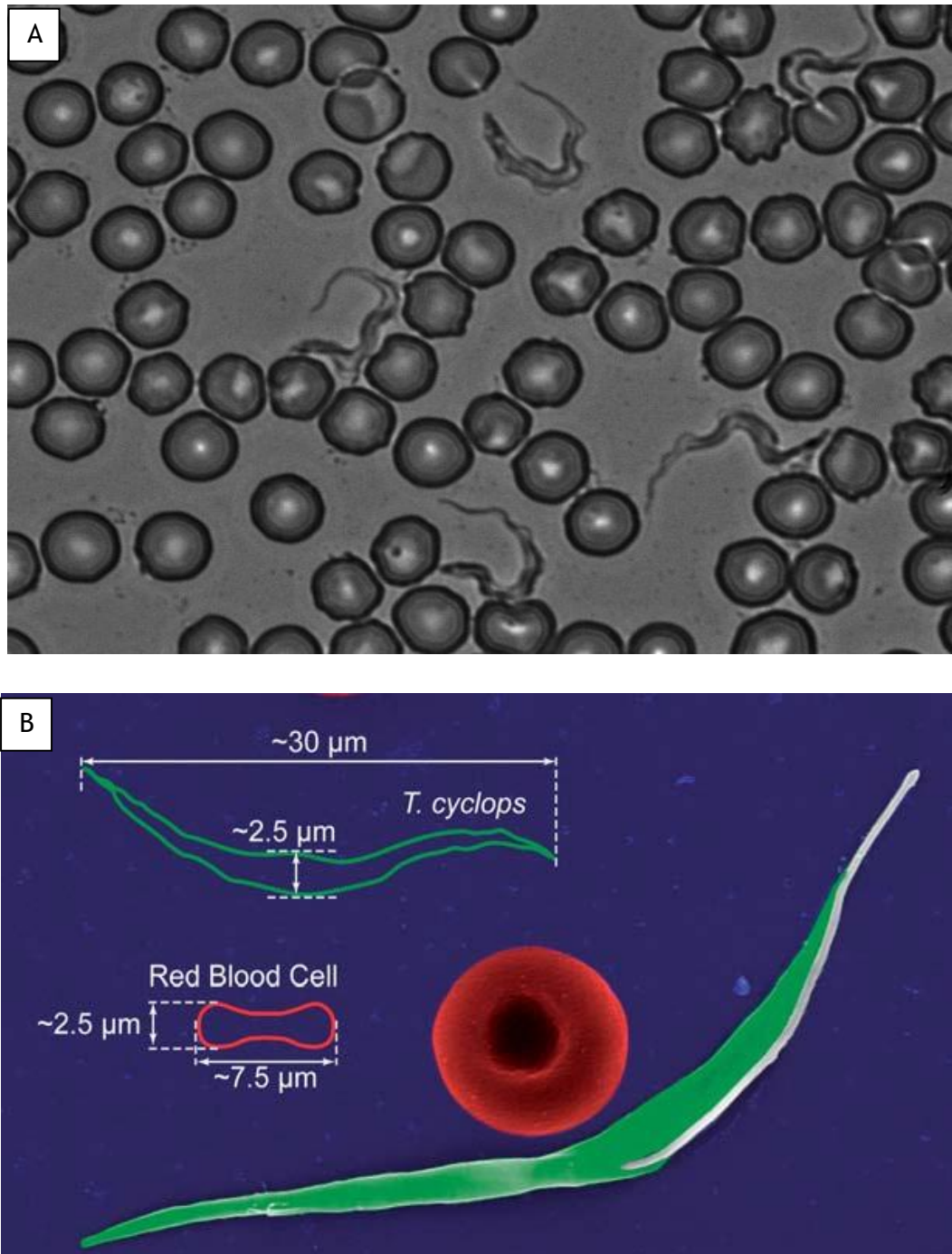


Figure 1.4: (A) Fixed thin blood smear of *Trypanosoma brucei brucei* (WT 427). This picture was taken using an oil immersion objective (100X). (B) Scanning electron microscope (SEM) picture of *Trypanosoma cyclops* and a red blood cell (Figure reproduced from Holm et al., 2011 by permission of The Royal Society of Chemistry).

### 1.3 Current Diagnostics

It is preferable that sleeping sickness is diagnosed before the parasites cross the blood-brain barrier although this is often not possible in rural populations. Currently, the diagnosis is done by microscopically identifying the presence of parasitic trypanosomes in blood, lymph node aspirates and cerebrospinal fluid. The Card Agglutination Test for Trypanosomiasis (CATT), widely used in large scale screening campaigns, is a serological test dependent upon an antigen gene expressed frequently in early stage infection. Although microscopy remains the gold standard for the screening, the sensitivity and further development of these tests is challenged by the ability of the trypanosomes to vary their surface antigens. The Mini Anion Exchange Centrifugation Technique (mAECT) - linked to microscopy, microhaematocrit centrifugation technique (MHCT) and quantitative buffy coat (QBC) methods are also used for diagnosing HAT (Chappuis et al., 2005; Lejon et al., 2002; FIND 2012).

CATT detects anti-trypanosomal antibodies in infected individuals but is poor in terms of sensitivity and specificity. The specificity of the CATT had been reported to be 95% but many false positives have also been reported (FIND, 2012). Moreover, it cannot be used to diagnose *T. b. rhodesiense* infections. The mAECT method of sample preparation uses ion-exchange to distinguish between blood cells and parasites, with the cell surface charges being the differentiating factor. This process is not consequential or reliable while being technically difficult to implement as well. While MHCT involves centrifugation of the blood in a capillary tube followed by the examination of interface between plasma and the buffy coat for the parasites, the QBC method involves collecting the blood in acridine orange coated capillaries and then examining these samples under special microscopes. Presently, there are many problems concerning the diagnosis of HAT using these methods. Moreover, the high costs associated with these techniques render them impractical to use clinically (Chappuis et al., 2005; FIND, 2012). Therefore, there is an urgent need to develop a sensitive and cost-effective diagnostic technique for HAT.

## 1.4 The Challenge

Blood is a complex non-Newtonian fluid with erythrocytes or red blood cells accounting for 99% of the haematocrit. The remaining 1% includes leukocytes or white blood cells and thrombocytes or platelets. The complex nature of the blood makes it difficult to analyse it efficiently in microfluidic devices (Bhagat et al., 2011). Also, low parasitaemia (100 - 10,000 cells mL<sup>-1</sup>), an important characteristic of trypanosomiasis infection, makes it more difficult to detect trypanosomes in blood efficiently (Matovu et al., 2010). Thus, enrichment of trypanosomes would boost the sensitivity of the detection for any given sensing method.

A critical factor in any sensing process is whether there is a requirement for the dilution of sample. Diluting the samples further decreases the number of parasites thus decreasing the detection limit. Diluting the sample before processing it often becomes necessary to make blood flow without clogging the microchannels, to adjust the conductivity (in dielectrophoresis) and to add reagents.

## 1.5 A Fresh Approach

Microfluidics, chemotaxis and density based separations provide a fresh approach to the problem where the required limit of detection is 1 parasite in 1  $\mu$ L drop of blood (which contains 1 million red blood cells, a detection sensitivity equivalent to 1 in 10<sup>6</sup>).

Microfluidics is a multidisciplinary field that studies the behaviour of fluids on the microscale. For most microfluidic devices bulk forces like gravity, buoyancy and momentum have very little effect on the fluid flow and factors such as inertia, viscosity and surface tension become dominant (Whitesides, 2006).

Carrying out the bio-analytical and diagnostic processes at microfluidic levels allows using minimum reagents, high sensitivity, rapid detection time and cost effectiveness. Moreover, these devices can be portable, which allows them to be used at the point-of-care or in the field. Sample preparation is an integral and arguably the most complicated part of any biochemical analysis (Pamme, 2007). One of the most important and widely used microfluidic developments has been that of continuous flow separations. Separation of sample components based on

size, charge, density, and magnetic properties is an integral part of many analytical processes (Toner and Irimia, 2005). Table 1.1 summarizes the commonly used microfluidic continuous separation techniques.

In continuous flow separation, the sample is introduced continuously into the device compared to chromatography or electrophoresis, which requires a onetime injection of a precise volume. Continuous sample injection also allows continuous readout and lateral separation of the sample components (Pamme, 2007).

Method	Driving force	Separation basis	Sample	References
Pinched flow fractionation	Laminar flow profile	Size	Microparticles, cells	Yamada et al., 2004; Jain and Posner, 2008
Field-flow fractionation	Perpendicular force fields	Size, density, polarizability, magnetization	Microparticles, cells	Giddings et al., 1976; Giddings 2003
Deterministic lateral displacement	Microstructure arrays	Size	Microparticles, cells, DNA, proteins	Huang et al., 2004; Inglis 2006
Hydrodynamic separation	Laminar flow profile	Size	Blood	Yang et al., 2006
Inertial focussing	Fluid and wall shear	Size	Microparticles, cells, DNA, proteins	Di Carlo et al., 2007; 2008)
Sedimentation	Gravity	Size, density	Microparticles, cells	Huh et al., 2007
Electrophoresis	Homogeneous electric field	Charge to size ratio	Microparticles, cells	Zhang and Manz, 2003
Dielectrophoresis	Non homogeneous electric field	Size, polarizability	Microparticles, cells	Dürr et al., 2003
Acoustophoresis	Acoustic pressure	Size, density	Microparticles, cells	Nilsson et al., 2004

Table 1.1: Common microfluidic continuous separation methods.

Using microfluidics has also its disadvantages such as sampling, sample introduction and epidemiology of disease. In most cases the sample preparation is carried out off chip and involves pre-processing of the samples before

analysis. Sample injection requires external pumps and constant power source to maintain fluid flow in the microchannels and becomes difficult to arrange for in resource poor settings.

Trypanosomes differ from both red and white blood cells. The trypanosomes are 20-30  $\mu\text{m}$  long, and 3-4  $\mu\text{m}$  in diameter compared to erythrocytes, which are discoid in shape and can have a diameter of 2-8  $\mu\text{m}$  (Figure 1.5). The parasites are also motile. This work explores how these fundamental physical differences can be used to provide a reagentless method to isolate and measure trypanosomes from within the blood matrix.

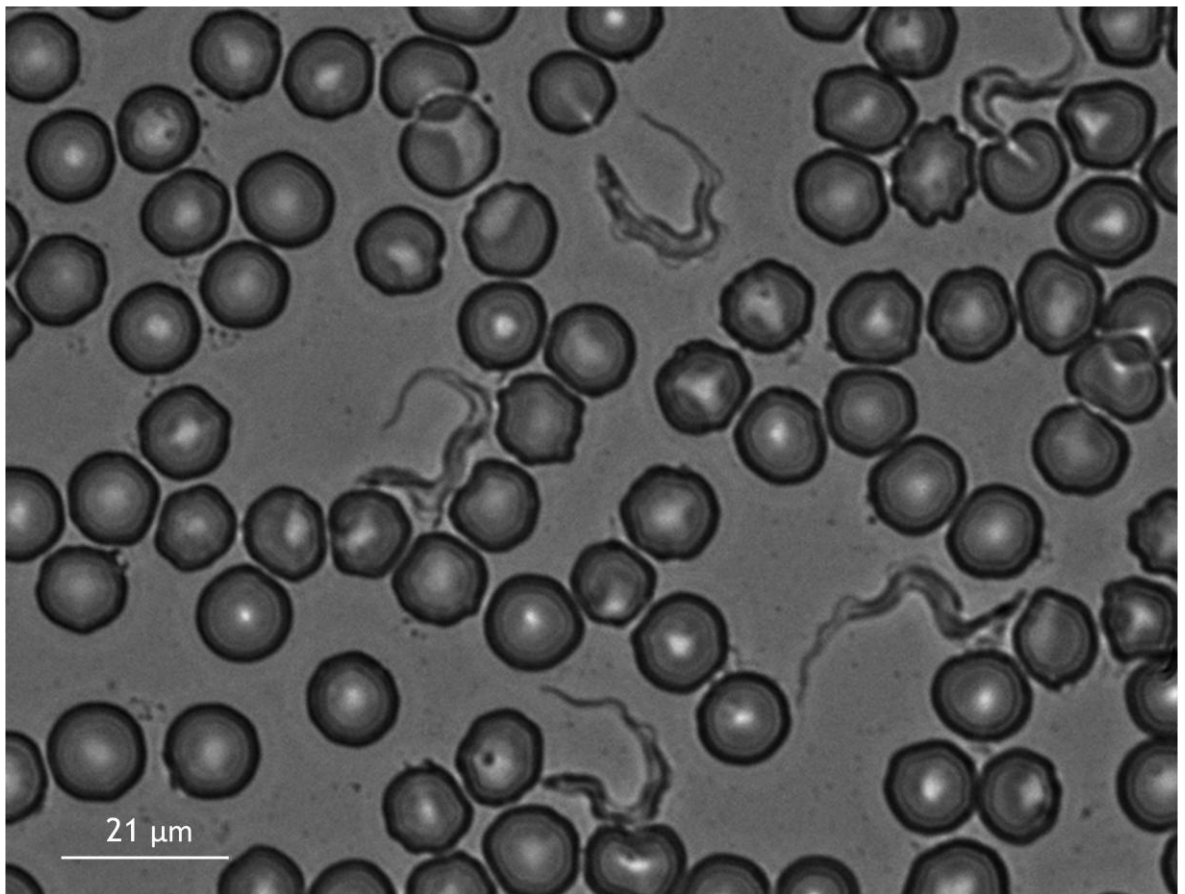


Figure 1.5: Fixed thin blood smear illustrating the physical differences between trypanosomes and red blood cells. The picture was taken using an oil immersion objective (100X).

## 1.6 Motivation

The diagnosis and treatment of diseases has improved with regular technological advances over the recent past. Although, the countries of the African subcontinent need more sensitive and portable diagnostic devices (Chappius et al., 2005), most of the current “point-of-care” instruments that have emerged through new technologies are available only for the diseases more prevalent in the West. Human African Trypanosomiasis (HAT) or sleeping sickness claims many thousands of lives and also causes adverse healthcare and socio-economic difficulties in Africa. For this disease, diagnostic tools remain rudimentary.

Microfluidics and lab-on-a-chip techniques hold the prospect to change the face of the medical diagnostics in the developing world. With manipulation of small sample volumes, microfluidic technologies are enabling miniaturisation and integration of laboratory tests into low cost, low power, hand-held microchip formats. This can allow complex medical diagnostic procedures to be carried out in remote locations where healthcare facilities are not adequate. The low-cost paper diagnostics developed by Martinez et al., (2007) offer promise mainly for the resource poor countries. As an alternative to conventional microfluidics systems, paper based diagnostic devices are inexpensive, easy to use and do not need mechanical pumping systems to drive fluid flows. Paper is available everywhere and its surface can be chemically modified to carry out a wide variety of functions. Martinez et al., (2007) developed a low-cost paper based platform to detect glucose and proteins in urine.

To eliminate sleeping sickness, the ability to diagnose the disease in humans and livestock at initial stages, before the parasites cross the blood brain barrier, is mandatory. Once the parasites cross the blood brain barrier, the diagnostic and treatment procedures become more complicated and risky (Barrett et al., 2003).

Presently, there are many problems concerning the diagnosis of HAT; therefore, the gold standard for the diagnosis remains microscopy (FIND, 2012). A point-of care device, that can rapidly and sensitively detect trypanosomes in human blood, is urgently needed. A device that would integrate all steps of a typical bio-chemical analysis, from sample preparation to sensitive detection, into a single platform not only would improve the chances of diagnosing the disease early, but would also help in enabling effective life saving treatments of

afflicted individuals. Importantly, it would also facilitate the entry of patients into clinical trials for urgently needed new drugs.

## 1.7 Introduction to Thesis

Following the introduction, Chapter 2 will introduce chemotaxis in *Trypanosoma brucei*. The experimental results for the demonstration of the chemotaxis of *T. brucei* towards D-glucose will be presented.

Chapters 3, 4 and 5 will introduce pinched flow fractionation (PFF), Dean flow and inertial migration based devices respectively, used to enhance particle separation. The working principles and the device design will be discussed. Application of the principle to microparticle separations and cell separations will be presented.

In Chapter 6, a novel density based separation of microparticles and cells will be described. The work involving density based separation of beads and whole blood was carried out at the George Whitesides Group, Department of Chemistry and Chemical Biology, Harvard University. The enrichment of trypanosomes was carried out at University of Glasgow.

Chapter 7 will introduce density based enrichment of trypanosomes using Surface Acoustic Waves (SAW). Finally, Chapter 8 will provide the over conclusions of the work.

## Chapter 2 - Chemotaxis in *Trypanosoma brucei*

### 2.1 Introduction

As discussed in Chapter 1, African trypanosomes cause the disease human African trypanosomiasis, a neglected tropical disease that has been targeted for elimination by 2020. A central tenet of the elimination programme will be the establishment of novel diagnostic tests that enable identification of cases of the disease. The fact that trypanosomes are frequently present in very low numbers in blood (e.g.  $100 \text{ mL}^{-1}$ ) adds difficulties to diagnosis. As trypanosomes are motile, we investigated chemotactic responses as a means to self-separate parasites from blood cells. Trypanosomes use D-glucose as their primary energy source. Fructose and glycerol are other reported energy sources. Trypanosomes demonstrate selective chemotaxis towards D-glucose but not the other energy sources.

A major impediment to current diagnostic algorithms is the low number of trypanosomes found in blood. This can drop to fewer than  $100 \text{ parasites mL}^{-1}$  of blood. Separation currently depends on centrifugation (the high density red blood cells leave lower density trypanosomes in a buffy coat after centrifugation at the suitable RCF, a property that we have investigated in a microfluidic enrichment device using acoustics, as detailed in Chapter 7. Recent applications of microfluidic based approaches including deterministic lateral displacement (Holm et al., 2011) and dielectrophoresis (Menachery et al., 2012) reveal how technological advances can be applied to improved separation of parasites from blood. Surface charge differences too can be exploited and mini anion exchange columns retain red cells whilst trypanosomes, uncharged at pH 7.4, elute from the column. Trypanosomes are flagellated motile organisms. While related *Leishmania* parasites have been shown to demonstrate both chemotaxis (Bray, 1983; Oliveira et al., 2000; Pozzo et al., 2007) and osmotaxis (Leslie et al., 2002), this has not been demonstrated for trypanosomes. A similar ability in trypanosomes might thus be exploited in allowing these cells to self-separate from blood.

## 2.2 Background

Chemotaxis, defined as the movement of an organism towards or away from a chemical, can be exploited to separate motile organisms from their environment. Separation or enrichment of trypanosomes from blood is seen as a major requirement for the establishment of novel diagnostic tools. Although chemotaxis has been previously reported for many microorganisms, the process has not yet been described for *Trypanosoma brucei*.

Chemotaxis in *Leishmania* was first reported by Bray in 1983. *Leishmania (mexicana mexicana, major and donovani)* promastigotes revealed chemotaxis towards various sugars and serum. However, the assay was relatively insensitive. Taxis was only apparent when high concentrations of attractant were used (ca. 20 mM). In 2000, Oliveira et al., developed an easy and sensitive assay modified from an earlier assay studying taxis in *E. coli* (Adler 1973). Conclusions that this assay showed *Leishmania* chemotaxis was challenged when use of a variety of carbohydrates or other chemical controls indicated the response was osmotactic (Leslie et al., 2002).

Recently, however, optical tweezers were used to study the behaviour (directionality and strength of force generated) of *Leishmania* under a glucose gradient and it was found that on sensing a glucose gradient, *Leishmania* promastigotes swim 3 - 5 times in circles and the force generated by them under glucose gradient is stronger and directed towards the gradient (Pozzo et al., 2007), reintroducing the notion that chemotactic responses in *Leishmania* are possible.

Ultimately, taxis in trypanosomes could be exploited in any algorithm aimed at separating or enriching trypanosomes from blood cells without requirement for centrifugation or ion exchange chromatography.

## 2.3 Experimental Details

### 2.3.1 Cultivation of Trypanosomes

Bloodstream forms of *Trypanosoma brucei brucei* (Strain 427) (Cross and Manning, 1973) were used as surrogates for *T. brucei gambiense* and *T. brucei rhodesiense* in experiments. *T. brucei* were cultured in Hirumi's Modified Iscove's medium (HMI-9, Appendix 10.1, Hirumi and Hirumi, 1989) supplemented with 10% foetal bovine serum (FBS, Gibco) and maintained at 37 °C and 5% CO<sub>2</sub>. The cells were cultured in 25 cm<sup>2</sup> tissue culture flask and passaged three times a week. Mouse blood spiked with *T. brucei* was used to conduct chemotaxis experiments. The trypanosomes were grown to a density of 2x10<sup>6</sup> mL<sup>-1</sup>. Before use, trypanosomes were washed with Carter's balanced salt solution (Appendix 10.2).

### 2.3.2 Dialysis

The dialysis membrane was boiled for 30 minutes in 10 mM sodium bicarbonate and 1 mM EDTA. The membrane was then rinsed thoroughly with distilled water and stored in ethanol at 4 °C. Before use, the membrane was washed with phosphate buffered saline (PBS, 2.7 mM KCl, 1.5 mM KH<sub>2</sub>PO<sub>4</sub>, 136.9 mM NaCl, 8.9 mM Na<sub>2</sub>HPO<sub>4</sub>•7H<sub>2</sub>O, pH 7.0 - 7.3). One end of the membrane was clipped and 1 mL of plasma carefully pipetted into it. Then the other end was clipped as well and the membrane was stirred in a beaker with 50 mL PBS at 4 °C. The PBS was replaced during and left stirring overnight.

### 2.3.3 Chemotaxis assay

The assay was similar to the *Leishmania* chemotaxis study reported by Leslie et al., 2002 and Oliveira et al., 2000. 0.1 M solutions of seven potential attractants (D-glucose; D-fructose; D-ribose; L-proline; L-arginine; L-lysine and kynurenine) and a negative control were made in molten 2% agarose in Eppendorf tubes. These compounds were chosen after screening the library of amino acids and sugars. Glass capillaries with an outer diameter of 1 mm and length of 100 mm were placed in each tube to let the solution flow into the capillary and set in such a way that a 1 cm gap remains at one of the end of the capillary tube. CBSS (Fairlamb et al., 1992) was then added to the open end of each capillary (8 µl).

The substances in the capillary tube diffuse towards the open end of the capillary tube creating a concentration gradient.

Trypanosomes were washed with CBSS at room temperature and re-suspended in 4 mL CBSS. The capillaries were then vertically immersed, with the CBSS filled end downwards, in Eppendorf tubes containing CBSS and bloodstream *T. brucei* at a density of  $10^6 \text{ mL}^{-1}$ .

The entire setup was incubated at room temperature for 1 hour. The capillaries were carefully removed from the Eppendorf tubes and the solution taken out from each one with a fine pipette. The cells were fixed with 1% formaldehyde (8  $\mu\text{l}$ ) for 15 minutes and were counted using a Neubauer haemocytometer. The experiment was performed five times in triplicate each time ( $n = 15$ ).

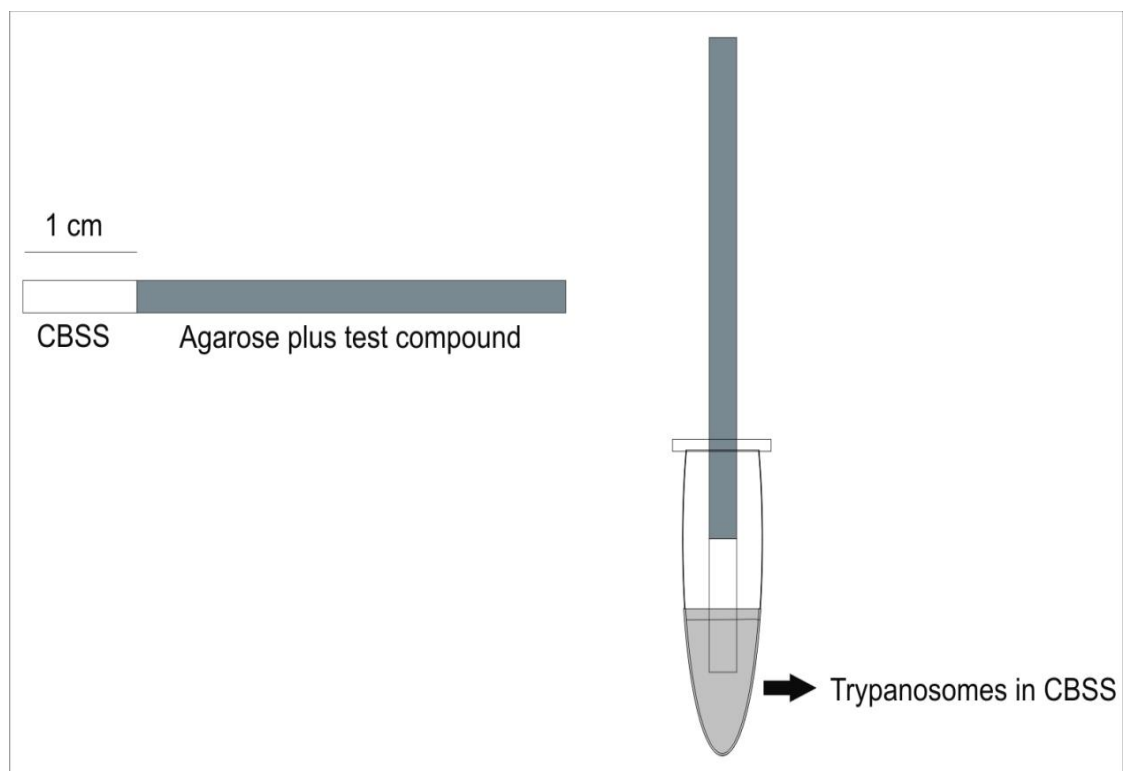


Figure 2.1: Schematic representation of the experimental setup.

### 2.3.4 Data Analysis

An unpaired, two-tailed t-test was used to determine the probability (p value) and a p-value  $\leq 0.05$  was considered significant. The two-tailed test was chosen to validate whether the attraction coefficient of the test compound was greater or less than that of the control group.

### 2.3.5 Diffusion of Glucose in the Capillary Tube

The gap to generate a concentration gradient inside the capillary was chosen to be 1 cm so that a well defined concentration gradient is established inside the capillary tube. To determine the extent of diffusion of glucose inside the capillary tube, the system was simulated using COMSOL Multiphysics 3.4 (Comsol Inc.) and also experimentally validated by measuring the glucose concentration at various time points using a glucometer (Accu-Chek® Aviva Nano) (Table 2.1).

Time (minutes)	Concentration from glucometer (mM)	Concentration from simulation (mM)
10	5.5	6.75
20	9.6	9.55
40	13	13.5
60	18	16.6

Table 2.1: Average concentration of glucose inside the capillary tube at various time points.

### 2.3.6 Simulation

COMSOL was used to model the diffusion of glucose inside the capillary tube filled with CBSS. The capillary tube was modelled three-dimensionally with a radius of 0.5 mm and height of 1 cm. The following Equation describes the concentration of the glucose in the system (Landau and Lifshitz, 1966).

$$\delta_{ts} \frac{\partial c}{\partial t} + \nabla \cdot (-D \nabla c) = R - u \cdot \nabla c \quad (2.1)$$

Where

Quantity	Value	Unit	Description
$\delta_{ts}$	1	-	Time scaling coefficient
$C_0$		mol/m <sup>3</sup>	Concentration
D	6e <sup>-10</sup>	m <sup>2</sup> /s	Diffusion coefficient of glucose (Stein, 1990)
R	0	mol/m <sup>3</sup> .s	Reaction rate
u	0	m/s	Velocity

Table 2.2: List of input data for material balance. At the inlet the concentration of glucose was set to 0.1 M and the boundary condition for outlet was set to convective flux. The simulation was solved for time dependent diffusion.

The reaction rate is zero because the concentration of glucose is not affected by any reaction. Figure 2.2 shows the solution at time one hour and figure 2.3 gives the concentration gradient along the length of the capillary tube.

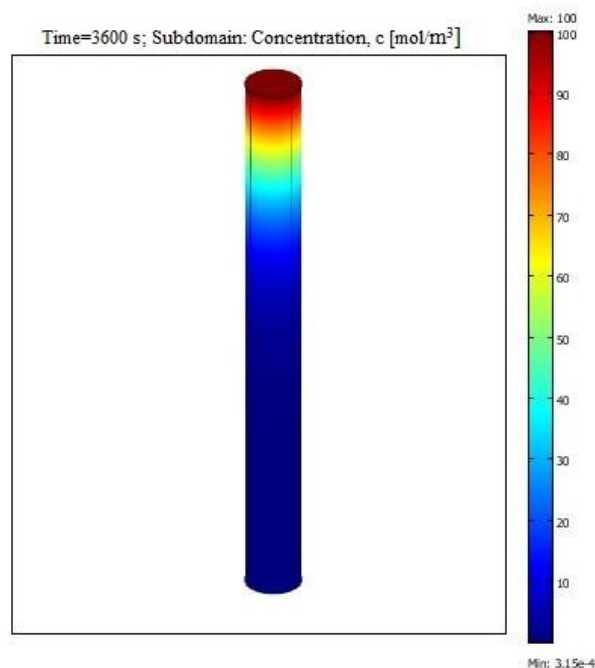


Figure 2.2: Simulation of the glucose gradient in the capillary tube at t=3600 seconds. The scale bar represents the concentration of the glucose in mM.

## 2.4 Results and Discussion

In initial experiments, trypanosomes were exposed to capillary gradients containing CBSS with the addition of 0.1 M solutions of various sugars and the number of trypanosomes entering each capillary then counted and compared to a negative control (where only CBSS was present in the agarose source). A mean movement of trypanosomes was calculated relative to a negative control for each substance to determine its attraction coefficient (Leslie et al., 2002). Thus an attraction coefficient of 1 meant no taxis. The attraction coefficients varied from 0.6 for ribose to 5 for glucose (Figure 2.4).

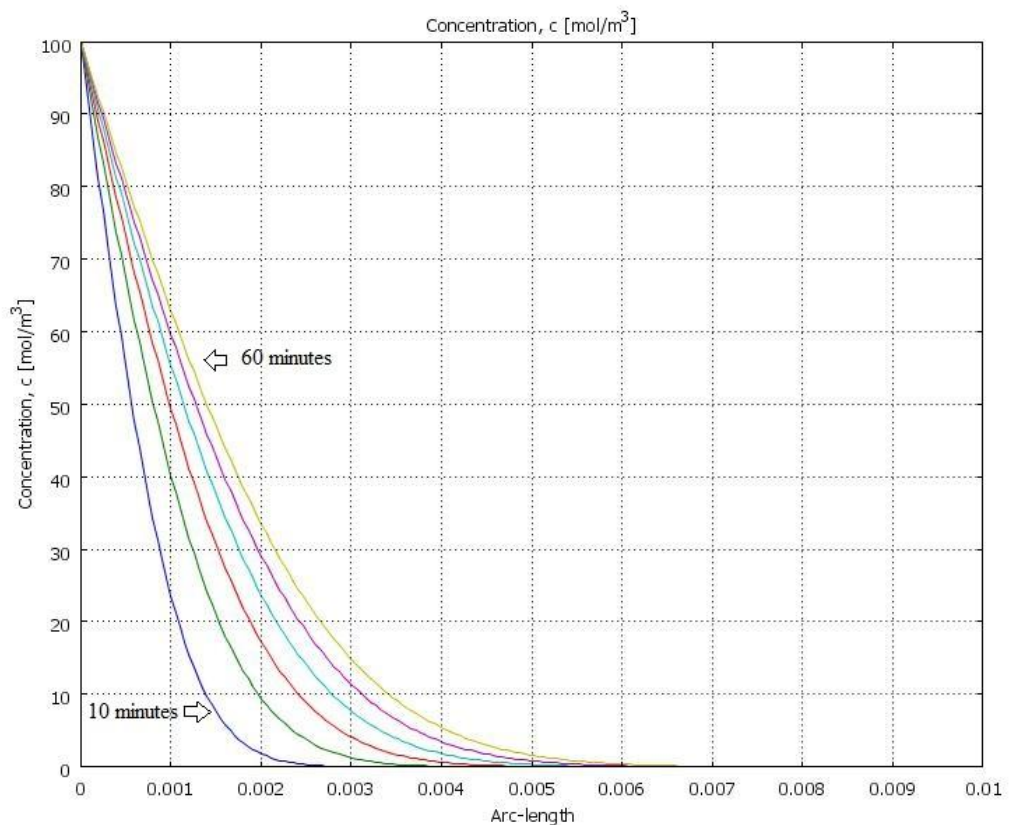


Figure 2.3: Concentration gradient profile of glucose along the length of the capillary tube from t=10 - t=60 minutes.

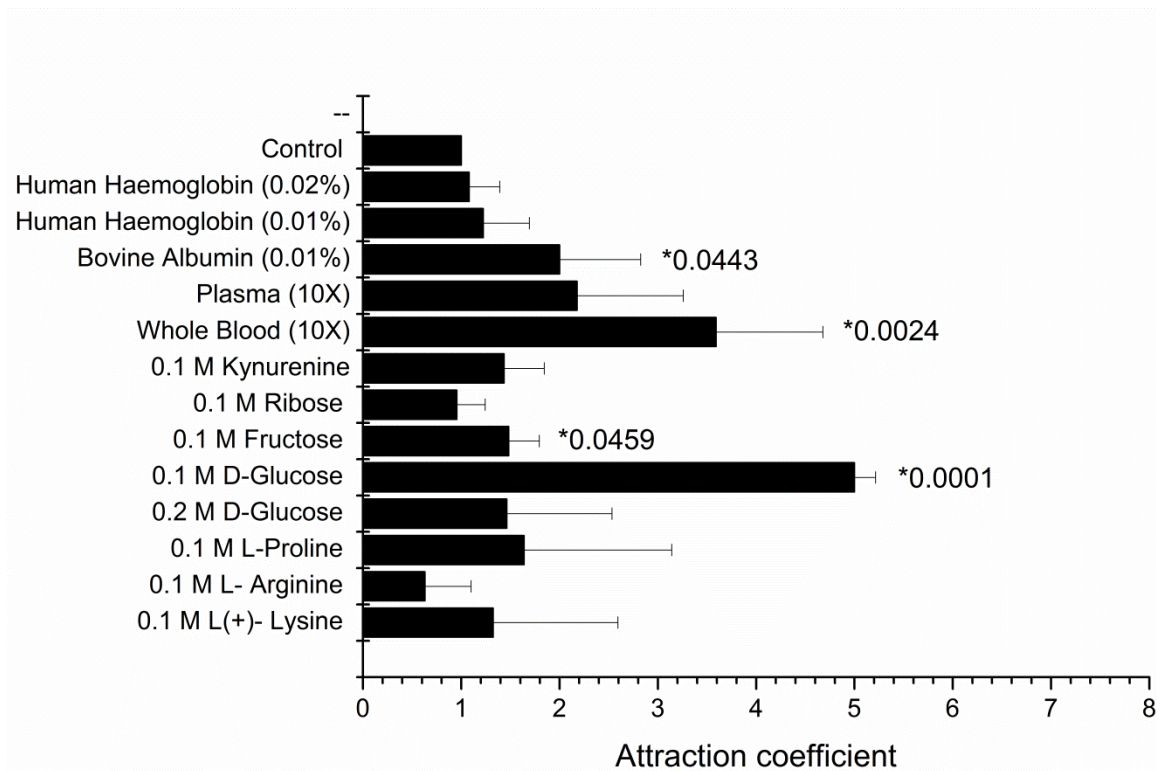


Figure 2.4: Attraction coefficients of test compounds including whole blood and plasma. Error bars indicate the standard error of the mean (n=5). The results have been normalized against the control. [\* statistically significant p-values].

Significant mobility towards D-glucose was evident whereas no other substrates appeared to promote the same effect. D-glucose is the principal substrate for trypanosome growth and energy provision. It is possible that the apparent migration involved enhanced flagellum motility in D-glucose. *T. brucei* uses both glucose and fructose as an energy source. Glycerol is also an excellent energy source but is cytotoxic at high concentrations (D'Hondt and Kondo, 1980). To test whether the movement of trypanosomes towards glucose was chemotaxis and not, for example, movement driven by enhanced flagellum motility in the presence of a robust energy source, an HMI-9 medium derivative was made where high concentrations of prospective energy sources were absent. Various energy sources were then added to incomplete medium separately to study the behaviour of trypanosomes. The trypanosomes grew normally and at the same rate at over 48 hours in HMI-9 supplemented with glucose and fructose although glycerol did not sustain similar growth, nor did galactose thus establishing the

fact that they show genuine chemotaxis towards glucose rather than a phenomenon dependent on energising the flagellum (Figure 2.5).

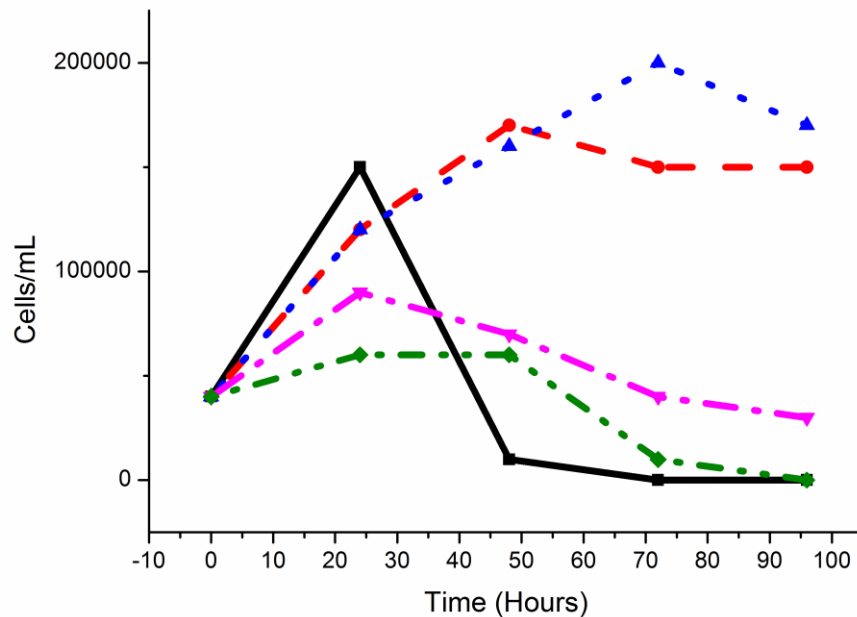


Figure 2.5: Growth curve of *T. brucei*. Parasites were grown in HMI-9 supplemented with 10% dialysed FBS and glucose (red), fructose (blue), glycerol (magenta) and galactose (green) as energy source and without an energy source (black).

D-fructose has previously been capable of sustaining *T. brucei* viability (Tetaud et al., 1997) and we show here that it is as effective as D-glucose as a carbon and energy source for growth in vitro. However, it did not act as a significant attractant to trypanosomes in the assay.

To further investigate this potential chemotaxis, whole blood, plasma, blood proteins and various concentrations of sugars were tested. Although blood, plasma and D-glucose all showed a higher taxis response compared to the rest of the compounds tested, the replicates showed substantial variability (Figures 2.4, 2.7). 0.1 M D-glucose showed a better taxis response than 0.2 M D-glucose. A t-test was conducted to compare 0.1 M D-glucose and 0.2 M D-glucose attraction coefficients. There was a very significant difference,  $p=0.0016$ , between the two data sets, suggesting that trypanosomes are selectively attracted to 0.1 M D-glucose.

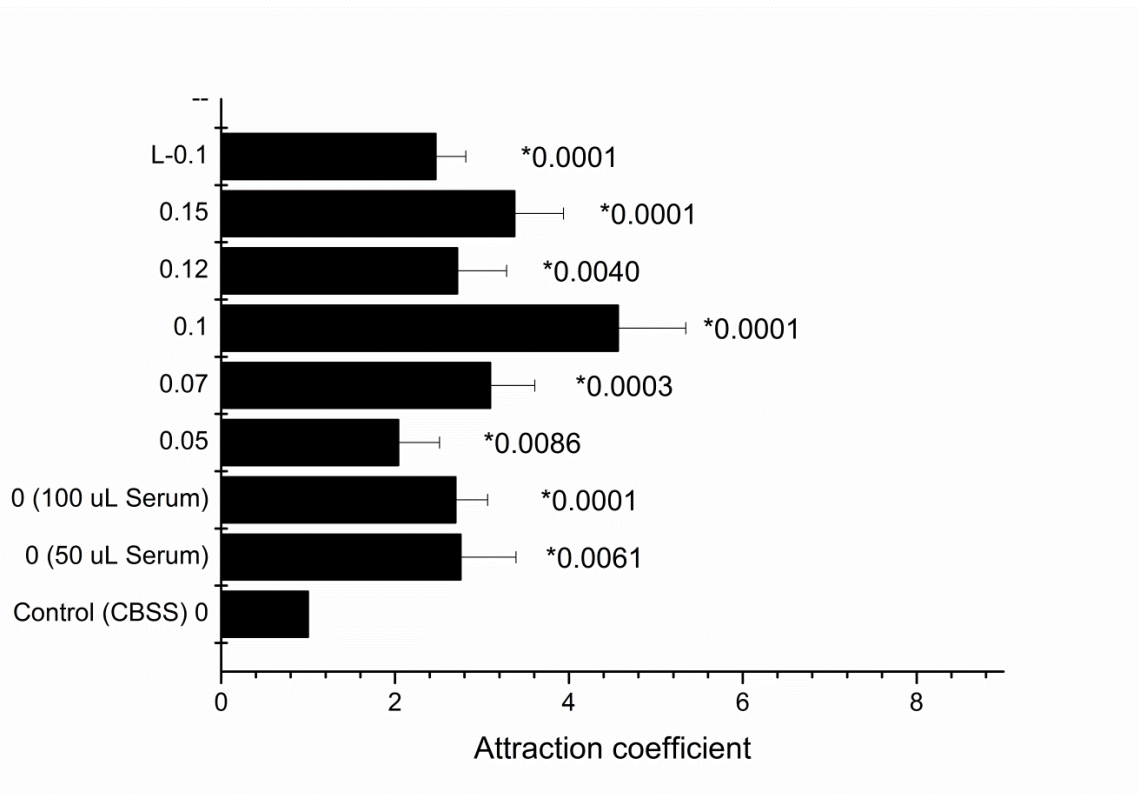


Figure 2.6: Attraction coefficient of dialysed plasma with different D-glucose concentrations. 100  $\mu$ L of dialysed serum was added to each sample unless stated otherwise. The control neither had serum nor any glucose. The results have been normalized against the control. Error bars indicate the standard error of the mean (n=5). [\* statistically significant p-values]

The chemotaxis experiments were further carried out with dialysed serum. Various D-glucose concentrations added to dialysed serum were tested (Figure 2.6). The attraction coefficient varied from 4.5 for 0.1 M D-glucose to 2 for 0.05 M D-glucose. Interestingly 0.1 M L-glucose showed a comparable taxis response to D-glucose, although former is not a substrate for trypanosome glucose transport or hexokinase (Tetaud et al., 1997; Ter Kuile and Opperdoes, 1991).

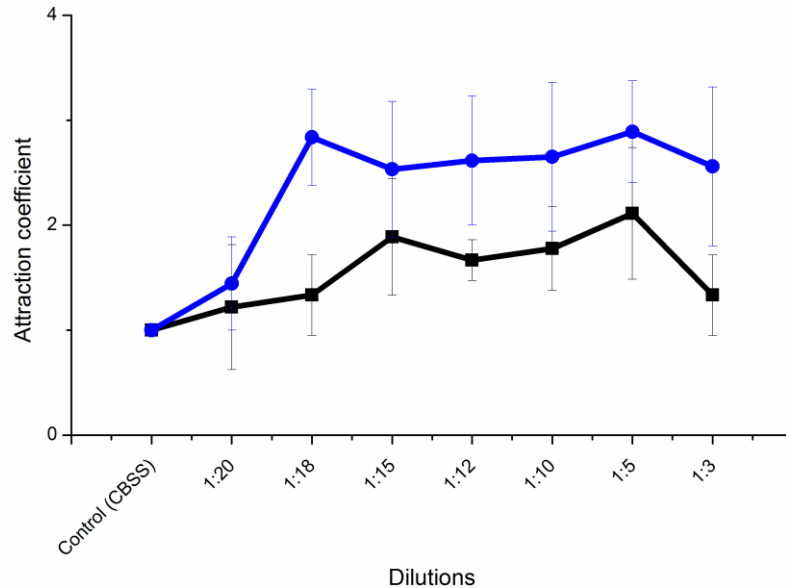


Figure 2.7: Attraction coefficient of various dilutions of whole blood (black) and plasma (blue). The dilutions were made in CBSS. The control (CBSS) does not contain any blood or plasma. Error bars indicate the standard error of the mean (n=3).

Chemotaxis experiments were also carried out with various dilutions of whole blood and plasma. This was done to study effect of concentration change of proteins and glucose present in the blood on the behaviour of trypanosomes (Figure 2.7). Blood and plasma were diluted in CBSS.

## 2.5 Conclusion

*T. brucei* swims towards higher concentrations of D-glucose in a gradient. These findings could be integrated with a microfluidic system to separate or enrich the parasites from the whole blood for sensitive diagnosis of HAT. It would be interesting to combine chemotaxis with microfluidics to study the behaviour of trypanosomes in the flow as well as for isolation of trypanosomes from the infected blood using glucose as a chemo-attractant. The H-filter, which is a microfluidic membrane-less filter that allows for continuous extraction of small molecules from complex fluids such as blood (Brody et al., 1997; Yager et al., 2006), could be an option.

## Chapter 3 - Pinched Flow Fractionation

### 3.1 Introduction

Size based particle separation is essential for many biochemical and analytical assays (Blankenstein and Larsen, 1998). Typically, membrane based filters have been used for separation of microparticles, but problems like clogging, dependence on pore size and high costs limit their use (Bhagat et al., 2009). In this chapter, a pinched flow fractionation based device for microparticle separation is described that overcomes the limitations of membrane based devices.

The pinched flow fractionation (PFF) is an effective technique for continuous size based particle separation. The concept of PFF for separation of microparticles was put forward by Yamada et al., in 2004. In PFF, two inlets are used to introduce fluids with and without particles. The inlets are followed by a pinched segment and a broadened segment. Inside the pinched segment, PFF uses laminar flow with low Reynolds number to assist size based separation. The Reynolds number ( $Re$ ) is the ratio of inertial and viscous forces. For most flows in microfluidic systems,  $Re$  is assumed to be low ( $Re \ll 1$ ) (Di Carlo, 2009).

$$Re = \frac{\rho ul}{\eta} \quad (3.1)$$

Where  $\rho$  is the density of the fluid,  $u$  is the velocity of the fluid,  $l$  is the characteristic length and  $\eta$  is the viscosity of the fluid.

Regardless of their sizes, the particles in the liquid are forced to align to one of the sidewalls of the pinched segment by another liquid without particles. As the particles approach the broadened segment, larger particles experience a force towards the centre of the channel by the spreading flow while the smaller particles are forced towards the sidewalls. This slight difference in the position of the particles in the pinched segment is however, amplified in the broadened segment, leading to the size based separation of particles perpendicular to the

bulk flow (Yamada et al., 2004; Jain and Posner, 2008). Figure 3.1 shows the schematic representation of the PFF principle.

The Navier-Stokes equation (3.6) is a fundamental equation of fluid dynamics and can be derived from Newton's second law using the principles of conservation of energy, mass and momentum (Andersen and Levinsen, 2007).

$$m \frac{d}{dt} u = \sum_j F_j \quad (3.2)$$

Dividing Equation 3.2 by volume gives density,  $\rho$ , and the force density,  $f$ .

$$\rho D_t u = \sum_j f_j \quad (3.3)$$

When using Newton's second law, particles have well defined positions. Replacing the time derivative with material derivative in Equation 3.3

$$D_t = \frac{\partial}{\partial t} + (u \cdot \nabla) \quad (3.4)$$

Using the material derivative expression in Equation 3.3

$$\rho \left( \frac{\partial}{\partial t} + (u \cdot \nabla) \right) u = \sum_j f_j \quad (3.5)$$

The Navier-Stokes equation for an incompressible fluid can be obtained by introducing the body forces acting on the fluid particles.

$$\rho \left( \frac{\partial u}{\partial t} + u \cdot \nabla u \right) = -\nabla p + \mu \nabla^2 u + f \quad (3.6)$$

Where  $u$  is the fluid velocity field,  $f$  is the vector field of the external forces acting on the fluid and  $p$  is the pressure field (Di Carlo, 2009).

For high aspect ratio channels (height $\gg$ width), at low  $Re$  and averaged depth, the Navier-Stokes equation can be reduced to Darcy's law. This equation is based on the assumption that the laminar flow streamlines will expand linearly as the flow enters the broadened segment and that the particles are completely aligned against the pinched segment wall (Jain and Posner, 2008). The difference between the particle positions ( $\Delta C$ ) in the broadened segment can be given by Equation

$$\Delta C = \frac{w_b \Delta D_p}{2 w_p} \quad (3.7)$$

Where  $\Delta D_p$  is the particle diameter and  $w_b$  and  $w_p$  are the widths of the broadened and pinched segment respectively (Jain and Posner, 2008).

The separation efficiency is determined by the flow rates of the particle stream and the buffer stream. The ratio of these two flows determines how much further the particles are pushed against the sidewall of the pinched segment. The boundary angle between the broadened and the pinched segment and the width of pinched segment also affect the separation efficiency as the particle alignment is determined by the flow profile in the microchannels (Yamada et al., 2004).

Another factor that affects the separation efficiency is the difference in particle sizes. It is assumed that, when pushed towards the wall of the pinched segment, the particles will follow a streamline corresponding to their central position. For a non-spherical particle, the separation is determined by the smallest dimension which has been demonstrated using red blood cells (Takagi et al., 2005).

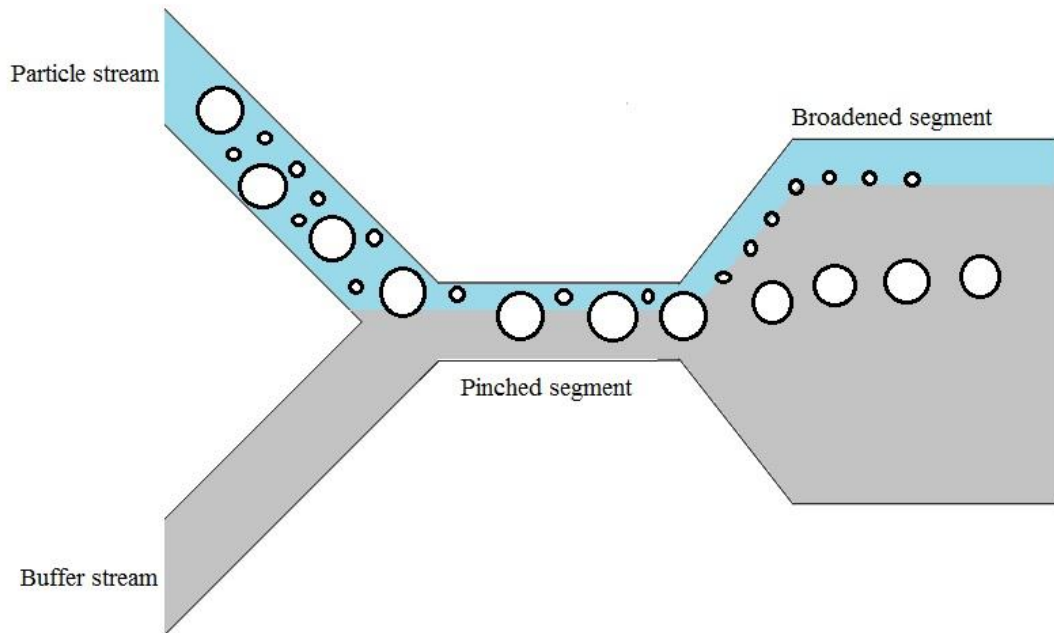


Figure 3.1: Principle of pinched flow fractionation. Schematic diagram showing particle behaviour in pinched and broadened segments.

Yapici et al (2009), calculated the migration of spherical particles (concentration of particles  $> 10\%$  w/v), for low  $Re$ . The interaction between particles was included in the calculations and was found to be dominant over particle migration across streamlines in a Poiseuille flow. They concluded that the particles migrate towards the centre of the channel due to the forces from interaction between particles and shear minimization.

Di Carlo et al., (2009), used COMSOL Multiphysics to calculate the migration of the particles of radius ' $r$ ' in square microchannels of width ' $w$ '. The concentration of particles was kept low compared to concentration used by Yapici et al., (2009). The ratio of  $2r/w$  was fixed to be above 0.1 and only beads with diameter greater than  $5\ \mu\text{m}$  were used. It was observed that the particle alignment against the channel wall was influenced by the effective lift force pointing towards the channel centre and away from the channel walls. However, the particles do not equilibrate in the channel centre as proposed by Yapici et al., in 2009 (Di Carlo et al., 2009).

### 3.2 Background

Yamada et al., 2004 used this technique to successfully separate 15  $\mu\text{m}$  and 30  $\mu\text{m}$  beads using pinched segments with widths between 47 and 82  $\mu\text{m}$ . Two boundary angles (angle between the pinched and the broadened segment), 60° and 180°, were tested for each pinched segment width. The channel depth was maintained between 45 and 55  $\mu\text{m}$  and the width of the broadened segment was fixed at 1 mm for all devices. The devices were fabricated in PDMS using rapid prototyping. For the pinched segment width of 50  $\mu\text{m}$ , they reported collection of 99% of 15  $\mu\text{m}$  particles from outlet 1 and 91.6% of 30  $\mu\text{m}$  particles from outlet 2.

The technique was later modified by Takagi et al., (2005) to enhance the separation. Multiple outlets with different channel dimensions were introduced instead of one broadened segment. Multiple branching enables different flow rate distributions in different channels and application of negative pressure to one of the outlets facilitated the separation of most of the liquid through the drain channel. The device was used to separate 1 to 5  $\mu\text{m}$  particles as well as blood cells and plasma (Takagi et al., 2005). An addition of a PDMS microvalve to control the flow rates further enabled separation of one, two and three  $\mu\text{m}$  particles and 0.5 and 0.8  $\mu\text{m}$  particles (Sai et al., 2006). They reported 90% particle collection for 0.5  $\mu\text{m}$  particles from outlet 1 and 82% particle collection for 0.86  $\mu\text{m}$  particles from outlet 2. Zhang et al., (2006) used an asymmetric PFF device to separate 10 and 28  $\mu\text{m}$  particles. PFF was also used to separate 2 and 15  $\mu\text{m}$  particles using a 15 - 30  $\mu\text{m}$  wide pinched segment and an aspect ratio of 20 - 30.

Though PFF has been used for focussing red blood cells (Takagi et al., 2005) and liver cells (Yamada et al., 2007), size based separation of other cells has not been reported yet.

### 3.3 Experimental Details

#### 3.3.1 Microfabrication and Soft Lithography

Microfluidic devices were fabricated using soft lithography in polydimethylsiloxane (PDMS) in the James Watt Nanofabrication Center (University of Glasgow). Masters for the microfluidic channels were fabricated on 4" silicon wafers using negative photoresist SU-8 3050 (Microchem Corporation). Details of the fabrication procedure are shown in Figure 3.2. The wafers were ultrasonicated with acetone, isopropyl alcohol (IPA) and methanol for 5 minutes each and finally cleaned with reverse osmosis (RO) purified water before use.

Approximately 4 mL of SU-8 3050 was dispensed onto the substrate directly from the bottle. The substrate was spun at a speed of 3000 rpm for 30 seconds. The substrate was then soft baked for 30 minutes on a hot plate at 100°C and allowed to cool to room temperature. A mask aligner (MA 6, Suss Microtech) was used for UV exposure of 40 seconds. The exposed substrate was then baked for one minute at 100°C before developing.

The substrate was developed in EC solvent (Dow Chemicals) for five minutes. After development, the wafer was rinsed with IPA and RO water and then blown dry. The width and height of the channel were measured using Dektak 6M Veeco profilometer (software version 8.30.005). The master was silanized with trichloro(1*H*,1*H*,2*H*,2*H*-perfluorooctyl)silane (Sigma Aldrich) for 45 minutes to yield a hydrophobic surface to aid the release of PDMS. PDMS (Sylgard 184, Dow Corning) was prepared by mixing the polymer and the curing agent in a ratio of 10:1, poured on to the master, degassed in a vacuum chamber for 45 minutes and then cured in a 90°C oven for one hour.

The PDMS was then carefully peeled off the master and cut with a scalpel. The fluid inlet and outlet were drilled on to a glass slides (VWR) for tube connections. The glass slide and the PDMS structures were treated with oxygen plasma (100 W) for 2 minutes before irreversible bonding.

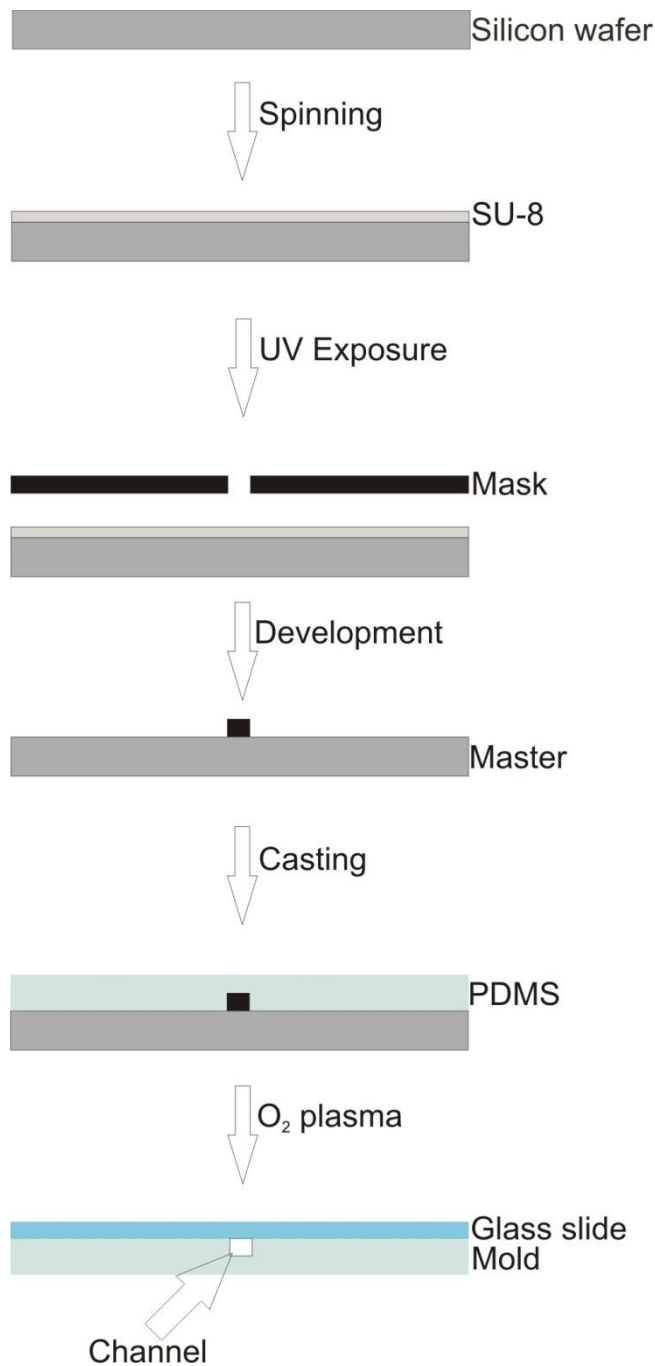


Figure 3.2: Schematic of the soft lithography process used to fabricate microfluidic devices. SU-8 3050 is dispensed on to a silicon wafer. Photolithography was used to define the structure of the device. The master was developed and PDMS mixed in a ratio of 10:1 is poured onto a finished master and baked for 45 minutes at 90 °C. The cured PDMS device was peeled from the master and oxygen plasma treated at 100 W for 2 minutes before being bonded to a glass slide.

### 3.3.2 Device Fabrication

The PFF devices (Figure 3.3) were fabricated, using soft lithography with an acetate mask. 3  $\mu\text{m}$ , 10  $\mu\text{m}$  and 25  $\mu\text{m}$  polystyrene beads were obtained from Bangs Laboratories, Inc. Microbore PTFE Tubing, 0.012"ID x 0.030"OD was obtained from Cole-Parmer. The device was mounted on a Zeiss Axio Imager A1 microscope. The sample was injected into the device through a syringe. The flow rates were varied between 1 - 50  $\mu\text{L min}^{-1}$  using a syringe pump (New Era). The samples were collected from the outlets and analyzed using a haemocytometer and a microscope. The designs had two inlets and three outlets.

For separation of 10  $\mu\text{m}$  and 25  $\mu\text{m}$ , the device dimensions used were as follows. The length and width of inlet channels was 1.5 mm and 100  $\mu\text{m}$  respectively. The pinched segment was 100  $\mu\text{m}$  wide and 1.50 mm long, the broadened segment was 1.5 mm long and 1 mm wide, and the boundary angle between the pinched and broadened segment was kept at 180° (Figure 3.3). The outlets were 1mm long and 300  $\mu\text{m}$  wide.

For separation of 3 and 10  $\mu\text{m}$  beads the device used has an inlet with the length and width of 500  $\mu\text{m}$  and 50  $\mu\text{m}$  respectively. The pinched segment was 15  $\mu\text{m}$  wide and 150  $\mu\text{m}$  long, the broadened segment was 750  $\mu\text{m}$  long and 250  $\mu\text{m}$  wide, and the boundary angle between the pinched and broadened segment was fixed at 90°. This device had three outlets with the length and width of 750  $\mu\text{m}$  and 50  $\mu\text{m}$  respectively (Figure 3.4).

### 3.3.3 Cultivation of Trypanosomes

*T. cyclops* were cultured in Cunningham's medium (Appendix 3) supplemented with 20% FBS and maintained at 27 °C. *T. cyclops* were passaged once a week and were grown to a density of  $2 \times 10^6 \text{ mL}^{-1}$ .

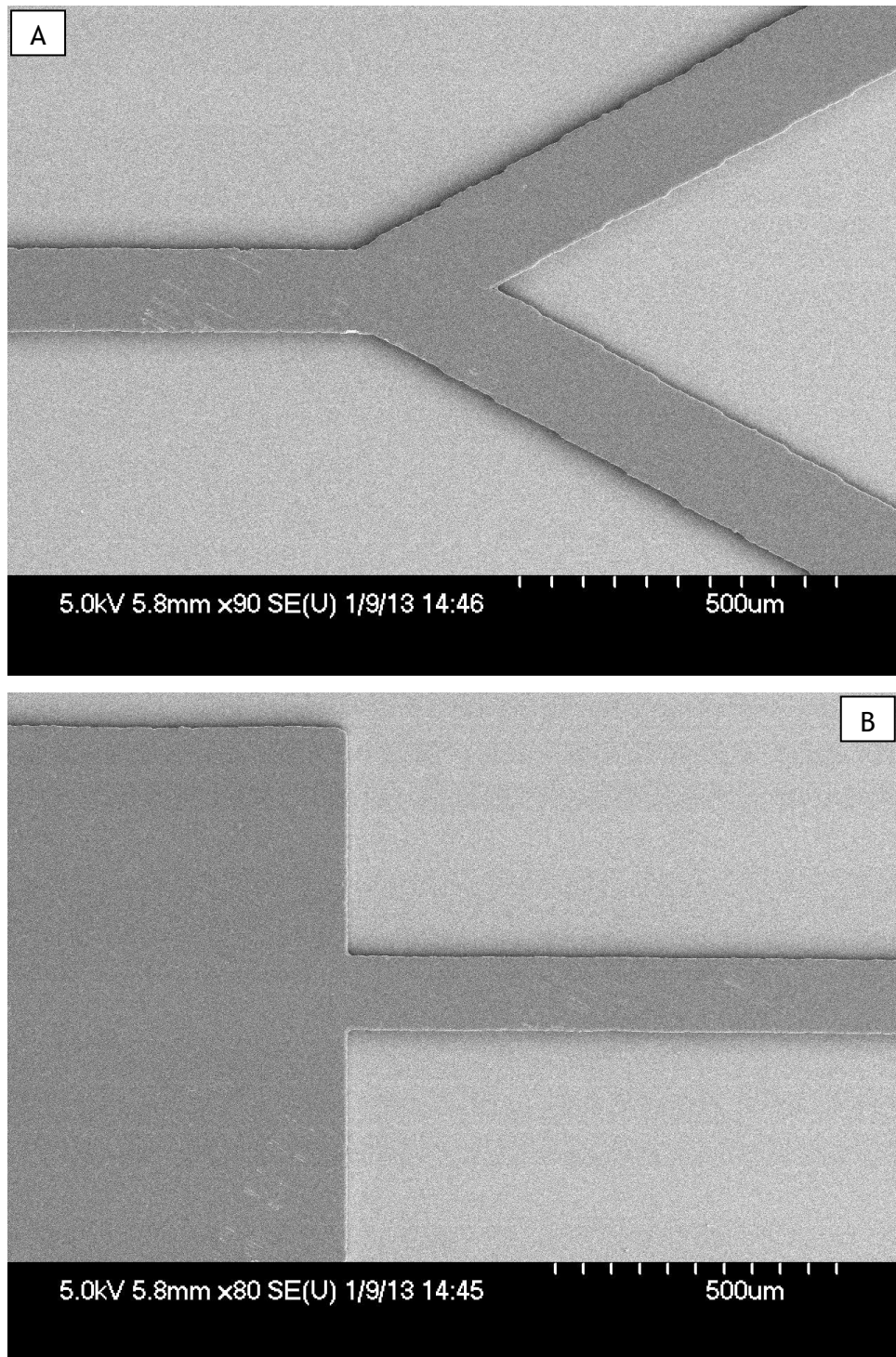


Figure 3.3: SEM of the PFF device for separation of 10.14 and 24.99  $\mu\text{m}$  beads. Length and width of inlet channels is 1 mm and 150  $\mu\text{m}$  respectively (A). The pinched segment is 100  $\mu\text{m}$  wide and 750  $\mu\text{m}$  long, the broadened segment is 1mm long and 1.5 mm wide (B). The length and width of outlets is 1mm and 300  $\mu\text{m}$  respectively. The picture was taken using Hitachi S-4700 operating at 5kV.

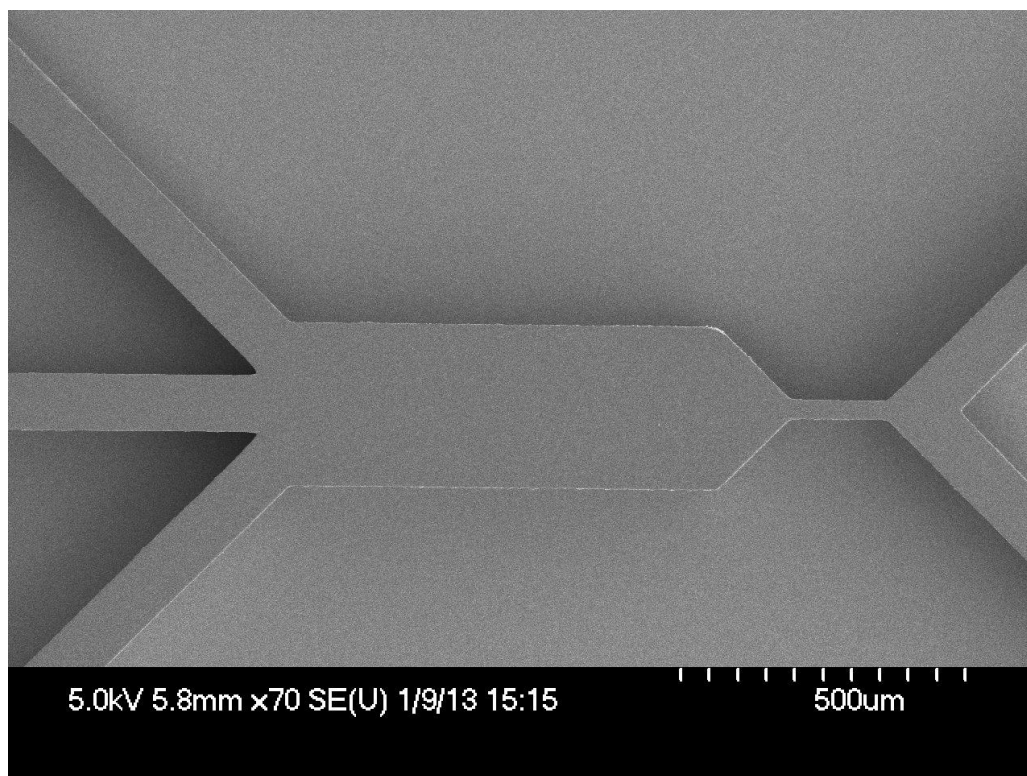


Figure 3.4: SEM of the PFF device. Length and width of inlet channels are 500  $\mu\text{m}$  and 50  $\mu\text{m}$  respectively. The pinched segment is 15  $\mu\text{m}$  wide and 150  $\mu\text{m}$  long, the broadened segment is 750  $\mu\text{m}$  long and 250  $\mu\text{m}$  wide. The length and width of outlets is 750  $\mu\text{m}$  and 50  $\mu\text{m}$  respectively. The picture was taken using Hitachi S-4700 operating at 5kV.

### 3.4 Results and Discussion

First the 10  $\mu\text{m}$  and 25  $\mu\text{m}$  polystyrene beads were separated using the device described in Figure 3.3. The pinched segment width was 100  $\mu\text{m}$  and the boundary angle between pinched and broadened segment was 180°. The flow rate of the particle steam was fixed at 5  $\mu\text{L min}^{-1}$  and that of buffer steam at 30  $\mu\text{L m}^{-1}$ . These flow rates were chosen as they resulted in best separation efficiency after testing a range of flow rates. Figure 3.5 shows the separation performance of the device.

Majority of the 10  $\mu\text{m}$  beads were collected from outlet 1 and the 25  $\mu\text{m}$  beads were collected from outlet 2. The residual 10  $\mu\text{m}$  and 25  $\mu\text{m}$  beads were collected from outlets 2 and 3 respectively. No 10  $\mu\text{m}$  were collected in outlet 3 and likewise no 25  $\mu\text{m}$  beads were collected from outlet 1. The length and width

of the pinched segment was found to be inefficient for separation of 3  $\mu\text{m}$  and 10  $\mu\text{m}$  beads. The 3  $\mu\text{m}$  and 10  $\mu\text{m}$  beads were chosen to mimic the red blood cells and parasites in the flow. Also, the boundary angle of  $180^\circ$  led to the occasional bubble formation in the corners of the broadened segment.

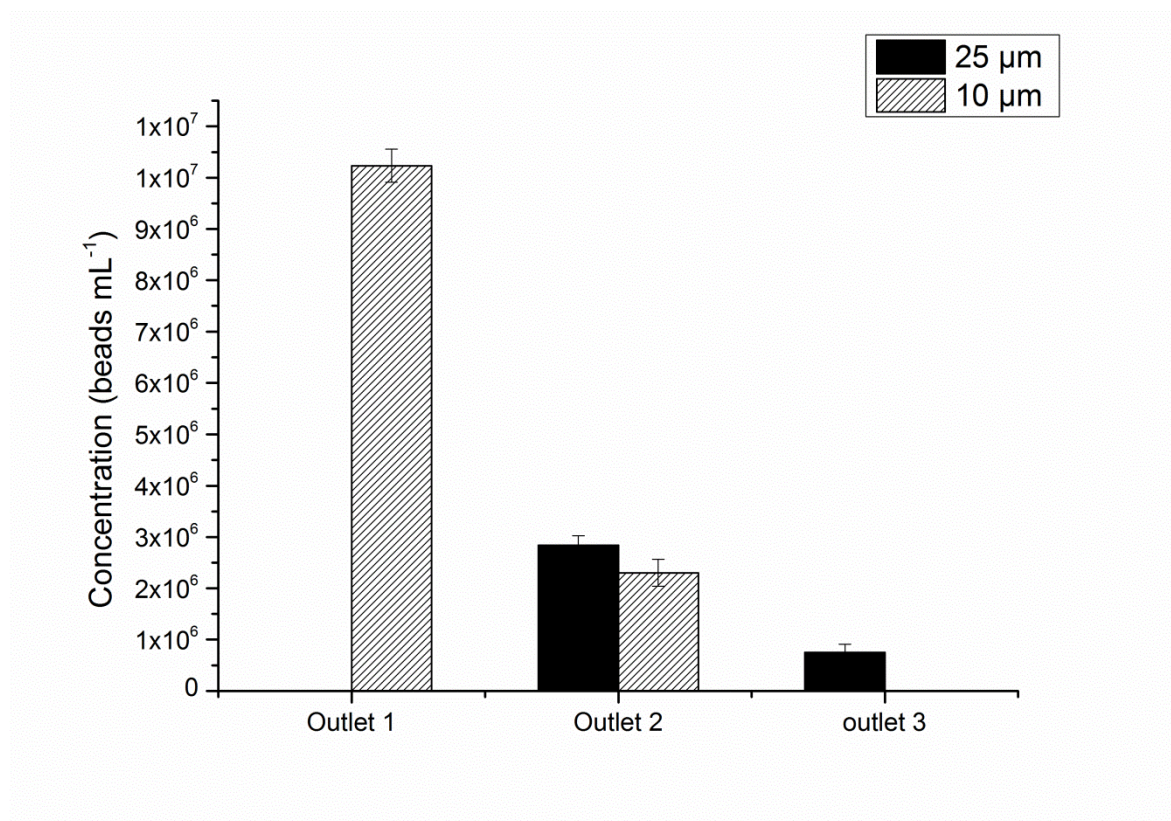


Figure 3.5: Separation performance of 10  $\mu\text{m}$  and 25  $\mu\text{m}$  beads. The width of the pinched segment was 100  $\mu\text{m}$  and a boundary angle of  $180^\circ$ . The beads were counted by haemocytometry in samples taken from outlets after separation. The data are means of 3 replicates and the error bars are standard deviation. The initial concentration of 10  $\mu\text{m}$  and 25  $\mu\text{m}$  beads was  $1.3 \times 10^6$  and  $3.6 \times 10^6 \text{ mL}^{-1}$  respectively.

To overcome these limitations, a new device with the pinched segment width of 15  $\mu\text{m}$  and boundary angle of  $90^\circ$  was fabricated (Figure 3.4). Figure 3.6 shows the separation efficiency of the device with 3  $\mu\text{m}$  and 10  $\mu\text{m}$  polystyrene beads. The flow rates used were kept unchanged ( $5 \mu\text{L min}^{-1}$  for the particle stream and  $30 \mu\text{L min}^{-1}$  for the buffer stream). 74% of the 3  $\mu\text{m}$  beads were collected from outlet 1 and 19% from outlet 2. 76% of the 10  $\mu\text{m}$  beads were collected from outlet 2 and 22% from outlet 3. The residual 10  $\mu\text{m}$  and 25  $\mu\text{m}$  beads were collected from outlets 2 and 3 respectively. No 10  $\mu\text{m}$  were collected in outlet 3 and likewise no 25  $\mu\text{m}$  beads were collected from outlet 1.

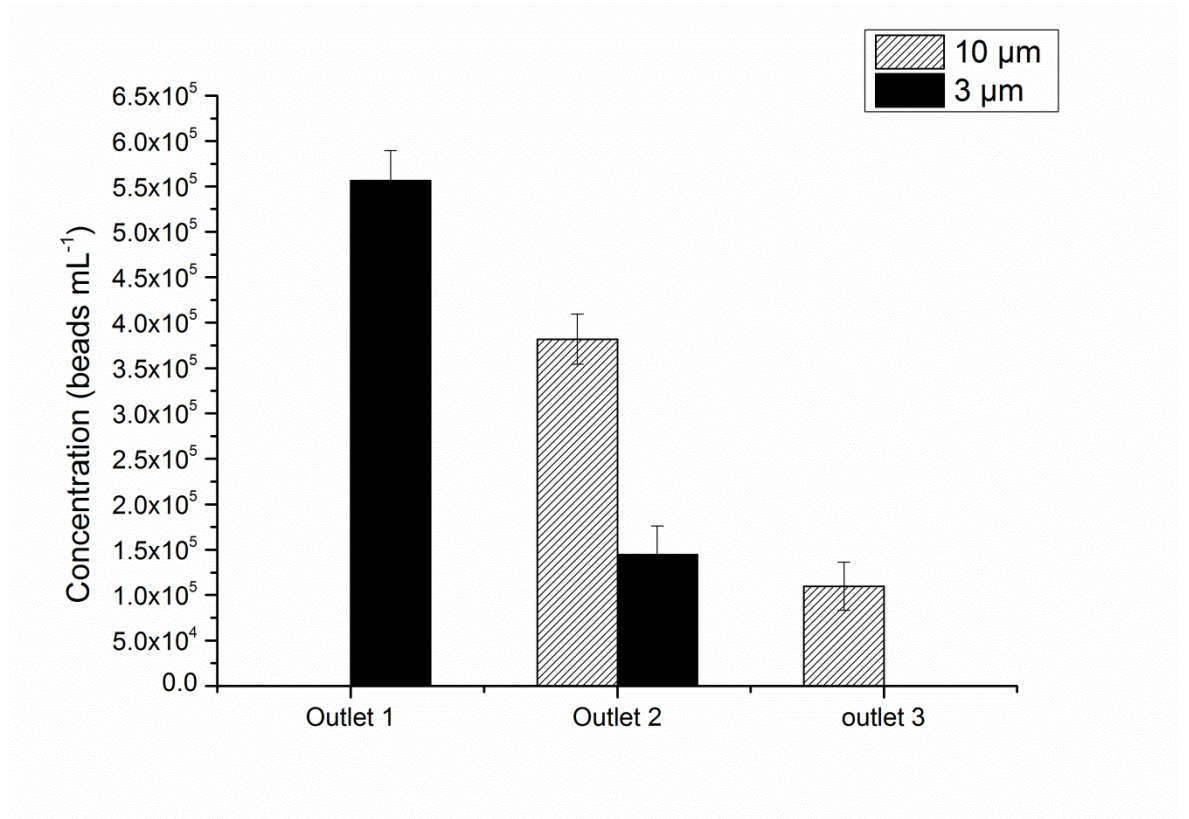


Figure 3.6: Separation performance of 3 µm and 10 µm beads. The width of the pinched segment was 20 µm and the boundary angle was 90°. The beads were counted by haemocytometry in samples taken from outlets after separation. The data are means of 3 replicates and the error bars are standard deviation. . The initial concentration of 10 µm and 3 µm beads was  $5 \times 10^5$  and  $7.5 \times 10^5$  mL<sup>-1</sup> respectively.

Though PFF was employed successfully to separate different particle sizes, separation of trypanosomes from blood cells proved to be inefficient. Figure 3.7 shows the separation efficiency of the device. The blood was diluted 20X in PBS and spiked with  $1 \times 10^6$  trypanosomes mL<sup>-1</sup>. Both trypanosomes and RBCs were collected from all three outlets. 50% of the RBCs were collected from outlet 1, ~30% from outlet 2 and the rest from outlet 3. ~30% of trypanosomes were collected from outlet 1, ~35% from outlet 2 and 12% from outlet three. A fraction of parasites was lost due to the dilution of the sample. The inefficient separation could be attributed to the fact that trypanosomes have a very different shape, when compared to red blood cells. They are elongated and thin, while the red blood cell can be approximated as a disk.

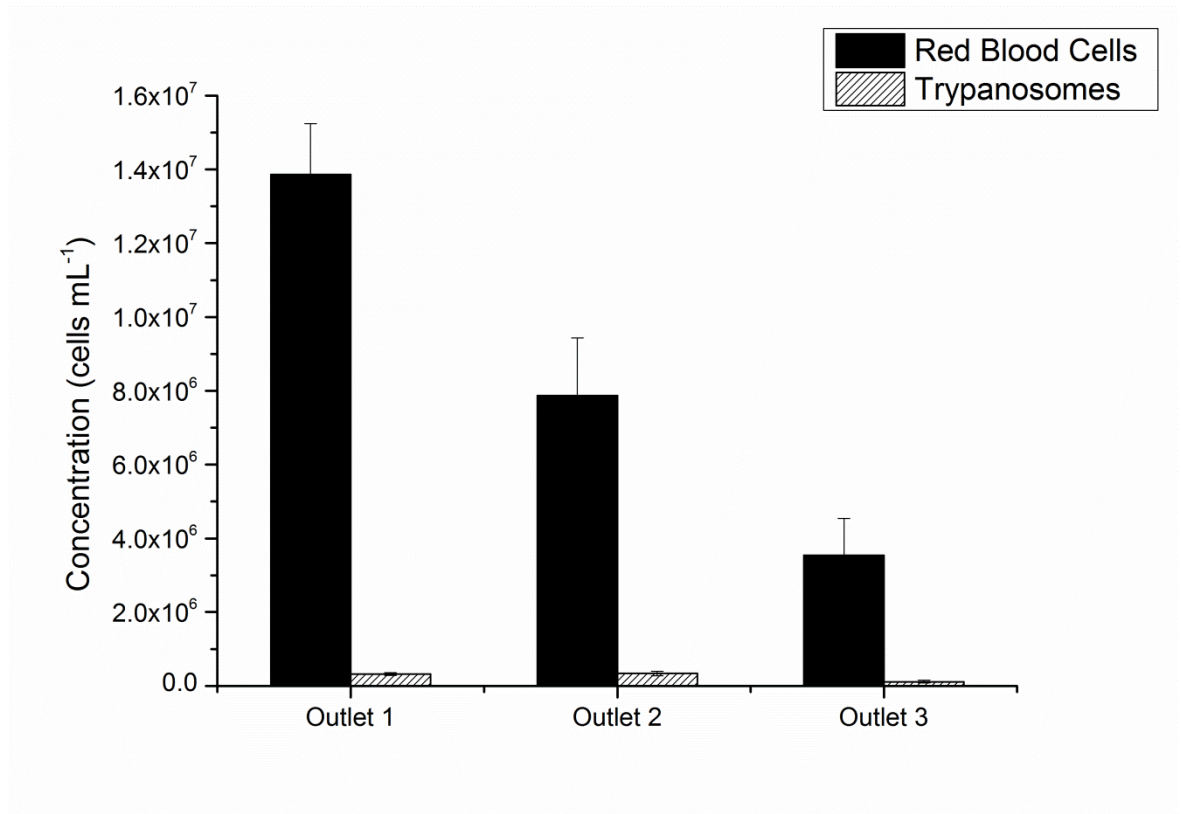


Figure 3.7: Separation performance of trypanosomes and red blood cells. The width of the pinched segment was 20  $\mu\text{m}$  and the boundary angle was 90°. The cells were counted by haemocytometry in samples taken from outlets after separation. The flow rates used were kept at 5  $\mu\text{L min}^{-1}$  for the particle stream and 30  $\mu\text{L min}^{-1}$  for the buffer stream. The data are means of 3 replicates and the error bars are standard deviation. The initial concentration of RBCs and trypanosomes was  $2.7 \times 10^7$  and  $1 \times 10^6$   $\text{mL}^{-1}$  respectively.

### 3.5 Conclusion

In PFF, the separation process is entirely based on particle size and should, in principle, separate trypanosomes from blood cells but the comparable diameters of trypanosomes and RBCs make the separation difficult. Though the fabricated device was capable of separating spherical particles, it did not efficiently separate blood cells from plasma. One reason could be the possible protein deposition on the microchannel walls that leads to clogging and disrupts the laminar flow inside the channels. As a result the sample needs to be diluted at least 50 times which further decreases the concentration of parasites in the sample and increases the sample volume to be processed and required sensitivity. A microfluidic device with spiral geometry, described in next chapter, was fabricated to overcome this limitation.

## Chapter 4 - Dean Flow

### 4.1 Introduction

Recently, inertial lift forces have been used extensively in microfluidics (Di Carlo, 2007; Seo et al., 2007a). Two counter-rotating vortices known as Dean vortices are formed in the top and bottom halves of the curvilinear channels. These vortices are generated by the centrifugal acceleration experienced by the fluid in a radially outward direction inside the channel (Dean, 1927; 1928). Dean number ( $De$ ) is used to quantify the magnitude of secondary flows generated in the spiral channels and is given by:

$$De = \frac{\rho u D}{\mu} \sqrt{D_h/2R} = Re \sqrt{D_h/2R_c} \quad (4.1)$$

where  $\rho$  is density of medium,  $u$  is the average velocity of the fluid,  $\mu$  is the viscosity of the fluid,  $R_c$  is the radius of curvature and  $D_h$  is the hydraulic diameter of the channel. In a spiral microchannel, the Dean number increases with the increase in Reynolds number, channel size and decrease in radius of curvature (Bhagat et al., 2008).

For a straight microchannel  $De = 0$  (Dean flow absent) and  $De > 0$  for a spiral microchannel. Stronger Dean forces can be generated by increasing the cross-section of the channels or by increasing the flow rates. Also the ratio of lift forces to Dean drag is greater for bigger particles as compared to the smaller ones (Kuntaegowdanahalli et al., 2009). The lift forces acting on the particles are size dependent leading to equilibration of different sized particles in different streamlines and hence size based separation (Park et al., 2009).

The average Dean velocity for a given  $De$  can be calculated from the expression formulated by Ookwara et al., (2004; 2006).

$$U_{Dean} = 1.8 \times 10^{-4} De^{1.63} \quad (4.2)$$

The particles are entrained in one of the two vortices, formed due to the transverse secondary Dean flows, depending on their size (Figure 4.1). The Dean drag force experienced by the particles can be obtained by the expression

$$F_D = 3\pi\mu D_p U_F \quad (4.3)$$

Where  $\mu$  is the fluid viscosity,  $D_p$  is the diameter of the particle and  $U_F$  is the flow velocity (Asmolov, 1999).

In a curvilinear channel, the particles experience pressure forces (Maxey and Riley, 1983) and inertial lift forces (McLaughlin, 1991; Asmolov, 1999) in addition to the Dean drag  $F_D$ . The inertial lift forces, also known as wall effect forces ( $F_{LW}$ ), force the particles in the laminar flow to migrate between streamlines to a specific position where the lift forces equilibrate the shear forces. In a parabolic flow profile developed in a straight channel, the fluid moving down the centre travels faster than along the walls but in a curved channel as a result of counter rotating Dean vortices, the fluid in the centre of the channel experiences a higher centrifugal force than the surrounding liquid, which ejects fluid from the high speed core towards the outer wall (Howell et al., 2004). The inertial forces direct the suspended particles away from the centre whereas the walls of the channel exert a lift force on the particles directing them away from the wall. The net force equilibrates the particles based on their size into focussed streams (Kuntaegowdanahalli et al., 2009).

A combination of Dean drag forces ( $F_D$ ) and inertial lift ( $F_{LS}$ ) acts on the particles flowing through a spiral microchannel. The magnitude and direction of these forces is determined by particle size and position across the microchannel cross-section. The lift forces dominate if the particles have  $D_p/D_h \geq 0.07$  (where,  $D_p$  is the particle diameter and  $D_h$  is the microchannel hydraulic diameter, Bhagat et al., 2008), and are responsible for the equilibration of the particles within the channels. In a rectangular microchannel, particle equilibration does not depend on the hydraulic diameter but instead depends on the shortest channel dimension (microchannel height) due to varying shear rates across the channel cross-section (Bhagat et al., 2008). Figure 4.1 demonstrates the principle of

Dean flow and the forces acting on the microparticles inside the spiral microchannel.

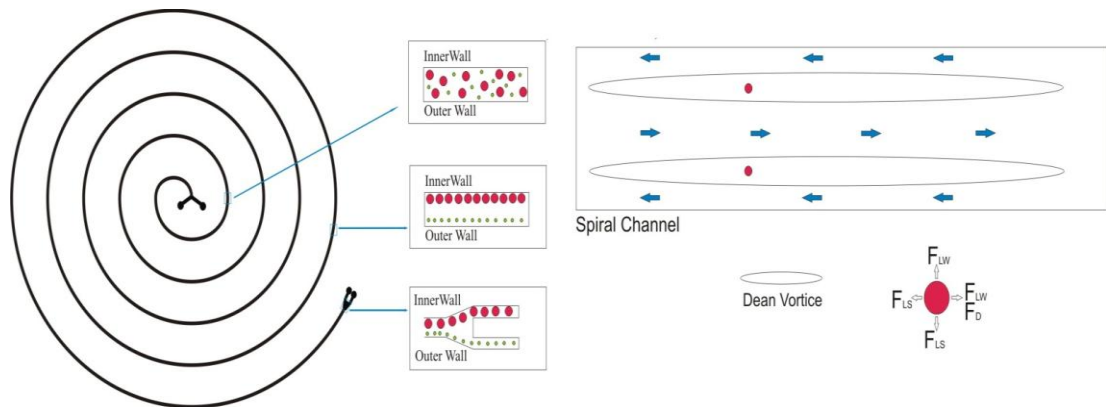


Figure 4.1: Schematic of size based separation of beads in spiral microchannels. Under the influence of counter acting lift forces and Dean Drag, the particles equilibrate according to the size along the inner wall of the spiral microchannel (where  $F_{LW}$  is inertial lift force exerted by channel wall,  $F_{LS}$  is the shear lift force and  $F_D$  is the Dean drag force).

## 4.2 Background

Centrifugal acceleration separation was first reported by Blatter et al., (2004). The used this technique to separate plasma from blood. The device consisted of an inlet for injecting blood into the microchannels with a  $90^\circ$  bend. The bend bifurcated into two channels, one for collecting plasma and other for collection of blood cells. The authors reported an 80% separation efficiency.

Gregoratto et al., (2007) used spiral microchannels, with aspect ratio ranging from 8 - 15, for separation of large volumes of dilute suspensions. The suspension consisted of  $1\ \mu\text{m}$ ,  $8\ \mu\text{m}$  and  $10\ \mu\text{m}$  polystyrene beads in water. The suspension was injected into the device that had an aspect ratio of  $\sim 10$ , at varying flow rates. At a flow rate of  $2\ \text{mL min}^{-1}$ , the authors reported a 3.5 fold increase for  $10\ \mu\text{m}$  particles and negligible concentration for  $1\ \mu\text{m}$  particles.

The Dean forces coupled with shear induced inertial forces have been used by Seo et al., (2007a) and Di Carlo et al., (2007) to demonstrate particle separation. Seo et al., (2007b) used an S shaped segment in the centre of spiral microchannels to demonstrate the principle. The particles were focussed in

equilibrium positions, channel periphery, due to inertial forces and Dean forces reduces the equilibrium position to just one. The design was used to separate 3  $\mu\text{m}$ , 6  $\mu\text{m}$  and 10  $\mu\text{m}$  polystyrene beads. A 9.3 times concentration was achieved for 6  $\mu\text{m}$  beads and 1.4 times concentration for 3  $\mu\text{m}$  beads.

Di Carlo et al., (2007, 2008) used asymmetric serpentine channel geometry to separate 2  $\mu\text{m}$  and 10  $\mu\text{m}$  particles. They observed that particles with  $D_p/D_h > 0.07$  tend to occupy a single equilibrium position. They used this principle to focus 10  $\mu\text{m}$  particles along the microchannel wall whereas, the 2  $\mu\text{m}$  particles remained dispersed across the entire length of the microchannel.

Bhagat et al., (2008) demonstrated the use of 5 loop spiral microfluidic device for separation of 3  $\mu\text{m}$  and 7  $\mu\text{m}$  polystyrene beads. They concluded that Dean forces dominate over lift forces in case of 2  $\mu\text{m}$  particles and vice versa in case of 7  $\mu\text{m}$  particles. Later in 2009, Kuntaegowdanahalli et al., used spiral microchannels to achieve continuous separation of 10  $\mu\text{m}$ , 15  $\mu\text{m}$  and 20  $\mu\text{m}$  polystyrene beads. The inertial microfluidic device exhibited a separation efficiency of 90%. They further used the device to separate neuroblastoma and glioma cells with 80% efficiency.

Inertial lift forces have also been used to successfully separate bacteria (*E. coli*) from human blood cells (Wu et al., 2009). To generate a soft inertial force on the fluid, the device relied on three inlets one each for sample, acting flow and protecting sheath flow. The asymmetric sheath flow forces the large particles away from the original flow streamline whereas the smaller particles stay near the streamline. The separation is size based and is influenced by parameters like curved and focussed sample flow segments and Reynolds number (Wu et al., 2009).

### 4.3 Experimental Details

The spiral was fabricated using soft lithography in polydimethylsiloxane (PDMS). Approximately 4 mL of SU-8 2025 was dispensed onto the substrate directly from the bottle. The substrate was spun at a speed of 2000 rpm for 30 seconds. The substrate was then soft baked for 30 minutes on a hot plate at 100°C and allowed to cool to room temperature. A mask aligner (MA 6, Suss Microtech) was used for UV exposure of 65 seconds. The exposed substrate was then baked for one minute at 100°C before developing.

The substrate was developed in EC solvent (Dow Chemicals) for five minutes. After development, the wafer was rinsed with IPA and RO water and then blown dry. The width and height of the channel were measured using Dektak 6M Veeco profilometer (software version 8.30.005). The master was silanized with trichloro(1H,1H,2H,2H-perfluorooctyl)silane (Sigma Aldrich) for 45 minutes to yield a hydrophobic surface to aid the release of master from PDMS. PDMS (Sylgard 184, Dow Corning) was prepared by mixing the polymer and the curing agent in a ratio of 10:1, poured on to the master, degassed in a vacuum chamber for 45 minutes and then cured in a 90 °C oven for one hour.

The PDMS was then carefully peeled off the master and cut with a scalpel. The fluid inlet and outlet were drilled on to a glass slides (VWR) for tube connections. The glass slide and the PDMS structures were treated with oxygen plasma (100 W) for 2 minutes before irreversible bonding.

The fabricated spiral consisted of 5 loops with two inlets and two outlets. The radius of the spiral was 75 mm and the total length of the spiral was 15 cm. with channel width and height 500  $\mu\text{m}$  and 40  $\mu\text{m}$  respectively. The spacing between channels was fixed to 500  $\mu\text{m}$  (Figure 4.2).

A mixture of 5  $\mu\text{m}$  and 10  $\mu\text{m}$  fluorescent polystyrene beads were initially used to demonstrate the separation. Later whole blood and whole blood spiked with *Trypanosoma cyclops* was used to demonstrate cell separations. Prior to use, whole blood was stored at 4 °C and diluted 50X in PBS. *T. cyclops* were cultured in Cunningham's medium in a 25 cm<sup>2</sup> tissue culture flask (Corning) and maintained at 27 °C and were diluted 50X in Cunningham's medium prior to their

use. *T. cyclops* were used as a surrogate for *T. brucei* due to regulatory safety rules, but are still useful to demonstrate the separation.

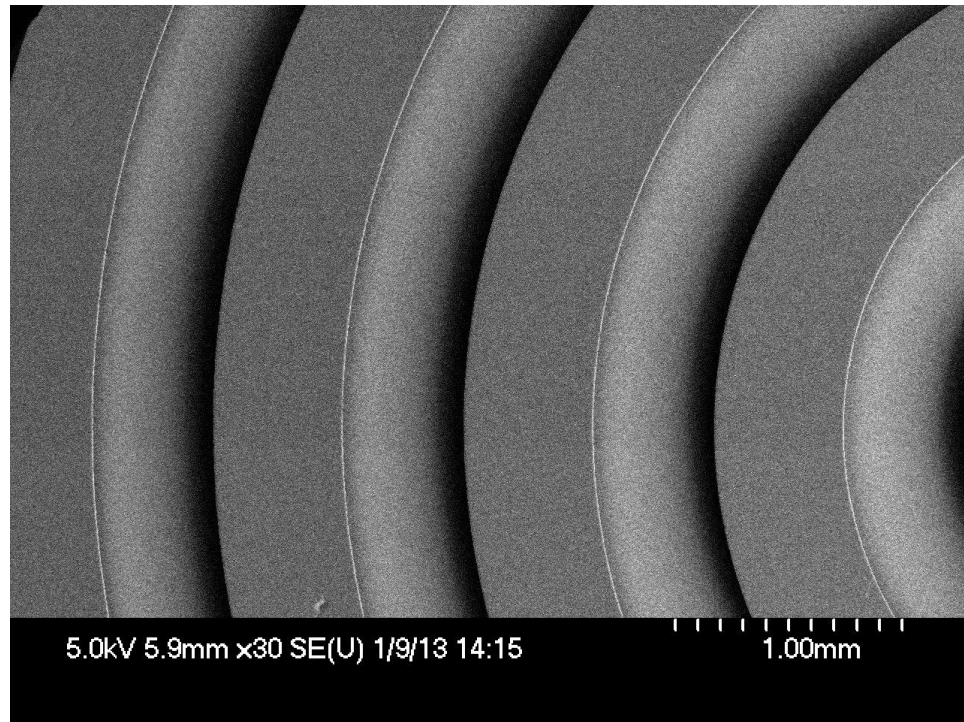


Figure 4.2: SEM image of the 5 loop spiral device. The design consists of two inlets and two outlets. The sample was introduced through the inner inlet. The spiral microchannel is 500  $\mu\text{m}$  wide and 40  $\mu\text{m}$  high. The picture was taken using Hitachi S-4700 operating at 5kV.

#### 4.4 Results and Discussion

The particle stream was injected into the spiral and the separation occurs based on particle mass. In spiral microchannels, the particles experience centrifugal acceleration which causes the particles to move towards the outer channel wall based on their size. The centrifugal forces also cause the particles to move across the width of the microchannel - in transverse direction. The magnitude of these opposing forces depends on the particle size and particle to channel dimension ratio ( $D_p/D_h$ ) causing the formation of streams according to the particle sizes. These particles can be collected individually at their respective outlets.

To achieve separation between the 5  $\mu\text{m}$  and 10  $\mu\text{m}$  polystyrene beads, a 5-loop spiral geometry with two inlets and two bifurcating outlets was fabricated.

Figure 4.3 illustrates the fabricated spiral microchannel. The microchannels were 500  $\mu\text{m}$  wide and 40  $\mu\text{m}$  high ( $D_h = 74 \mu\text{m}$ ) with 500  $\mu\text{m}$  spacing between two successive loops and a radius of curvature of 1 cm. The microchannel cross-section was designed such that the  $D_p/D_h$  criterion was satisfied for 10  $\mu\text{m}$  diameter particles ( $\sim 0.13$ ) but not for 5  $\mu\text{m}$  diameter particles ( $\sim 0.06$ ). The total length of the microchannel was  $\sim 15$  cm (Figure 4.2).

The equilibrating effect of counter acting inertial lift forces and Dean drag forces was exploited to focus 5  $\mu\text{m}$  and 10  $\mu\text{m}$  polystyrene beads in spiral microchannels. The flow rate of  $15 \mu\text{L min}^{-1}$  was used to achieve separation. The 5  $\mu\text{m}$  beads were focussed towards the centre of the microchannel whereas the 10  $\mu\text{m}$  beads were focussed along the inner channel wall (Figure 4.3). Further increasing the flow rate led to defocusing of the beads as a result of Dean drag forces dominating the inertial lift forces. Similar observations have been reported by Di Carlo et al., 2008 and Kuntaegowdanahalli et al., 2009.

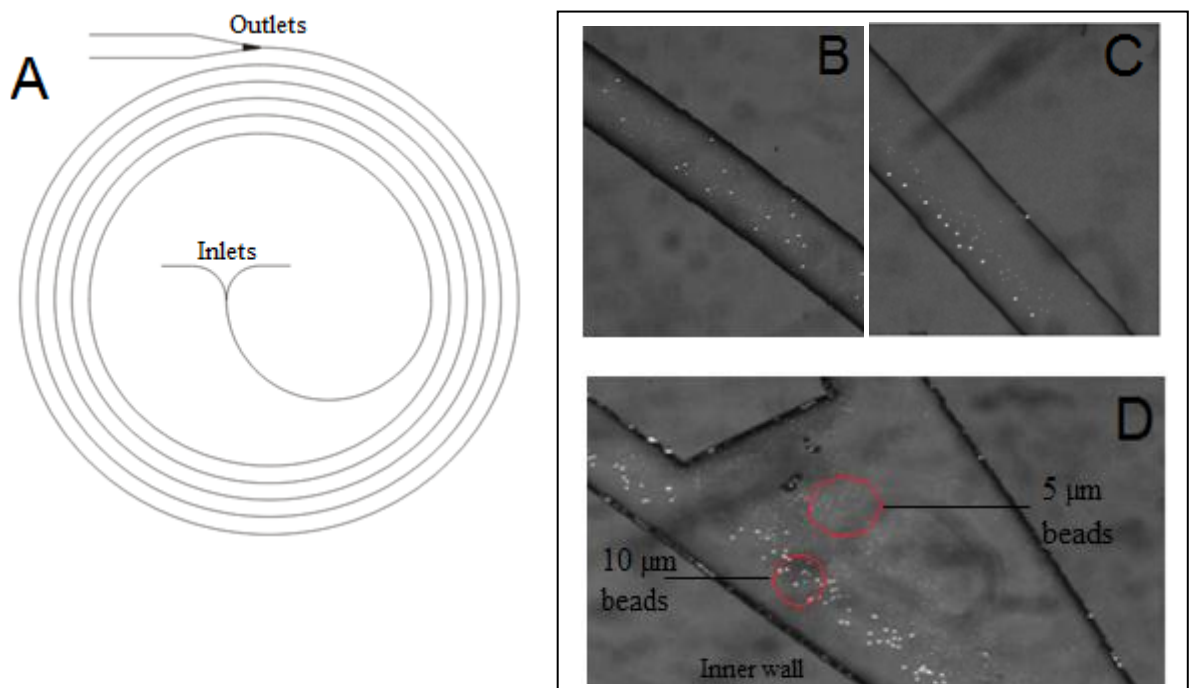


Figure 4.3: (A) Schematic of the 5-loop spiral with two inlets and two outlets. The device was fabricated in PDMS using soft lithography. (B) Picture of the first loop of the spiral with 5  $\mu\text{m}$  and 10  $\mu\text{m}$  polystyrene beads. (C) Picture of the 5<sup>th</sup> loop of the spiral. The 10  $\mu\text{m}$  beads are focussed along the inner wall whereas 5  $\mu\text{m}$  beads are focussed towards the centre of the channel. (D) Picture of the separation at the outlet.

Figure 4.4 gives the distribution of 5 and 10  $\mu\text{m}$  particles at  $De = 0.06$ . The 10  $\mu\text{m}$  particles were collected from the inner outlet with an efficiency of 78%. The 5  $\mu\text{m}$  particles were weakly focussed along the outer channel wall with a separation efficiency of 60%. The output samples were collected separately and analysed by haemocytometry.

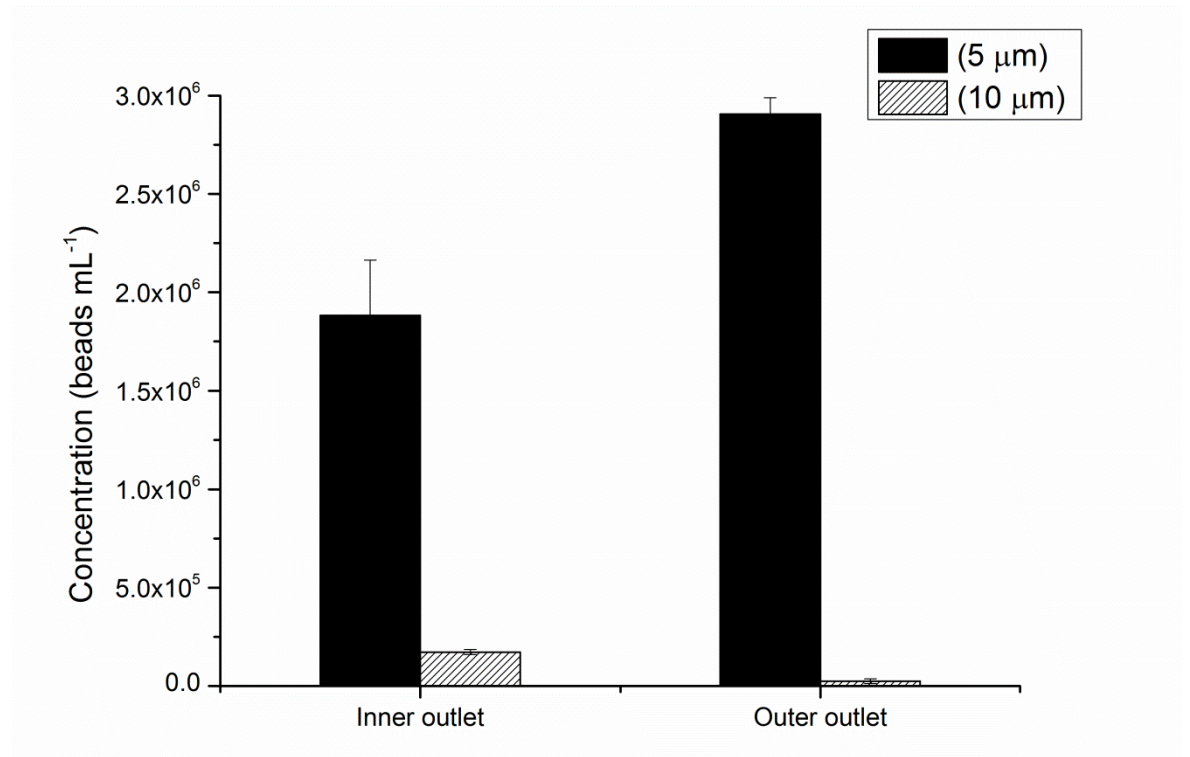


Figure 4.4: Distribution of 5  $\mu\text{m}$  and 10  $\mu\text{m}$  particles in the inner (outlet 1) and outer (outlet 2) outlets of the spiral device. The separation was achieved at a flow rate of 15  $\mu\text{L min}^{-1}$  and  $De = 0.06$ . The error bars represent the standard deviation ( $n = 3$ ). The initial concentration of 5  $\mu\text{m}$  and 10  $\mu\text{m}$  beads was  $5.2 \times 10^6$  and  $2.2 \times 10^5$   $\text{mL}^{-1}$  respectively.

To further demonstrate the separation capability of the device, the same design was used to separate blood cells and plasma. The blood was diluted 50 times in PBS before being introduced into the device. Figure 4.5 shows the microscopic images of blood cells and plasma separation. For flow rates of 15  $\mu\text{L min}^{-1}$ , the blood cells focussed along the inner channel wall whereas the plasma was collected from the outer outlet. 77% of the blood cells were collected in the inner outlet and 21% at the outer outlet (Figure 4.6). The output samples were collected separately and analysed by haemocytometry.

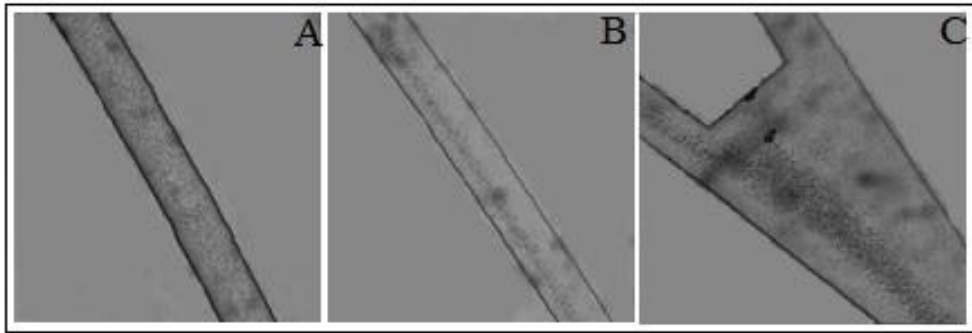


Figure 4.5: (A) Picture of 1<sup>st</sup> loop of the device with unsorted whole blood. (B) Picture of the 5<sup>th</sup> loop. The blood cells focus along the inner wall whereas the plasma is focussed along the out wall. (C) Picture of the outlet showing separation of blood cells and plasma into inner and out outlets respectively. Pictures were cleaned digitally using GIMP to remove dust and adjust orientation.

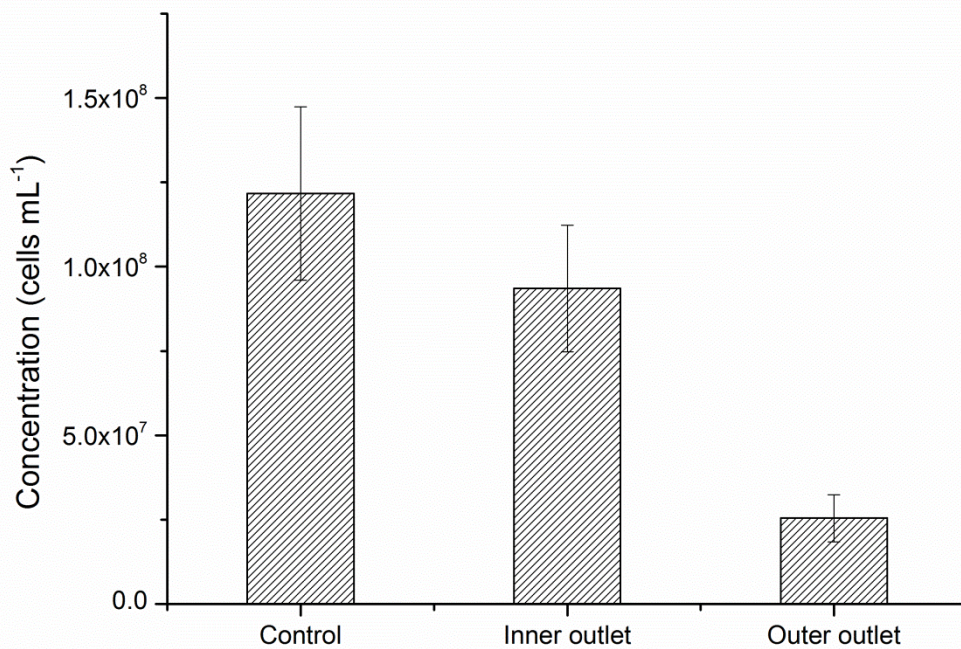


Figure 4.6: Distribution of blood cells and plasma in the inner and outer outlets of the spiral device. The blood cells were collected mainly from the inner outlet (outlet 1) where as the plasma was collected from the outer outlet (outlet 2). The separation was achieved at a flow rate of  $15 \mu\text{L min}^{-1}$  and  $De = 0.06$ . The error bars represent the standard deviation ( $n = 3$ ). Control is the input ( $50\text{X}$  diluted blood with a concentration of  $1.2 \times 10^8 \text{ cells mL}^{-1}$ ) and cells collected from outlets are the output.

It was observed that the spiral channels do not work efficiently with concentrated cell solutions (whole blood). The device works better with low cell concentrations. Using higher cell concentration leads to clogging and disrupted flow inside the microchannels. Finally, whole blood spiked with  $10^5$  trypanosomes  $\text{mL}^{-1}$  and diluted 50 times in PBS was introduced into the device. No significant separation of trypanosomes and blood cells was observed using the spiral microchannels.

#### **4.5 Conclusion**

A microfluidic device with spiral geometry that takes the advantage of the combination of Dean forces and inertial forces was described in this chapter. The device was successfully used to demonstrate the separation of microparticles and blood cells from plasma. The enrichment of trypanosomes from infected blood was inefficient though. The next chapter describes the fabrication of a microfluidic device that exploits inertial migration to achieve particle separation.

## Chapter 5 - Inertial Microfluidics

### 5.1 Introduction

Inertial lift forces have been used quite extensively in microfluidics (Di Carlo, 2007; Seo et al., 2007a), albeit only with a few commercial applications. In a parabolic flow profile, both normal and shear stress forces act on the particles yielding drag and lift forces that are parallel and perpendicular to the direction of main flow respectively. The drag forces are responsible for particle acceleration whereas the shear forces are responsible for their lateral displacement. The shear induced lift forces direct the suspended particles away from the centre whereas the walls of the channel exert a lift force “wall effect” on the particles directing them away from the wall. The net force equilibrates the particles into focussed streams based on their size (Di Carlo, 2009).

The magnitude and direction of these forces is determined by particle size and position across the microchannel cross-section. The lift forces dominate if the particles have  $D_p/D_h \geq 0.07$  (where,  $D_p$  is the particle diameter and  $D_h$  is the microchannel hydraulic diameter, Bhagat et al., 2008), and are responsible for the equilibration of the particles within the channels. In a rectangular microchannel, particle equilibration does not depend on the hydraulic diameter but instead depends on the shortest channel dimension (microchannel height) due to varying shear rates across the channel cross-section (Bhagat et al., 2009).

The effect of inertial forces on particle migration was first reported by Segré and Silberberg (1962). In their experiment, they studied the behaviour of neutrally buoyant particles with a finite Reynolds number in cylindrical channels. They concluded that in a tube, neutrally buoyant particles equilibrate at a radial position of  $0.6 r$  from the centreline of the microchannel (where  $r$  is the radius of the channel, Segré and Silberberg, 1962a). This equilibrium shifts more towards the wall with increasing Reynolds number ( $Re$ ) (Asmolov, 1999).

In a microchannel with finite length, the particles focus along the channel walls at equilibration given  $D_p/D_h \geq 0.07$  (Segré and Silberberg, 1962a, b; Di Carlo et al., 2007). At low  $Re$  ( $<100$ ), the shear gradient is uniform on all sides of a square microchannel and hence leads to eight equilibrium positions. As the  $Re$  increases to 500, the equilibrium positions are reduced to four (four corners of

the channel, Figure 5.1, Chun and Lad, 2006). In channels with high  $AR$ , the particles focus along the longer channel dimension as a result of the shear rate modulation (Bhagat et al., 2009).

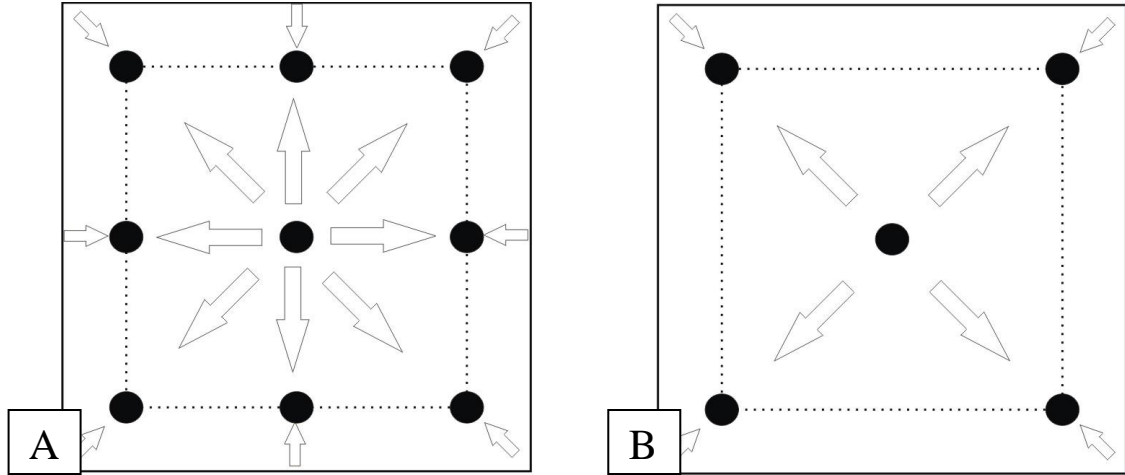


Figure 5.1: Inertial migration of particles in a square microchannel for  $Re < 100$  (A) and  $Re \geq 500$  (B).

An efficient particle equilibration along the sidewalls of channels can be achieved in a straight microchannel without any contraction-expansion array (Figure 5.2). (Bhagat et al., 2009). However, the contraction-expansion arrays have been shown to enhance the particle separation by preferentially focusing the particles along the channel walls. (Park et al., 2009). When a particle enters the expanded region from contracted region, the distance of the particles from the channel walls increases, causing shear induced lift forces to push the particles away from the centre. The combination of shear induced lift forces produced by high aspect ratio and contraction-expansion regions enhances the efficiency of the microparticle separation (Bhagat et al., 2011).

The lift and drag forces acting on particles in a flow can be obtained using Navier-Stokes equation (Di Carlo, 2009), also shown as Equation 3.6

$$\rho \left( \frac{\partial u}{\partial t} + u \cdot \nabla u \right) = -\nabla p + \mu \nabla^2 u + f \quad (5.1)$$

Where  $\rho$  is the fluid density,  $u$  is the velocity field of fluid,  $p$  pressure field and  $f$  is the external forces vector field. Viscous drag force and the net lift forces are the two critical forces involved in migration of particles in the device channels. The drag force ( $F_D$ ), a function of particle size and flow velocity, can be estimated as

$$F_D = 3\pi\mu D_p U_F \quad (5.2)$$

Where  $\mu$  is the fluid viscosity,  $D_p$  is the diameter of the particle and  $U_F$  is the flow velocity (Asmalov, 1999). The lift forces ( $F_L$ ) can be predicted as

$$F_L = \rho G^2 C_L D_p^4 \quad (5.3)$$

Where  $\rho$  is density of the fluid,  $G$  is the fluid shear rate,  $C_L$  is the lift coefficient. Lift coefficient is a dimensionless quantity and is a function of Reynolds number and cross-sectional position of the particle in the microchannel. The average value of  $C_L$  can be assumed to be -0.5 for flows with  $Re$  less than 100 (Di Carlo, 2009). The fluid shear rate  $G$  is can be calculated using the following equation.

$$G = 2 U_F / D_R \quad (5.4)$$

The flow velocity needed for a particle to focus in a channel can be determined using particle Reynolds number ( $Re_p$ ), a dimensionless parameter related to  $Re$  by ratio of particle to channel length (Bhagat et al., 2011; Di Carlo, 2009).

$$Re_p = Re(D_p/L_c)^2 \quad (5.5)$$

Where  $D_p$  is the particle diameter and  $L_c$  is the characteristic length. Particle migration is faster in flows with higher particle  $Re$  (Bhagat et al., 2011).

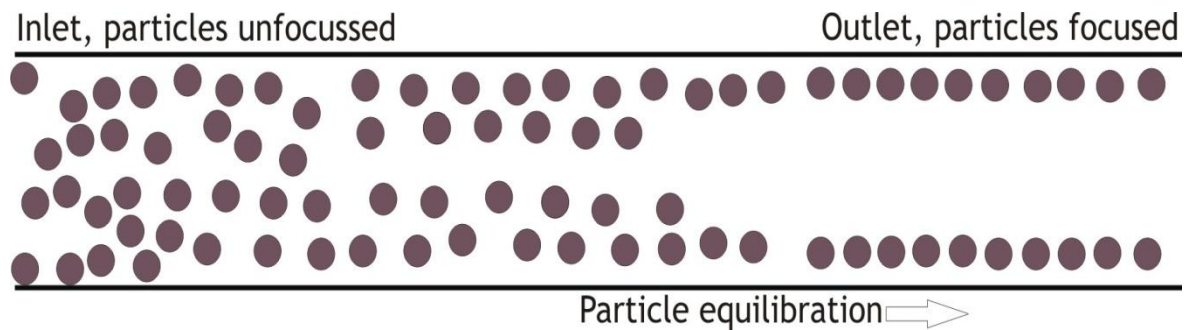


Figure 5.2: Schematic of a rectangular microchannel showing the equilibration of the particles. The particles are randomly distributed at the inlet and align along the channel walls as they reach the outlet.

Inside the microchannels, the particles attain equilibrium under the influence of only viscous drag and inertial lift forces irrespective of channel length. From Equations 5.2 and 5.3, it can be interpreted that the lift ( $F_L$ ) and drag forces ( $F_D$ ) depend on the particle size ( $D_p$ ) with the lift forces increasing more rapidly compared to the drag force for increasing particle size. Thus, particle separation can be achieved by varying these two forces. As shown by recent studies, for  $D_p/D_h \geq 0.07$ , the inertial lift forces dominate and result in particle equilibration within a short channel length (Di Carlo et al., 2007; Bhagat et al., 2008).

The shear rate is higher along the width of the channels, forcing the cells to focus along the channel height. When *Trypanosoma* spiked blood was injected into the device, the cells were initially dispersed near the inlet but as they travel along the channel the shear rate modulation causes the cells to align in two streams along the walls leaving the trypanosomes in the centre of the channel.

To separate the blood cells and trypanosomes, it is critical that the blood cells should be tightly focussed along the channel walls. The width of the channel is critical when using a high aspect ratio device for focussing cells (Bhagat et al., 2009). During the experiments, the width of the pinched units was considered to be critical and was fixed to 10, 15, 20 and 30  $\mu\text{m}$ , in a series of flow experiments.

## 5.2 Background

Inertial microfluidics has been mostly used to separate microparticles. Di Carlo et al., (2007) used inertial migration to separate 2 - 17  $\mu\text{m}$  particles in channels with asymmetric geometry. They reported the mass sorting rate of  $1 \text{ g hr}^{-1}$  for 1% particle solution (2  $\mu\text{m}$  and 10  $\mu\text{m}$ ) at a flow rate of  $1.5 \text{ mL min}^{-1}$ . By tuning the channel geometry they were also able to separate 4  $\mu\text{m}$  and 7  $\mu\text{m}$  particles although at a lower throughput. Di Carlo et al., (2008) used the same principle to achieve 90 - 100% separation of rigid particles, emulsion and platelets from diluted blood at a throughput of  $1 \text{ mL min}^{-1}$ .

Bhagat et al., (2009) used both square and rectangular microchannels to show inertial migration of particles. They concluded that the cross-section of the channel is critical for particle equilibration rather than the hydraulic diameter. At  $Re = 20$  flow, they showed complete separation of 2  $\mu\text{m}$  and 590 nm particles.

Wu et al., (2009) used inertial force induced migration to separate *E. coli* from erythrocytes using a flow rate of  $18 \mu\text{L min}^{-1}$ . The sample used a high cell concentration ( $> 10^8 \text{ cells mL}^{-1}$ ) and a 300 fold enrichment of bacteria was reported.

Bhagat et al., 2010 further developed inertial force induced particle migration to enrich circulating tumour cells from blood. They demonstrated that flowing MCF-7 spiked blood (diluted to 2% haematocrit) through the microchannels at  $400 \mu\text{L min}^{-1}$  led to recovery of more than 80% of the tumour cells. The device was capable of processing  $10^8 \text{ cells min}^{-1}$ , translating to processing time of ~50 minutes for 1 mL whole blood.

## 5.3 Experimental Details

### 5.3.1 Device Design

Masks were designed using L-Edit v14.1 (Tanner EDA Software). The inertial migration designs used for separation of trypanosomes from blood cells are based on published work by Bhagat et al., 2011. The device geometry is illustrated in Figure 5.3. The device consisted of one inlet and three (one central and two outer) outlets. The devices were fabricated in PDMS using soft lithography. It consisted of 1.5 cm long rectangular contraction-expansion array

that opens into a 300  $\mu\text{m}$  wide rectangular block before bifurcating into centre and side outlets each 100  $\mu\text{m}$  wide (Figure 5.4). The channel is divided into 75 alternating pinched and expanded regions (Figure 5.5). Each subunit has a pair of contraction-expansion region, the length of each region being 100  $\mu\text{m}$ . The width fixed at 90  $\mu\text{m}$  for expanded regions and 30  $\mu\text{m}$  for the first 70 contraction region and 10  $\mu\text{m}$  for the last five.

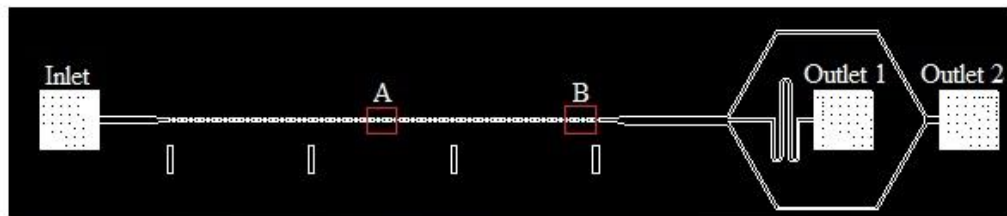


Figure 5.3: Schematic of the inertial microfluidic device for separating trypanosomes from infected blood. The device has one inlet and two outlets. The channel has 75 alternating pinched and expanded units. The length of each unit is 100  $\mu\text{m}$  and the width of the expanded units is 60  $\mu\text{m}$ . The total length of the channel is 1.5 cm.

Approximately 4 mL of SU-8 3050 was dispensed onto the substrate directly from the bottle. The substrate was spun at a speed at 1000 rpm for 30 seconds. The substrate was then soft baked for 30 minutes on a hot plate at 100  $^{\circ}\text{C}$  and allowed to cool to room temperature. A mask aligner (MA 6, Suss Microtech) was used for UV exposure 65 seconds. The exposed substrate was then baked for one minute at 100  $^{\circ}\text{C}$  before developing.

The substrate was developed in EC solvent (Dow Chemicals) for ten minutes. After development, the wafer was rinsed with IPA and RO water and then blown dry. The width and height of the channel were measured using Dektak 6M Veeco profilometer (software version 8.30.005). The depth was measured to be 50  $\mu\text{m}$  (aspect ratio of 2.5). The master was silanized with trichloro(1H,1H,2H,2H-perfluorooctyl)silane (Sigma Aldrich) for 45 minutes to yield a hydrophobic surface to aid the release of master from PDMS. PDMS (Sylgard 184, Dow Corning) was prepared by mixing the polymer and the curing agent in a ratio of

10:1, poured on to the master, degassed in a vacuum chamber for 45 minutes and then cured in a 90 °C oven for one hour.

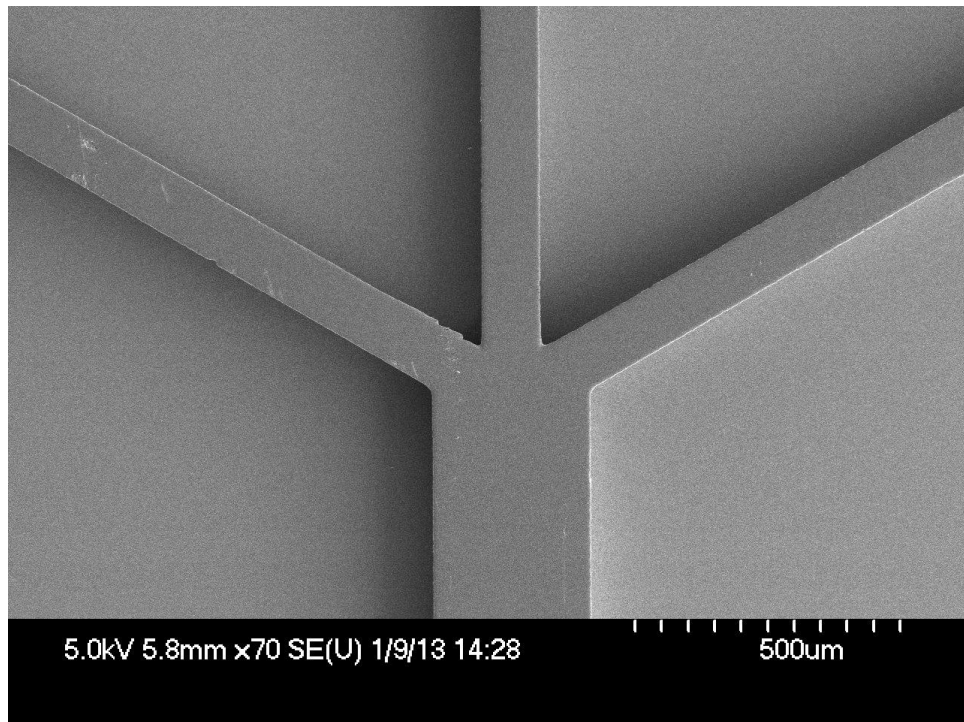


Figure 5.4: SEM of the channel outlets. The device has one central outlet for collection of trypanosomes and two outer outlets for the collection of blood cells. Each outlet is 100  $\mu\text{m}$  wide. The picture was taken using Hitachi S-4700 operating at 5kV.

The PDMS was then carefully peeled off the master and cut with a scalpel. The fluid inlet and outlet were drilled on to a glass slide (VWR) for tube connections. The glass slide and the PDMS structures were treated with oxygen plasma (100 W) for 2 minutes before irreversible bonding.

They consist of a high aspect ratio 1.5 cm long rectangular contraction-expansion array that opens into a 300  $\mu\text{m}$  wide rectangular block before bifurcating into centre and side outlets each 100  $\mu\text{m}$  wide (Figure 5.3). The channel is divided into 75 alternating pinched and expanded regions. Each subunit has a pair of contraction-expansion region, the length of each being 100  $\mu\text{m}$ . The width was varied between 60 and 90  $\mu\text{m}$  for expanded regions and 20 and 30  $\mu\text{m}$  for the contraction region.

Later the channel design was modified to include five pinched segments at the end to further enhance the enrichment capability of the device. Whilst the width of the first 70 pinched units is 20  $\mu\text{m}$ , the last five pinched units are 10  $\mu\text{m}$

wide. This was done so that the unfocussed parasites would be collected from the centre outlet and the blood cells from the outer outlet.

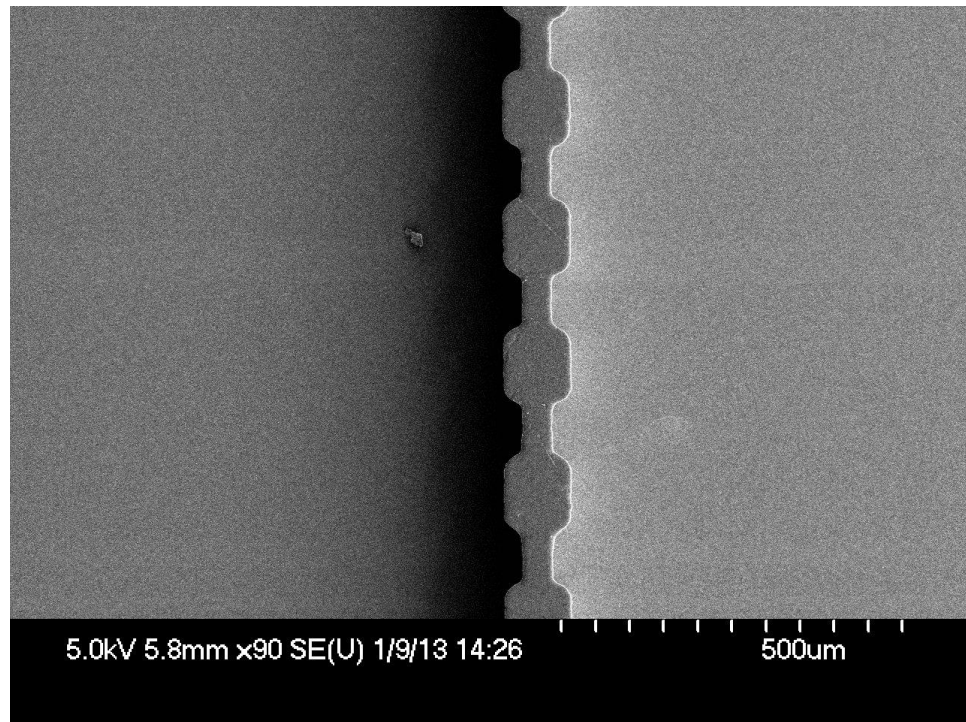


Figure 5.5: SEM of the expansion-contraction regions of the channel. The expansion regions are 100  $\mu\text{m}$  long and 90  $\mu\text{m}$  wide. The contraction regions are 100  $\mu\text{m}$  long and 30  $\mu\text{m}$  wide. The height of the channel is 50  $\mu\text{m}$ . The picture was taken using Hitachi S-4700 operating at 5kV.

### 5.3.2 Device Characterization

The device was mounted on a Zeiss Axio Imager A1 microscope. The sample was injected into the device through a syringe. The flow rates were varied between 50 - 500  $\mu\text{L min}^{-1}$  using a syringe pump (New Era). The separation was viewed and captured using Photran SA-1 fastcam and Vision Research Phantom Miro M310 fastcam. Frame rates between 10,000 - 54,000 per second were used to capture and analyse the data. The samples were collected from the outlets and analyzed using a haemocytometer (Neubauer).

### 5.3.3 Cultivation of Trypanosomes

*T. cyclops* were cultured in Cunningham's medium supplemented with 20% FBS and maintained at 27 °C. *T. cyclops* were passaged once a week and were grown to a density of  $2 \times 10^6 \text{ mL}^{-1}$ .

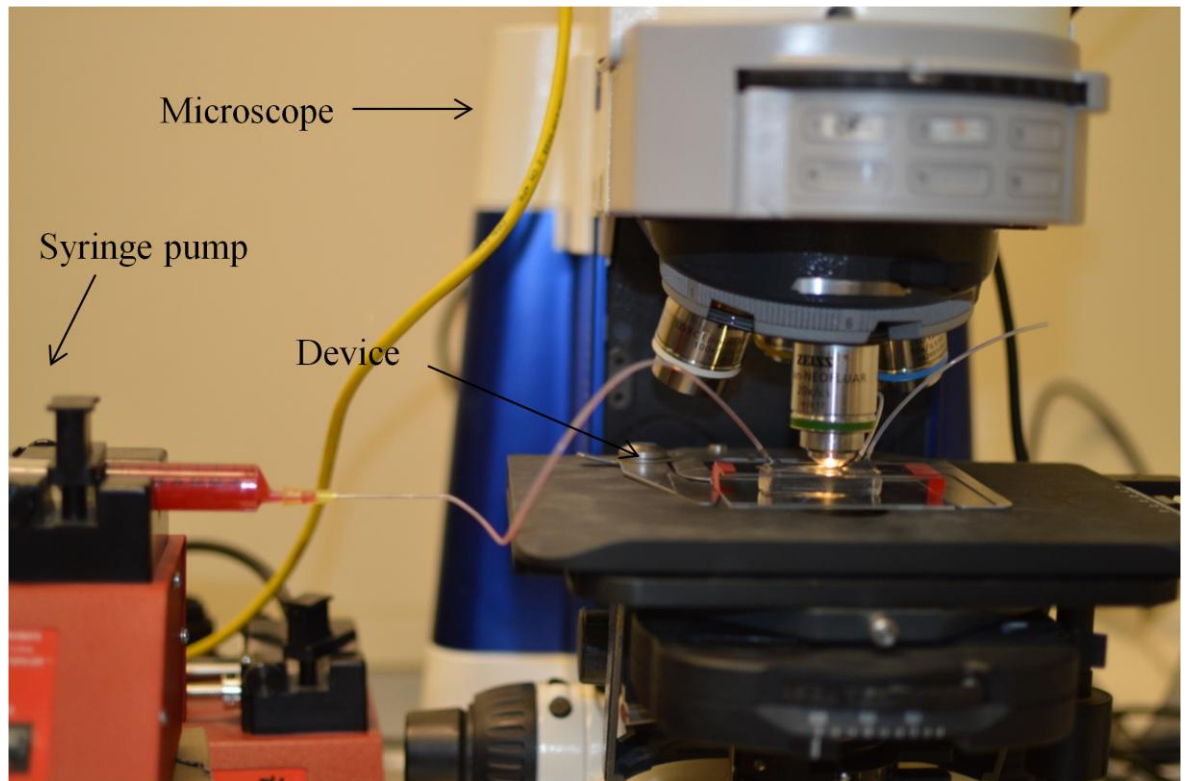


Figure 5.6: Picture of the experimental setup showing the microscope, syringe pump and the microfluidic device.

## 5.4 Results and Discussion

As discussed earlier, blood is a complex non-Newtonian fluid with erythrocytes or red blood cells accounting for 99% of the haematocrit (Bhagat et al., 2011). Trypanosomes are 20-30  $\mu\text{m}$  long and  $\sim 3 \mu\text{m}$  wide (Barrett et al., 2003), Red blood cells on the other hand are discoid bodies with a diameter of 8  $\mu\text{m}$  (Vona et al., 2000). For calculating the  $Re$ , the density and viscosity used for blood was  $1060 \text{ Kg m}^{-3}$  (Cutnell and Johnson, 2009) and  $0.0035 \text{ Pa}\cdot\text{s}$  (Olgac et al., 2008) respectively.

High aspect ratio ( $AR = 2.5$ ) rectangular microchannels  $100 \times 50 \mu\text{m}^2$  ( $D_h = 67$ ) (Figure 5.7) were used to enrich trypanosomes in the blood. The high AR meant that the particles preferentially focused along the height rather than the width of the channel as the lift forces acting along the width are larger than those acting along the height (Bhagat et al., 2009). The device was tested at flow rates  $100 - 500 \mu\text{l min}^{-1}$  ( $Re$  10 - 54). The cell size to critical channel dimension

(which in this case is the smallest channel dimension  $D_p/L_c$ ) was 0.12 for the red blood cells and 0.06 for the trypanosomes. For particles to migrate inside the microchannel,  $D_p/L_c$  should be greater than 0.07 (Serge and Silberberg, 1962; Di Carlo et al, 2007).

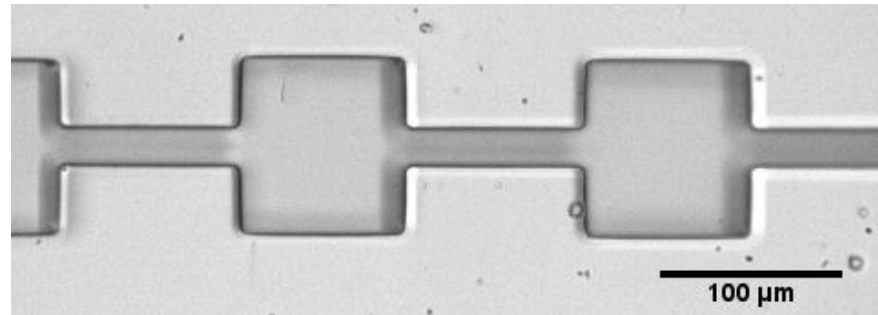


Figure 5.7: Picture of the PDMS microchannel. The length and height of each unit is 100 and 50  $\mu\text{m}$  respectively.

At the inlet, the cells were randomly distributed for each flow rate used. For flow rate  $100 \mu\text{l min}^{-1}$ , the particles remained randomly distributed throughout the channel, indicating no migration (Figure 5.8B). At  $200 \mu\text{l min}^{-1}$ , the cells started to loosely focus along the cell walls (Figure 5.8C). For flow rate  $300 \mu\text{l min}^{-1}$ , the cells focused more tightly along the microchannel walls (Figure 5.8D) compared to  $100$  and  $200 \mu\text{l min}^{-1}$ , indicating cell migration.

The best particle migration was achieved at  $400 \mu\text{l min}^{-1}$  as the increasing the  $Re$  increased the lift forces that allowed the blood cells to overcome the viscous drag equilibrating along the channel walls at a distance of  $0.2L_c$  from the walls (Figure 5.8E). Table 5.1 summarizes the  $Re$  and  $Re_p$  for red blood cells and trypanosomes for each flow rate used.

Further increasing the flow rate to  $500 \mu\text{l min}^{-1}$ , indicated no particle migration as the particles did not focus along the channel walls. Flow rates higher than  $500 \mu\text{l min}^{-1}$  could not be tested as the devices were unable to withstand the pressure and failed mainly near the inlet.

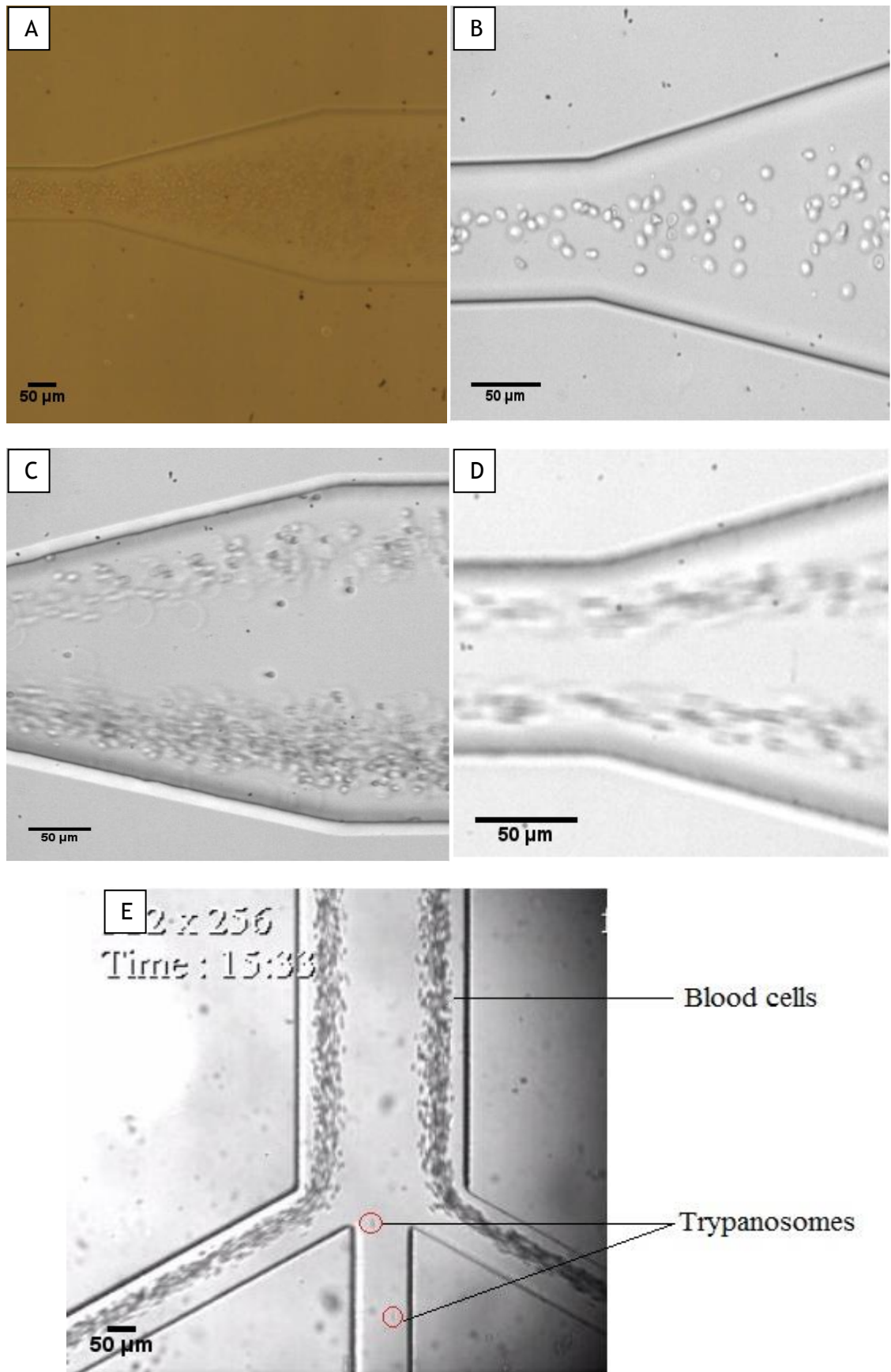


Figure 5.8: Pictures of *Trypanosoma cyclops* spiked blood in various flow conditions inside the microfluidic device. (A) No flow (B) 100 μL min<sup>-1</sup> (C) 200 μL min<sup>-1</sup> (D) 300 μL min<sup>-1</sup>, and (E) 400 μL min<sup>-1</sup>. These pictures have been extracted from videos. A, B, C and D are the pictures of broadened segment that leads to the outlets and E is the picture of the broadened segments with the three outlets.

Flow Rate ( $\text{min}^{-1}$ )	Reynolds number ( $Re$ )	Particle Reynolds number ( $Re_p$ ) RBC	Particle Reynolds number ( $Re_p$ ) trypanosomes
100	10.12	1.62	0.40
200	20.18	3.23	0.81
300	30.28	4.85	1.21
400	40.40	6.45	1.62
500	53.79	8.60	2.15

Table 5.1: List of Reynolds numbers and particles Reynolds numbers associated with different flow rates.

Whole blood spiked with *Trypanosoma cyclops* was used for the experiments after establishing the optimal conditions. *T. cyclops* ( $1 \times 10^5 \text{ mL}^{-1}$ ) spiked blood was diluted 20 times in PBS before being injected into the device at a flow rate of  $400 \mu\text{L min}^{-1}$  ( $Re = 40.40$ ). The width of the pinched region was fixed to  $20 \mu\text{m}$ . The device had two side outlets for collection of blood cells and one centre outlet for collection of trypanosomes. The trypanosomes were counted using a Neubauer haemocytometer.

The required limit of detection is 1 parasite in a  $1 \mu\text{L}$  drop of blood, which contains 1 million red blood cells (a detection sensitivity equivalent to 1 in  $10^6$ ). Figure 5.9 indicates that at outlet 1, there are 10 trypanosomes per every blood cell counted. In experiments conducted with *T. cyclops* spiked blood,  $\sim 99\%$  of the blood cells were removed facilitating the use of haemocytometry for the detection of the parasites. A single device can process  $\sim 10^8$  cells per minute at a flow rate of  $400 \mu\text{L min}^{-1}$ , that is,  $\sim 50$  minutes to process a mL of whole blood.

A small number of blood cells were also collected from the centre outlet along with the parasites. To counter this problem and achieve a more efficient enrichment, the devices could in future be multiplexed. The centre outlet from the device one can be connected to the inlet of device two and so on. Multiplexing not only will completely eliminate the presence of the blood cells in the centre outlet but will also reduce the analysis time considerably.

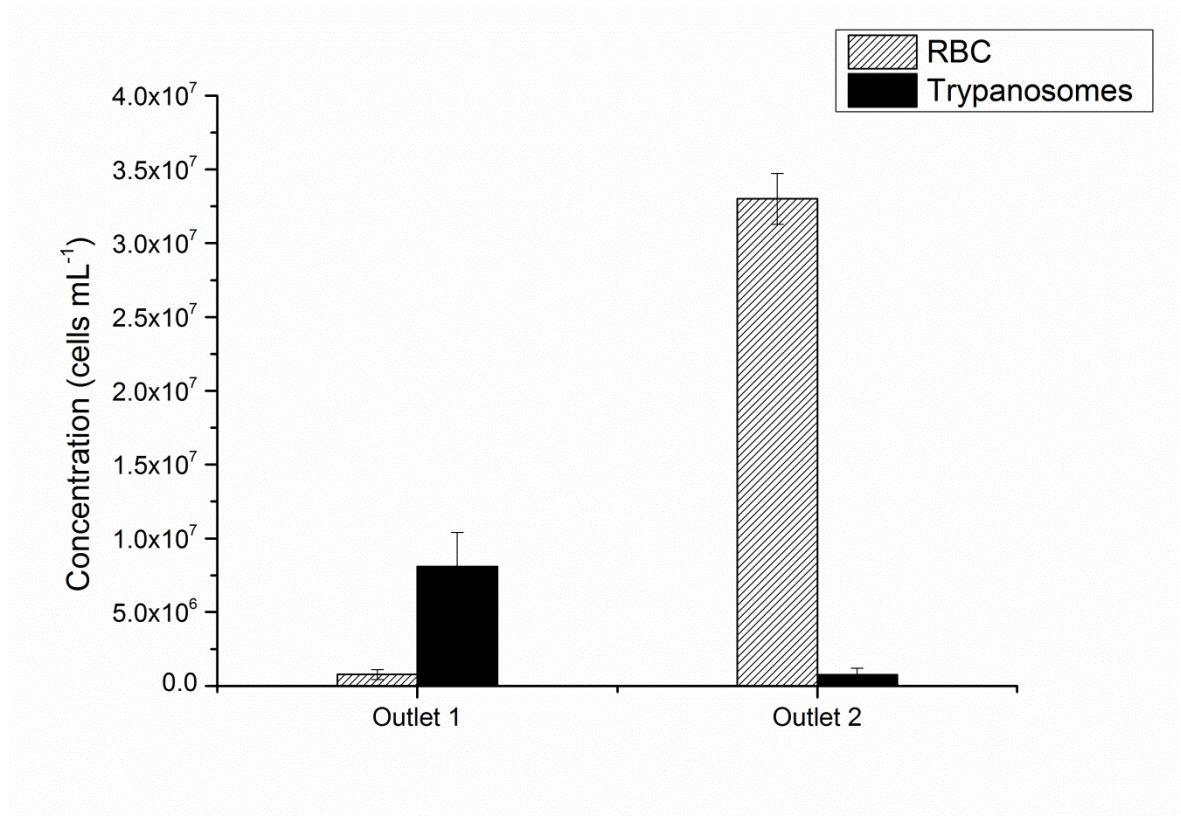


Figure 5.9: The enrichment effect of inertial microfluidics on *Trypanosoma cyclops* spiked blood. The blood was injected in to the device at a flow rate of  $400 \mu\text{L min}^{-1}$ . Trypanosomes were mainly collected at the outlet 1 and the red blood cells at outlet 2. The error bars represent the standard deviation ( $n = 3$ ). The initial concentration of RBCs and trypanosomes was  $2.13 \times 10^7$  and  $1 \times 10^5 \text{ mL}^{-1}$  respectively.

## 5.5 Conclusion

This chapter describes inertial microfluidics separation of the trypanosomes from blood cells using a contraction-expansion array. Inertial migration is a continuous flow separation technique based on preferential migration of microparticles due to shear induced lift forces in channels with high aspect ratio. In experiments conducted with *T. cyclops* spiked blood, ~99% of the blood cells were removed facilitating the use of haemocytometry for the detection of the parasites. Based on the experiments carried out with microfluidics devices (Chapters 3, 4 and 5), it was observed that fundamentally it is difficult to work with the whole blood which causes problems like protein and blood cells deposition on channel walls and clogging.

## Chapter 6 - Density Based Separation of Whole Blood and Enrichment of Trypanosomes

### 6.1 Introduction

The characterization of different cellular components of human whole blood plays an important role in medical diagnoses (Bunn and Aster, 2011). This is often accomplished by isolating or enriching a specific cellular population or sub-population. Whole blood is composed of cells—leukocytes, platelets, and erythrocytes—suspended in protein-rich plasma; each type of cell is useful in the evaluation of the health of a patient. Automated haematology analyzers (e.g., Coulter counters and flow cytometers) are often used to separate and analyze the cellular components of whole blood from plasma (Bunn and Aster, 2011). In settings that do not have access to these instruments (for example, laboratories and clinics in rural or low-resource areas), simpler isolation and quantification methods are required; the isolation of different components of blood based on differences in their density is an attractive and feasible approach. Current density-based techniques, however, can only separate two sub-populations without changing the morphology of cells or resorting to demanding laboratory procedures (Bøyum et al., 1991). In addition, a sub-population of interest (e.g., disease-associated microorganisms or cells) may be very dilute and would be examined more easily through concentration—a capability that current density-based methods lack (Brakke and Daly, 1965).

Aqueous two-phase systems (ATPSs) were used to separate and concentrate the components of blood based on density. ATPSs are immiscible phases consisting of solutions of polymers in a common aqueous medium (Albertsson, 1958). An ATPS generated from a mixture of aqueous solutions of Dextran (a polyglucose) and Ficoll (a polysucrose) was used to separate the cellular components of human whole blood into fractions enriched in different types of cells. The concentration of dilute cells from a three-dimensional suspension to a two-dimensional interface is also described. This localization facilitates the visualization and collection of enriched species after separation.

The major cellular components of whole blood are erythrocytes (red blood cells, or RBCs) ( $\rho = 1.080\text{-}1.095 \text{ g cm}^{-3}$ , Leif and Vinograd, 1964), leukocytes (white blood cells, or WBCs) ( $\rho = 1.050\text{-}1.085 \text{ g cm}^{-3}$ , Shortman et al., 1967), and

platelets (Plts) ( $\rho = 1.062\text{--}1.084 \text{ g cm}^{-3}$ , Corash et al., 1977). WBCs, as a group, include many different types of cells, but can be classified broadly into two groups: mononuclear cells (MNCs) (i.e., lymphocytes and monocytes) and polymorphonuclear cells (PMNs) (i.e., basophils, eosinophils, and neutrophils). Recent advances in the measurement of the density of individual cells demonstrate the importance of the densities of blood cells as measures of health (Grover et al., 2011).

Although the ranges of density of different types of cells overlap, density-based techniques can provide useful separations. The most basic density-based method uses centrifugation through a single medium, which acts as a barrier in density, to separate two sub-populations. Commercially available media with a density of  $1.077 \text{ g cm}^{-1}$  (e.g., Lymphoprep) at physiological osmolarities ( $295 \pm 15 \text{ mOsmkg}^{-1}$ ) are designed to separate MNCs from the other cellular components of whole blood (Bøyum et al., 2002). To resolve more than two sub-populations using a single medium, researchers use hypertonic solutions with higher densities (e.g., Polymorphprep) (Kalmar et al., 1988). The osmotic stress of the hypertonic medium causes RBCs to release water; this release has the dual effect of making these cells denser, and of reducing the local density of the medium. This interplay between tonicity and density allows the separation of three sub-populations: MNCs, PMNs, and RBCs. By design, these media expose blood cells to non-physiological conditions and thus will not preserve cellular morphology, especially in the case of RBCs.

Layered gradients are density—layers comprising different concentrations of solutes in a common solvent (e.g., solutions of Ficoll (Glinski et al., 1976) or bovine serum albumin (Geha et al., 1973) in an aqueous buffer)—can separate more than two populations of blood cells. These gradients in density enable separations by allowing a type of cell with a specific density to sediment to an equilibrium position between regions of higher and lower density. Careful layering is required to prepare clearly defined regions of different density, and the boundaries between these regions broaden over time due to diffusion. As a result, the separation and subsequent collection of species in these media can be difficult. A simple and thermodynamically stable system capable of enriching sub-populations of cells based on their density at physiological conditions would

combine the strengths of existing techniques, and provide a new tool for the fractionation of whole blood and other biological particulates.

Aqueous two-phase systems, ATPSs, are generated from mixtures of immiscible solutions of solutes in water that separate spontaneously into two phases; these phases order, on settling or on centrifugation, according to density (Albertsson, 1958). Each phase of an ATPS consists predominantly (60-95% w/v) of water, and contains concentrations of solutes ranging from 1-40% w/v), and a combination of both solutes. These compositions determine the physical properties of the phases of an ATPS (e.g., density, viscosity and refractive index).

Many ATPSs are biocompatible (Albertsson, 1961) and have been used for relatively low-yield separations of cells (SooHoo and Walker, 2009; Frampton et al., 2011); these separations rely on partitioning cells between the phases of an ATPS—a process driven by the preferential affinity of the surfaces of cells for the components of these phases (Fisher, 1981). Density-based separations, however, offer a new set of applications for ATPSs. The interface between phases in an ATPS marks a discontinuity (on the molecular scale) between regions of different density. The densities ( $\rho_A$  and  $\rho_B$ ) of the phases on either side of the interface establish the range of densities for components ( $\rho_C$ ) that will localize at the interface ( $\rho_A > \rho_C > \rho_B$ ). The interfacial surface energy between the phases of an ATPS is astonishingly low (Hatti-Kaul, 2001) and the cells that pass through the interface when driven by centrifugal forces suffer minimal damage.

## 6.2 Background

The first density based separation of *Trypanosome brucei* was reported by Hirumi et al., in 1977. They used Lymphoprep (density  $1.077 \text{ g ml}^{-1}$ ) to separate trypanosomes from mouse blood by density gradient centrifugation. The infected mouse blood was centrifuged at 350 g for 15 minutes at 4 °C to achieve separation. They also used buffy coat method to do the same and found no significant differences between the two techniques.

De Titto et al., (1981) separated *Trypanosoma cruzi* from human peripheral lymphocytes by density gradient centrifugation. They used continuous and discontinuous gradients of Ficoll-Hypaque (F-H) system to obtain the separation.

Most of the trypanosomes were confined in the region with a density range between 1.051 - 1.057 g ml<sup>-1</sup> whereas the lymphocytes were recovered from the regions with density between 1.046 - 1.080 g ml<sup>-1</sup>. More than 80% trypanosomes were confined in the region with the density of 1.077 g ml<sup>-1</sup>. Further to obtain trypanosome free lymphocytes, a discontinuous F-H system with two layers (densities 1.060 and 1.077 g ml<sup>-1</sup>) was used.

Ogbunude and Magaji (1982) used a silicone fluid (specific gravity 1.075 g cm<sup>-3</sup>) to detect low numbers of *Trypanosoma brucei*, *Trypanosoma gambiense*, *Trypanosoma congolense* and *Trypanosoma vivax* in rat blood. After centrifugation of the sample through the silicone fluid, the trypanosomes remained suspended in the plasma whereas the red blood cells were collected as a pellet. The results were comparable to miniature anion-exchange centrifugation technique and quantitative buffy coat technique.

Schmatz et al., (1983) also reported density based separation of *T. cruzi* using a continuous Hypaque gradient. They prepared 12.5 - 25% solutions of Hypaque in culture medium to separate mixed populations of slender and broad forms of *T. cruzi*. They reported an 88 - 89% recovery for the separation procedure.

## 6.3 Experimental Details

### 6.3.1 Reagents

The following polymers were used in the experiments: poly(ethylene glycol) (Sigma-Aldrich; MW = 20000 Da), Ficoll (Sigma-Aldrich; MW = 70000 Da and 400000 Da), dextran (Spectrum Chemical; 500000 Da), and poly(vinyl alcohol) (Polysciences; MW = 3000 Da). Phosphate-buffered saline was from Lonza at 10× concentration and diluted it to 1× using distilled, deionized water from a Milli-Q water purification system (Millipore). For stains, a Hemacolor® stain set from Harleco was used, consisting of three solutions: (i) methanol, (ii) phosphate-buffered eosin solution, and (iii) phosphate-buffered thiazine solution. All reagents were used without further purification.

Human whole blood, collected over sodium heparin as an anticoagulant, from single healthy donors (vendor certified syphilis<sup>-</sup>, HTLV<sup>-</sup>, HIV<sup>-</sup>, HepB<sup>-</sup>, and HepC<sup>-</sup>) was purchased from Research Blood Components (Boston, MA).

### 6.3.2 Formation and Analysis of Aqueous Two-Phase Systems

The stock solutions of polymers were prepared at concentrations higher than those used in applications of density based separation. Depending on the application, buffer salts or NaCl was added to the stock solution. Density measurements were performed to characterize stock solutions and to ensure uniformity across multiple preparations of each solution. To prepare ATPSs, equivalent volumes of polymer solutions (either at stock concentrations or a dilution) were added into a container (e.g., Eppendorf tube or plastic cuvette), thoroughly mixed by vortexing for 30 seconds, and phase separated by centrifugation (2 - 10 minutes at 2000 g). Phase separation in ATPSs due to gravity alone occurs inconveniently slowly (minutes to hours) because the difference in density between layers of an ATPS was small ( $\Delta\rho \approx 0.001\text{-}0.100 \text{ g cm}^{-3}$ ).

An aliquot of each phase (2 mL) was sampled to analyze the density of each layer by oscillating U-tube density/specific gravity meter (Anton Paar DM35N). For experiments using blood, the final osmolarities of the phases of an ATPS are important to ensure biocompatibility. The osmolality was measured by freezing point depression using an Advanced Model 3300 Osmometer (Advanced Instruments, Inc.).

### 6.3.3 Separation of Blood

The separation experiments were performed within 4-12 hours of the blood being drawn. If blood is mixed with an ATPS, the liquid plasma, which is miscible with water, will dilute the system. Since the volume of blood that is plasma differs between people, mixing would not be a reliable method of sample introduction to ATPSs for density-based separations. Therefore, the blood was introduced to the top phase of the ATPS as a layer in all experiments. The top phase of the ATPS is an effective barrier to mixing, and ensures the steps in density produced by the ATPS are reproducible.

### 6.3.4 Extraction of Fractions of Cells after Separation

For separations performed in conical tubes (Figure 6.1), samples were removed from each interface. After the blood sample is fractionated in the ATPS, a blunted pipette was used to remove 500  $\mu\text{L}$  from the boundary between the

ATPS and the plasma, as well as the interface of the ATPS. To ensure that remaining WBCs at these areas do not contaminate the bottom sample, the supernatant above the pellet was removed before removing 500  $\mu$ L from the pellet. A small amount of the pellet is not recovered in this process. Some cells are removed with the supernatant and also are lost on the walls of the pipette tip used for extraction.

For separations performed in plastic capillaries, the fractions that contained the fractionated cells were isolated by cutting the capillary into sections with a razor. The polymer/cell sample was deposited from each section onto a glass microscope slide by applying pressure through a pipette tip on the other end of the segmented tube.

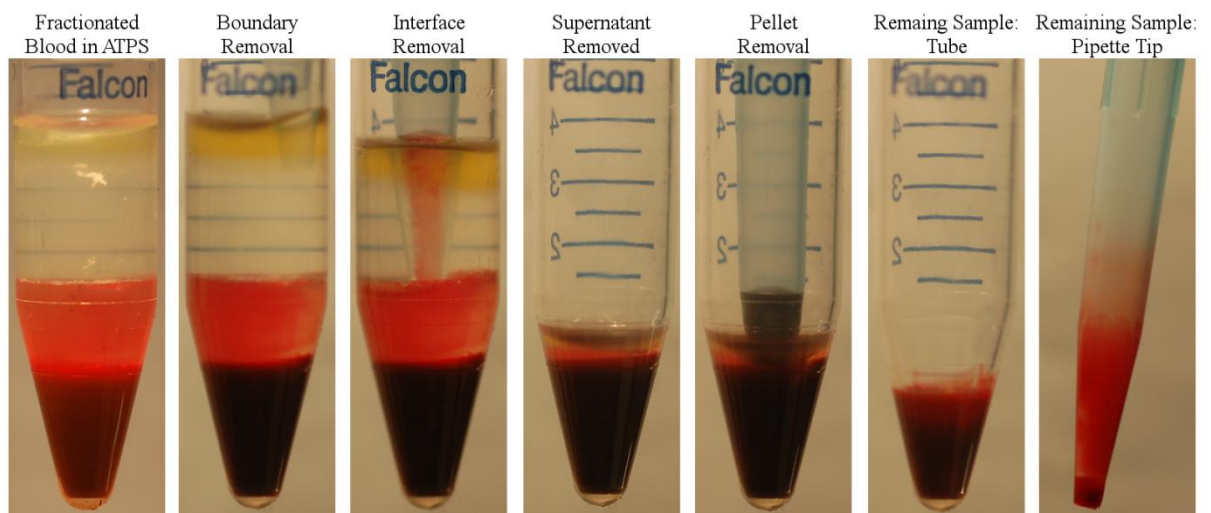


Figure 6.1: Procedure to recover cellular components after separation by ATPS. Each image depicts a single step in the protocol to isolate 500- $\mu$ L fractions of cells from the interfaces of an ATPS by pipette: the boundary between the plasma and the top phase is removed first, followed by the interface between phases, the remaining supernatant, and, finally, the pellet. Some cell loss occurs due to non-quantitative isolation of fractions and some non-specific binding.

### 6.3.5 Density Based Enrichment of Trypanosomes

Dextran (Mr - 500,000) from *Leuconostoc* and phosphate buffered saline (PBS) were purchased from Sigma and Ficoll PM 400 from GE Healthcare. 30% w/v stock solutions of Dextran and Ficoll were prepared. The osmolality of the solutions was fixed at 300 mOsm by adding NaCl solution. Density, osmolality and

pH measurements were used to characterize stock solutions and to ensure uniformity across multiple preparations of each solution. To prepare working solution of the Dextran Ficoll system, the stock solution was diluted with PBS. Centrifugation was used to increase the rate of separation of phases in ATPSs.

An aliquot of each phase (2 mL) was removed in order to analyze the density of each layer by oscillating U-tube density/specific gravity DA-510 (Kyoto Electronics Manufacturing) and the osmolality was measured by freezing point depression using an Advanced Model 3300 Osmometer (Advanced Instruments, Inc.).

To conduct the experiments, human whole blood was spiked with *T. cyclops*. *T. cyclops* were cultured in Cunningham's medium supplemented with 20% FBS and maintained at 27 °C. *T. cyclops* were passaged once a week and were grown to a density of  $2 \times 10^6 \text{ mL}^{-1}$ . 3 mL of ATPS was added to a 15 mL Falcon tube and centrifuged at 2000 g for 5 minutes to accelerate phase separation. Then 1 mL of spiked blood was carefully poured in to the Falcon tube over the phases. The samples were centrifuged at 2000 g for 60 - 90 minutes to achieve the separation. The fractions were extracted as explained in section 6.3.4.

#### 6.3.6 Selection of ATPSs

The Dextran-Ficoll ATPS exhibited a small difference in density between the top and bottom phases, and the bottom phase is dense enough to exclude most leukocytes. A 1:1 mixture of 20.5% (w/v) Dextran and 20.5% (w/v) Ficoll, produced a top phase with a density of  $1.076 \text{ g cm}^{-3}$  and a bottom phase with a density of  $1.080 \text{ g cm}^{-3}$ . Without additives, Dextran-Ficoll ATPSs prepared in distilled, deionized water that are in the density range of blood cells are acidic and hypotonic. The pH was titrated to 7.40 with NaOH and HCl. NaCl was then added to the solutions to reach a final osmolality of  $295 \pm 15 \text{ mOsmkg}^{-1}$  (i.e., isotonic).

The poly(ethylene glycol)-Ficoll ATPS exhibited differences in density between phases that were greater than  $0.030 \text{ g cm}^{-3}$ . A top phase with a density significantly greater than that of plasma ( $\rho = 1.026 \text{ g cm}^{-3}$ ) could not be produced while keeping the osmolality of the phases isotonic; this ATPS was, thus, not suitable for blood separations. The density ranges were, however,

suitable for separating polystyrene microspheres from Dynabeads. A 1:1 mixture of 15% (w/v) poly(ethylene glycol) and 20% (w/v) Ficoll (70000 Da) produced a top phase of  $1.025 \text{ g cm}^{-3}$  and a bottom phase of  $1.074 \text{ g cm}^{-3}$ . For experiments with microspheres, a small amount of surfactant was added, 0.01% Tween-20 (v/v), to the ATPS to prevent adhesion of the particles to the wall of the plastic capillary.

The poly(ethylene glycol)-Dextran ATPS had similar characteristics to the poly(ethylene glycol)-Ficoll ATPS. The poly(vinyl alcohol)-poly(ethylene glycol) ATPS could not produce a bottom phase that was dense enough to separate most WBCs from RBCs in the range of osmolality that is required for the separation of cells.

### 6.3.7 Separations Using Small Steps in Density

The only means to produce stable steps in density for the separation of biological species is the use of an ATPS. Some applications of the separation of cells may require a small step in density to isolate a sub-population of cells that are characterized by a narrow range of densities. Density standard floats (“beads”)—of known and calibrated densities— were used to test the ability of an ATPS with a small step in density to separate objects before using the systems with cells (Figure 6.2). An ATPS prepared from a 1:1 mixture of 21% (w/v) Dextran and 21% (w/v) Ficoll ( $\rho_{\text{top}} = 1.0783 \text{ g cm}^{-3}$ ;  $\rho_{\text{bottom}} = 1.0806 \text{ g cm}^{-3}$ ), and three beads with densities of  $1.0770 \text{ g cm}^{-3}$ ,  $1.0790 \text{ g cm}^{-3}$ , and  $1.0810 \text{ g cm}^{-3}$  were used. Due to their large size, the beads sedimented under a standard gravitational field (i.e., 1 g) after 6 hours to their equilibrium positions at one of the three interfaces of the ATPS: (i) the air/top phase interface, (ii) the interface between phases, or (iii) the interface between the bottom phase and the container. The use of centrifugation (2000 g for 10 minutes) accelerated the sedimentation of the beads through the ATPS. The difference in density between the bottom phase and the densest bead is only  $0.0004 \text{ g cm}^{-3}$ , which exemplifies the exceptional level of resolution of density-based separation using ATPS.

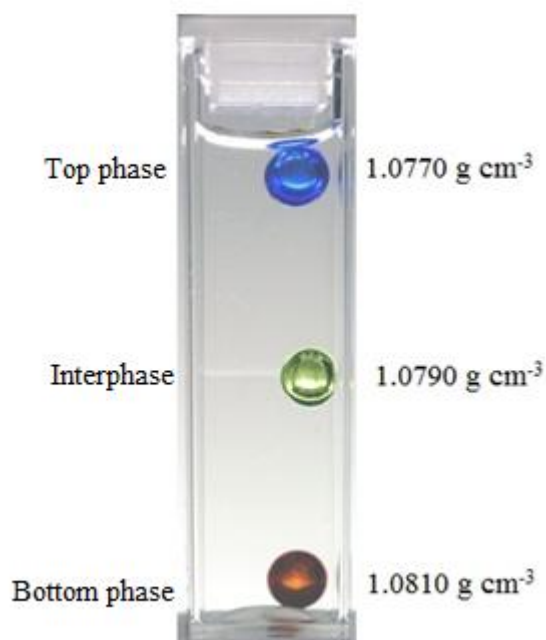


Figure 6.2: An image of Dextran-Ficoll ATPS ( $\rho_{\text{top}} = 1.0783 \text{ g cm}^{-3}$ ,  $\rho_{\text{bottom}} = 1.0806 \text{ g cm}^{-3}$ ; 21% (w/v) Ficoll and 21% (w/v) Dextran) separating three density standard beads with a density difference between each bead of  $0.0020 \text{ g cm}^{-3}$ .

### 6.3.8 Filtration of Particles Based on Density Using ATPSs

The interface between phases of an ATPS discriminates species based on density alone, rather than by their volume. There are conditions, however, where the interfacial tension between phases of an ATPS cannot be neglected and can compete with the balance of gravitational and buoyant forces that lead to density-based separations. These conditions result in the retention of objects at the interface that are denser than either phase; this effect scales with the magnitude of the interfacial tension and the particle size. For the separation of micron-sized particles, we overcome this effect by using a sufficiently large density step between phases.

This capability was demonstrated by separating polystyrene microspheres ( $\rho = 1.05 \text{ g cm}^{-3}$ ) and Dynabeads ( $\rho = 1.14 \text{ g cm}^{-3}$ ), particles with equivalent sizes ( $2.8 \mu\text{m}$ ) but different densities, using a poly(ethylene glycol)-Ficoll ATPS (Figure 6.3). The densities of the top and bottom phases of this ATPS were  $1.025 \text{ g cm}^{-3}$  and  $1.074 \text{ g cm}^{-3}$ , respectively, when prepared from a 1:1 mixture of 15% (w/v) poly(ethylene glycol) and 20% (w/v) Ficoll. A suspension containing ~250000 particles (polystyrene, Dynabeads, or a mixture of particle types) in water was

added to a plastic capillary that contained the ATPS. A bubble of air was introduced into the capillary to separate the ATPS and the suspension of particles; this separation ensured that the suspension and the ATPS would not mix prior to the experiment. After two minutes of centrifugation at 13700 g in a microhaematocrit centrifuge (CritSpinStatSpin; Iris Sample Processing, Inc.), (i) the bubble of air migrated against the applied centrifugal field due to buoyancy to allow the suspension of particles to contact the top phase of the ATPS, (ii) polystyrene particles sedimented through the top phase and concentrated at the interface between phases, (iii) the denser Dynabeads passed through both phases and concentrated at the interface between the bottom phase and the container, and (iv) a mixture of both types of beads sedimented by density independently, resulting in homogenous populations at separate interfaces (Figure 6.3).

#### **6.3.9 Analysis of the Components of Blood**

Thin smears of the samples were then prepared, stained (Harleco, Hemacolor® stain), and imaged by optical microscopy to examine the cellular contents of each section (Figure 6.4). The morphologies between micrographs of cells before and after centrifugation through the ATPS were found to be similar. The samples from experiments with the blood of five individuals were analyzed using a haematology analyzer (Siemens Advia 2120). For each whole blood sample used, aliquots of the original blood provided a baseline. Cells recovered from the ATPS fractions were washed with phosphate-buffered saline twice prior to analysis with the haematology analyzer. The average results from these individuals demonstrate the ability to isolate fractions of different cellular compositions (Table 6.1). Analysis of the reticulocytes revealed a high enrichment of reticulocytes at the liquid/liquid interface of the ATPS. The protocol that was used to extract cells from the ATPS prior to quantization using the haematology analyzer results in an apparent “loss” of cells when unprocessed whole blood is compared to the fractions isolated from the interfaces of the ATPS (Figure 6.6).

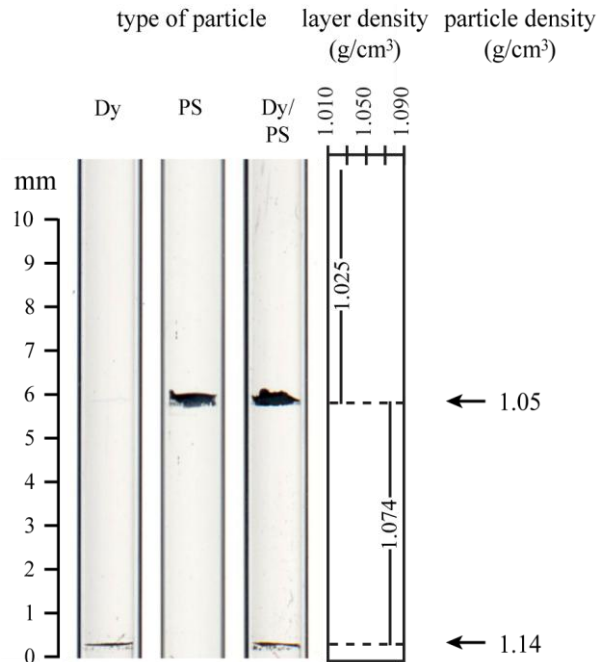


Figure 6.3: Density-based filtration of particles using an ATPS. The density step produced by a poly(ethylene glycol)-Ficoll ATPS ( $\rho_{top} = 1.025 \text{ g cm}^{-3}$ ,  $\rho_{bottom} = 1.074 \text{ g cm}^{-3}$ ; 15% (w/v) poly(ethylene glycol) and 20% (w/v) Ficoll) selectively filters particles of equivalent size ( $d = 2.8 \mu\text{m}$ ) based on their differences in density. Around 250000 particles were added to a microhaematocrit tube containing the ATPS. After centrifugation, the density step produced by the ATPS filtered solutions containing: (A) superparamagnetic microspheres only (Dynabeads (Dy);  $\rho = 1.14 \text{ g cm}^{-3}$ ), (B) polystyrene only (PS;  $\rho = 1.05 \text{ g cm}^{-3}$ ), and (C) a mixture of Dynabeads and polystyrene (Dy/PS).

The plasma that remained above the ATPS was evaluated for total protein content. The total protein content of plasma samples was quantified with a standard Bradford assay. A 96 well plate was prepared, and 250  $\mu\text{L}$  of Quick Start Bradford 1X dye reagent (Biorad) added to each well. A serial dilution of plasma samples was prepared and 5  $\mu\text{L}$  of each added to a well. The contents of each well were mixed well via pipetting. The concentration of protein in each well was determined with a calibration curve prepared from purified bovine serum albumin (0-2000  $\mu\text{g mL}^{-1}$ ). Absorption measurements (at 595 nm) were performed on a SpectraMax M2 microplate reader (Molecular Devices). The samples of plasma taken from the top of the Dextran-Ficoll ATPS were analyzed and protein levels compared to plasma taken from the same blood samples spun down in a centrifuge (Galaxy Centrifuge; VWR) for 15 minutes at 1000 g. The mean corpuscular volume (MCV) and the mean corpuscular haemoglobin (MCH) of RBCs isolated from five random donors before and after separations by ATPS were also analyzed. These quantitative results support the hypothesis that

sedimentation through the ATPS does not affect the morphology or the contents of cells.

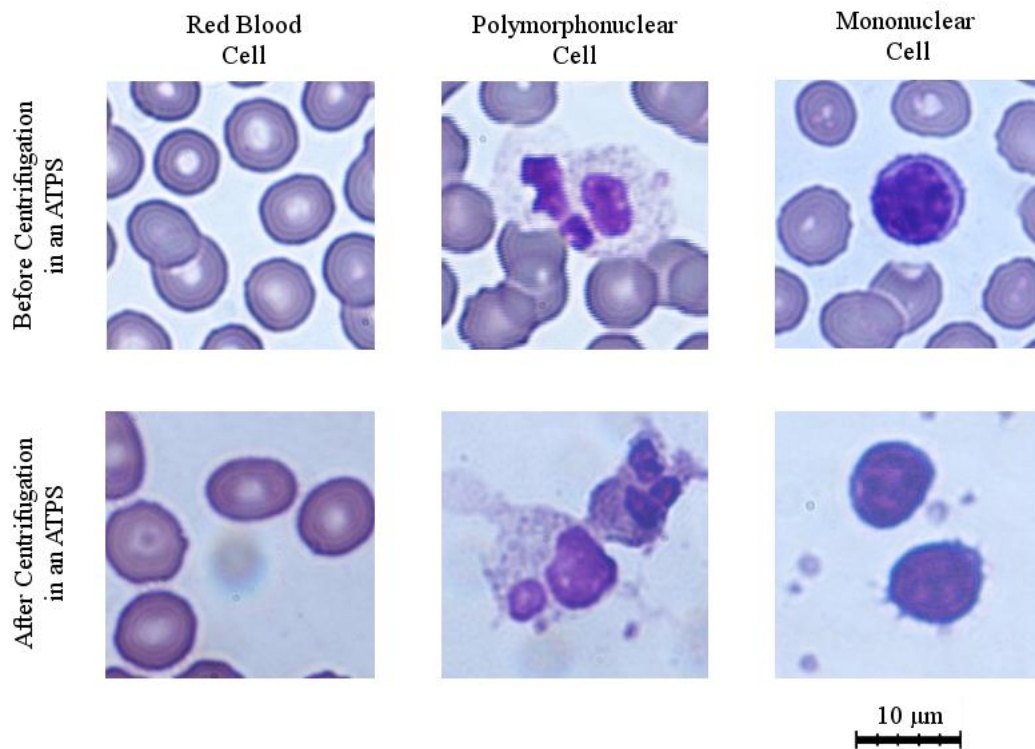


Figure 6.4: Morphology of cells after separation using an ATPS. Representative micrographs of red blood cells, polymorphonuclear cells, and mononuclear cells before and after centrifugation in an ATPS demonstrate no significant morphological change as a result density-based separation.

### 6.3.10 Analysis of *Trypanosoma* Enrichment

Thin smears of the samples were then prepared for trypanosomes and imaged by optical microscopy to examine the cellular contents of each section (Figure 6.5). The morphologies between micrographs of cells before and after centrifugation through the ATPS were found to be similar.

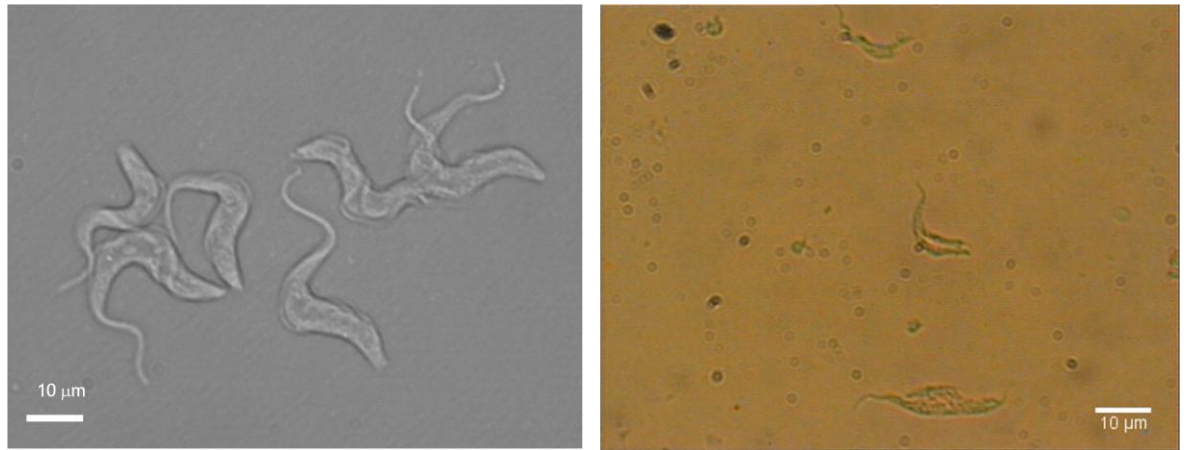


Figure 6.5: Morphology of trypanosomes before (*T. brucei*, phase contrast image) and after (*T. cyclops*, brightfield) separation using an ATPS. Representative micrographs before and after centrifugation in an ATPS demonstrate no significant morphological change.

## 6.4 Results and Discussion

### 6.4.1 Separation of Whole Blood

Several previously reported ATPSs [e.g., poly(ethylene glycol)-Ficoll (SooHoo and Walker, 2009), poly(ethylene glycol)-Dextran (Albertsson, 1958), Dextran-Ficoll (SooHoo and Walker, 2009), and poly(vinyl alcohol)-poly(ethylene glycol) (Albertsson, 1958)] were surveyed for their potential application in the density-based separation of cells. Dextran-Ficoll was chosen for its ability to satisfy two selection criteria: (i) values for the density of each phase required to separate different types of cells (e.g., MNCs, PMNs, and RBCs) from plasma, and (ii) isotonicity with plasma and to the ability to maintain physiological pH to avoid damaging the cells during separation. In blood, the physiological reference range for pH is 7.38-7.44, and for osmolality is 285-295 mOsm kg<sup>-1</sup> (Kratz et al., 2004). Changes to either of these parameters will result in changes in the morphology and density of blood cells.

The volume of blood to be separated depends on the particular needs of the setting. In a research or clinical laboratory, millilitres of blood, acquired by venupuncture or an arterial blood draw, may be required for use in assays or studies. In point-of-care testing, only a finger-prick may be available for blood collection; finger-prick volumes are limited to tens of microlitres. To demonstrate relevance to both of these settings, samples were evaluated with

volumes in two ranges: 1 mL of whole blood in a 15-mL conical tube and 10  $\mu\text{L}$  of whole blood in a plastic capillary tube. In each case, the samples were centrifuged to ensure that blood cells would reach their equilibrium point in the ATPS rapidly.

Larger volumes of whole blood made it possible to analyze the separation of cells quantitatively. Centrifugation was used to sediment the cells from the blood plasma through a Dextran-Ficoll ATPS ( $\rho_{\text{top}} = 1.076 \text{ g cm}^{-3}$ ,  $\rho_{\text{bottom}} = 1.080 \text{ g cm}^{-3}$ ). After centrifugation, clarified plasma (containing  $< 150 \text{ cells } \mu\text{L}^{-1}$  after separation) was retained on top of the ATPS and high concentrations of cells were visible at three locations (Figure 6.6). A Bradford assay was performed to quantify the protein content of the plasma retained above the top phase of the ATPS (Supporting Information). This fraction contained 76% of the protein content of blood plasma ( $54.6 \text{ g L}^{-1}$  of  $71.5 \text{ g L}^{-1}$  expected), and could be used in further analysis. Some plasma may be carried into the ATPS with the cells. Protein was found in all the phases of the ATPS, but we did not establish conclusively whether the protein was derived from plasma or from lysed cells. Approximately 76% of cellular components were recovered from the fractions of the ATPS after their separation from whole blood. The loss was attributed to our extraction protocol (Figure 6.1). The morphologies of all isolated cells were consistent with that of cells observed on smears made from the original sample of whole blood (Figure 6.4). The mean corpuscular volume (MCV) and mean corpuscular haemoglobin (MCH) of the RBCs from the bottom of the ATPS were also consistent with the MCV and MCH from the original sample; it was concluded, therefore, that minimal changes to cellular morphology occurred due to the pH or osmolality of the ATPS, interactions with the polymers comprising the ATPS, or interactions with the liquid/liquid interface during centrifugation.

The cells separated at each of the three ATPS interfaces were quantified using a haematology analyzer (Siemens, Advia 2120). Table 6.1 details the average distribution of cells of the isolated sub-populations from five individuals.

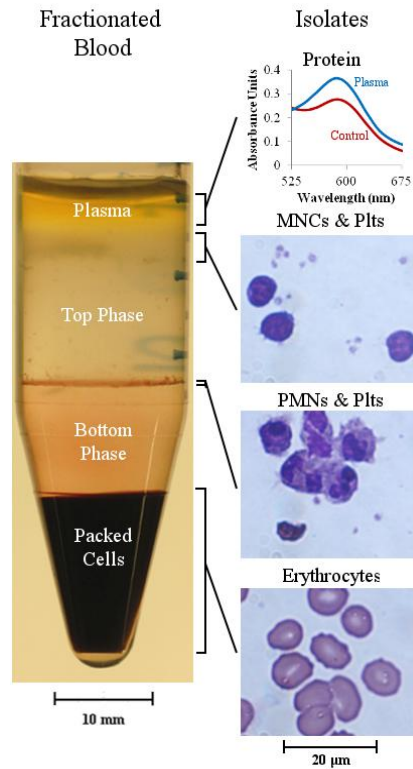


Figure 6.6: Enrichment and concentration of cells by density from 1 mL of whole blood. 3 mL of the Dextran-Ficoll ATPS ( $\rho_{top} = 1.076 \text{ g cm}^{-3}$ ,  $\rho_{bottom} = 1.080 \text{ g cm}^{-3}$ ; 20.5% (w/v) Ficoll and 20.5% (w/v) Dextran) was used to separate the cellular components of human blood based on density. After 100 minutes of centrifugation at 2000 g, the top and bottom phase of the ATPS are intact and separate different isolates of blood (Fractionated Blood). The contents of each isolate were examined; the protein content of the plasma fraction was evaluated with a Bradford assay and cellular contents were evaluated for morphology using optical microscopy (Isolates). A mixture of cells was present in each fraction; micrographs depict the cell types that were most prevalent.

Blood Component	Number of cells ( $\times 10^3 \mu\text{L}^{-1}$ )	Distribution of components in ATPS (%)		
		Boundary	Interface	Bottom
MNCs		28	33	38
PMNs	2.89	2	6	91
PLTs	140	8	20	73
RBCs	3930	0	< 1	> 99

Table 6.1: Average distribution of sub-populations of the cellular components of blood that are enriched at the interface and boundaries of an ATPS. Blood was analyzed from five different individuals. Whole blood (1 mL) was centrifuged over a Dextran-Ficoll ATPS ( $\rho_{top} = 1.076 \text{ g cm}^{-3}$ ,  $\rho_{bottom} = 1.080 \text{ g cm}^{-3}$ ; 20.5% (w/v) Ficoll and 20.5% (w/v) Dextran). The components of blood separated into four fractions: (i) above the ATPS (plasma), (ii) at the boundary between the plasma and the ATPS (boundary), (iii) at the liquid/liquid interface of the ATPS (interface), and (iv) below the ATPS (bottom). The plasma fraction contained less than 150 cells  $\mu\text{L}^{-1}$ . A haematology analyzer counted cells from the bottom three fractions (“boundary”, “interface”, and “bottom”).

The boundary between the ATPS and the plasma was depleted of RBCs and contained a mixture of WBCs and platelets. The ratio of MNCs per PMN was 7.4, a 12-fold enrichment from the starting ratio of 0.6. A population of WBCs that is free of RBCs would provide a measure of the function of an individual's immune system. The liquid/liquid interface was also enriched for WBCs and platelets, and the ratio of MNCs per PMN was 2.9, more than a four-fold increase from the starting ratio. RBCs were not completely depleted at this interface, and they accounted for one-third of the cellular components. Young RBCs and reticulocytes (immature RBCs) have lower densities than older RBCs (Leif and Vinograd, 1964). Reticulocytes normally account for between 1-2% of all RBCs. Further analysis revealed that over 31% of the RBCs at the liquid/liquid interface were reticulocytes. Concentrated populations of young RBCs and reticulocytes would provide a measure of haematopoiesis, which is important in characterizing anaemia and other diseases of the blood (Brugnara, 2003). The packed cells below the ATPS contained a mixture of all cellular components, 97% of which were RBCs. In this fraction, the ratio of MNCs per PMN was 0.2, a three-fold reduction of the starting ratio; most MNCs did not pass below the bottom phase.

A similar separation profile was observed (Figure 6.7) using a smaller volume of blood (10  $\mu$ L; a finger-prick), although a sufficient number of cells to rigorously quantify the number of each type of cell in each fraction could not be obtained. Blood plasma was retained as a separate, clarified liquid layer above the top phase of the ATPS, and clusters of cells were visible at three locations: (i) PMNs, MNCs, and platelets were present at the diffuse boundary between the blood plasma and the top phase, (ii) PMNs and MNCs were present at the interface between the immiscible phases, and (iii) PMNs, MNCs, and RBCs were present at the fluid-solid interface at the bottom of the capillary.

The effect of concentrating cells to an interface could allow for a rough quantification of cell types. For example, the vast majority of RBCs sediment to the bottom of this ATPS, and these packed cells provide a measure of the haematocrit—a critical marker of health. The haematocrit is the RBC volume percentage of whole blood, and it can be calculated by comparing the packed volume of sedimented RBCs to the volume of the retained blood plasma (Figure 6.7). A close agreement was found between the haematocrit measured in the ATPS with that measured using whole blood alone. Although the haematocrit can

be measured without the use of an ATPS, fractionating the remaining cells to separate interfaces could enable more thorough haematological analyses in limited-resource settings.

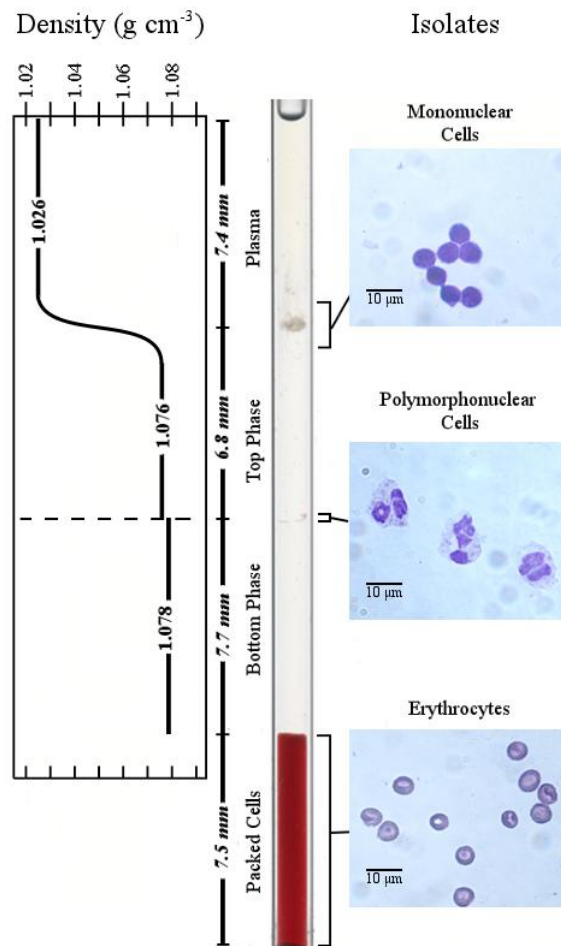


Figure 6.7: Enrichment and concentration of cells by density from 10  $\mu\text{L}$  of whole blood. The ATPS was Dextran-Ficoll ( $\rho_{\text{top}} = 1.076 \text{ g cm}^{-3}$ ,  $\rho_{\text{bottom}} = 1.080 \text{ g cm}^{-3}$ ; 20.5% (w/v) Ficoll and 20.5% (w/v) Dextran). Leukocytes (i.e., mononuclear cells and polymorphonuclear cells) and platelets segregated into two bands—one at the top of the ATPS and one at the liquid/liquid interface of the ATPS. Each band contained a mix of all three types of cells. Erythrocytes and leukocytes sedimented below the ATPS. Micrographs depict the types of cells that were most prevalent in each band (Isolates).

#### 6.4.2 Enrichment of Trypanosomes

Human whole blood spiked with 20,000 *T. cyclops* was used for developing the proof of concept. To demonstrate enrichment of trypanosomes using ATPS, 1 mL of the spiked blood was carefully layered over 3 mL Ficoll-Dextran system. The sample was then centrifuged (2000 g for 90 minutes) to sediment the cells from the blood plasma through a Dextran-Ficoll ATPS ( $\rho_{\text{top}} = 1.076 \text{ g cm}^{-3}$ ,  $\rho_{\text{bottom}} = 1.082 \text{ g cm}^{-3}$ ). After centrifugation, the cells were extracted from the top phase,

the interface and the bottom phase and analysed using a haemocytometer. Figure 6.8 illustrates the number of cells and trypanosomes extracted from each phase.

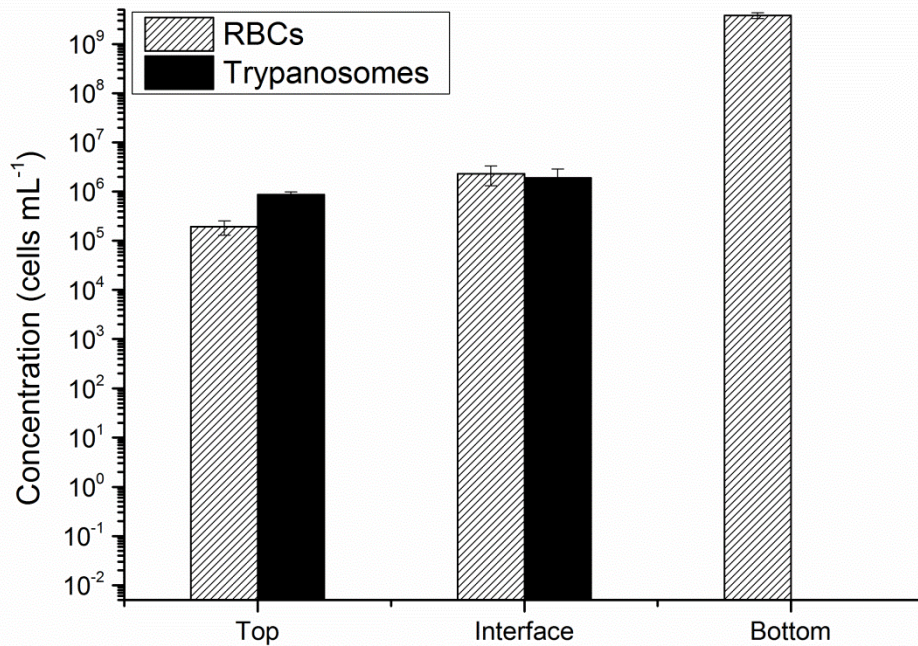


Figure 6.8: Enrichment and concentration of cells by density from 1 mL of spiked blood. 3 mL of the Dextran-Ficoll ATPS ( $\rho_{\text{top}} = 1.076 \text{ g cm}^{-3}$ ,  $\rho_{\text{bottom}} = 1.082 \text{ g cm}^{-3}$ ) was used for separation.

The trypanosomes were confined to the top layer (boundary between the ATPS and the plasma) and the interface of Ficoll-Dextran system. No trypanosomes were found in the RBC pellet. Table 6.2 gives the average distribution of the recovered cells. Top phase was depleted of RBCs and contained a mixture of WBCs and platelets. The liquid/liquid interface was also enriched for WBCs and platelets but the RBCs were not completely depleted at this interface. The majority of the RBCs sedimented as the pellet and were collected from the bottom phase. Blood plasma was retained as a separate, clarified liquid layer above the top phase of the ATPS.

Cells	Control (mL <sup>-1</sup> )	Cells recovered (mL <sup>-1</sup> )		
		Top layer ( $\rho = 1.076 \text{ g cm}^{-3}$ )	Interface	Bottom layer ( $\rho = 1.076 \text{ g cm}^{-3}$ )
Trypanosomes	$2 \times 10^4$	$8.67 \times 10^5$	$1.90 \times 10^6$	-
Red blood cells	$7 \times 10^8$	$1.92 \times 10^5$	$2.32 \times 10^6$	$3.83 \times 10^9$

Table 6.2: Average distribution of trypanosomes and blood cells at the interface and boundaries of ATPS. The blood separated into four fractions: (i) above the ATPS (plasma), (ii) at the boundary between the plasma and the ATPS (top layer), (iii) at the liquid/liquid interface of the ATPS (interface), and (iv) below the interface (bottom layer).

The effect of concentrating trypanosomes to an interface could allow for an easy diagnosis of sleeping sickness. In experiments conducted with *Trypanosoma cyclops* spiked blood, ~99% of the blood cells were removed from the top phase and the interphase, enriching the WBCs and trypanosomes, facilitating the use of haemocytometry for the detection of the parasites.

## 6.5 Conclusion

Separating human blood based on differences in the density of cells is a promising technique to isolate and quantify the cellular sub-populations of blood, but only layered gradients in density were capable of separating more than two sub-populations at once without changing the morphology of cells. The instability of layered miscible systems, and the difficulty of preparing them, has limited their use primarily to academic laboratories. Density-based separations through an ATPS provide a new method to separate sub-populations of interest. ATPSs combine the biocompatibility of aqueous media with the thermodynamic stability of separated phases. An appropriately formulated ATPS is capable of enriching and concentrating blood cells into three fractions: a relatively pure sub-population of MNCs, a mixture of WBCs and young erythrocytes, and the vast majority of erythrocytes.

This system provides a first step towards developing a simple, new blood test that could give several important measures of health, and have applications both

in the developing world and in high-technology medicine. In low-resource settings, this approach to the fractionation of whole blood and enrichment of trypanosomes could enable an easier detection of sleeping sickness, and a number of options for low-cost centrifuges are being developed to enable these applications (Wong et al., 2008; Brown et al., 2011). This technique can also be coupled with inertial microfluidic separation to enhance the separation efficiency of the device.

## Chapter 7 - Rapid Ultrasonic Isopycnic Separation of Trypanosomes

### 7.1 Introduction

Mainly the sample enrichment techniques used in disease diagnosis either exploit different mechanical properties of cells or target ligand-receptor interactions (Chin et al., 2011). Centrifugation, one of the most commonly used techniques, relies on differences in the density while techniques like magnetic-activated cell sorting or fluorescent-activated cell sorting require the addition of a label to generate a contrast. However, these limitations render the use of these techniques for diagnosis in resource poor environments difficult, given the constraints of costs and assay complexity (Chin et al., 2011; Urdea et al., 2006; Wong et al., 2008).

This chapter describes a novel method to achieve low cost and low power separation of cells, using a microseparation technique based on an acoustically actuated microchip (Figure 7.1A) for the enrichment of *T. brucei* from blood cells. The technique is based on developing unique flow patterns generated by the interaction of ultrasonic surface acoustic waves (SAWs) with blood, which, when coupled with an isopycnic density gradient, results in the separation of parasites from RBCs (Figure 7.1B, C). This technique needs only a few microlitres of blood (equivalent to a fingerprick) and eliminates the need for tubes, pumps or centrifuges.

#### 7.1.1 Diagnosis of Sleeping Sickness

As discussed previously, currently the diagnosis of sleeping sickness requires identification of the parasitic trypanosome in the blood (see chapter 1). The performance of a more recently introduced serological test which is now the main primary test for detection in large scale screening campaigns, the Card Agglutination Test for Trypanosomiasis (CATT), is poor in terms of sensitivity. The specificity of the CATT had been reported to be 95% but many false positives have been reported (FIND, 2012). Moreover, CATT is not useful in detecting sleeping sickness caused by *Trypanosoma brucei rhodesiense* (Chappius et al., WHO, 2006).

Presently, there are many problems concerning the diagnosis of HAT; therefore, the gold standard for the diagnosis remains microscopy. Another method of

sample preparation uses ion-exchange to distinguish blood cells and parasites, with the cell surface charges being the distinguishing or differentiating factor. This process is, however, technically difficult to implement as well (FIND, 2010).

Microfluidics and lab-on-a-chip techniques hold the prospect to change the face of the medical diagnostics in the developing world. With manipulation of small sample volumes, microfluidic technologies are enabling miniaturisation and integration of laboratory tests into low cost, low power, hand-held microchip formats. This can allow complex medical diagnostic procedures to be carried out in remote locations where healthcare facilities are not adequate (Yager 2006; 2008). For example, the low-cost paper diagnostics developed by Martinez et al., (2007).

Another promising microfluidics-based approach involves actuating fluid on a planar surface using surface acoustic wave (SAW) streaming (Wixforth, 2006). SAWs are mechanical waves that are induced by applying a voltage to an interdigitated transducer (IDT) at the surface of a piezoelectric substrate. When a drop of liquid is placed in the path of the SAW, the mechanical waves refract inside the droplet, generating fluid streaming (Shiokawa et al., 1989; Friend and Yeo, 2011). This streaming effect can be used to manipulate the droplets on a surface and several functions have already been reported, such as mixing (Tseng et al., 2006; Sritharan et al., 2006), moving (Tan et al., 2007; Bourquin et al., 2010), jetting (Tan et al., 2009; Bourquin et al., 2011a), nebulising (Kurosawa et al., 1995) and manipulation of particles (Tan et al., 2007; Bourquin et al., 2010). This SAW based streaming has found application in immunoassays (Bourquin et al., 2011b), PCR (Reboud et al., 2012), interface for mass spectrometry (Heron et al., 2010; Ho et al., 2011) and an actuation method for a lab-on-a-disk (Glass et al., 2012). Building upon these new applications, the enrichment of trypanosomes from blood cells will therefore not only provides an important challenge but also demonstrates the versatility of this technique.

Phononics is a term used to describe the field of engineering that deals with the tailored dispersion of acoustic energies. The phononic crystals possess periodic ordering of regions having a contrast in the elastic modulus (Sigalas and Economou, 1993, Kushwaha et al., 1993). These ordered arrays act as a waveguide that scatters the acoustic waves as a function of its direction or

frequency. These arrays are often simple close packed 3-D structures (cubic or hexagonal) or 2-d structures (square, hexagonal or honeycomb, Wilson et al., 2011).

In an array of periodic ordering regions, the waves propagate in all possible directions and fill all available space after being dispersed. Depending on the geometry and frequency of the phononic crystals, the waves can interfere constructively or destructively.

Sigalas and Economou (1993) were the first to develop a phononic band gap. The full band gap has since then found application as acoustic waveguides (Wilson et al., 2011), filters (Pai et al., 2004) and strong resonators (Wu et al., 2004). Wilson et al., (2011) used phononic crystals to manipulate fluid flows. They showed how different configurations of phononic crystals can be used as filters or waveguides to concentrate particles in a microdroplet. Bourquin et. al., (2011a) used phononic crystals to control jetting and ejection of droplets in a number of directions.

## **7.2 Background**

The technology described in this chapter relies both on the optimisation of the density of the blood and upon generating a unique pattern of streaming using SAW within a small droplet of blood obtained from a fingerprick. The particular flow patterns were generated by using acoustic streaming on the surface of the piezoelectric substrate. Asymmetric actuation of the drop with the SAW (Figure 1a) causes a circular rotational motion, thereby inducing secondary flows (Raghavan et al., 2010), illustrated in Figure 7.2, in a manner similar to Batchelor flows in the droplets.

The interface between the piezoelectric substrate and the droplet behaves as a no-slip boundary (equivalent to the stationary disk) and the top surface of the droplet behaves as a surface with the largest azimuthal velocity due to absence of friction with air (equivalent to the rotating disk). The azimuthal velocity is smaller at the bottom than at the top of the droplet as a consequence of frictional effect at the surface of the chip, causing the fluid to travel inward at the interface with the piezoelectric surface and drawing the RBCs to the centre of the drop. Additional constraints arising from the capillarity and volume

conservation results in the fluid recirculating upward in the middle of the droplet and downward at the free surface as illustrated in Figure 7.2. Under normal circumstances, this upward flow is not strong enough to lift the cells, in part as their buoyancy is too low.

The overall behaviour of RBC in the drop results from the interplay between the drag force ( $F_D$ ), the buoyancy ( $F_B$ ) and the force due to the gravity ( $F_g$ ). The separation of cells based upon density alone could not occur spontaneously within blood as  $F_B + F_D < F_g$ . It has already been shown that increasing the power, hence the velocity of the fluid  $U$  and the drag force  $F_D$ , will lead to lysis of the RBCs - a technique which has already been exploited in nucleic acid testing (Reboud et al., 2012).

Instead, in this chapter, an isopycnic gradient is used, adjusting the density of the fluid so that it is higher than that of the trypanosomes but lower than that of the RBCs ( $\rho_{\text{try}} \leq \rho_f < \rho_{\text{RBC}}$ ). Under these circumstances the buoyancy becomes sufficiently strong to dominate the overall forces, lifting the trypanosomes and allowing an isopycnic separation, as described in Figure 7.2. As a consequence, the RBCs are concentrated in the centre of the droplet while the trypanosomes are enriched at the periphery. The enriched material is easily isolated and analysed.

## 7.3 Materials and Methods

### 7.3.1 Device Fabrication

Two configurations were investigated in this chapter, (i) using SAW device on lithium niobate ( $\text{LiNbO}_3$ ) wafer, and (ii) using phononic superstrate. The SAW devices used in the experiments were fabricated with the help of Dr. Yannik Bourquin and Dr. Julien Reboud.

#### 7.3.1.1 SAW Device on $\text{LiNbO}_3$

The SAW device was fabricated on a  $128^\circ$  Y-cut X-propagating 3 inch  $\text{LiNbO}_3$  wafer. It consisted of 10 pairs of fingers to form a slanted finger interdigitated transducer (SFIDT). The width of the tapered fingers and the space between them varied linearly from  $62.5 \mu\text{m}$  to  $125 \mu\text{m}$  along the aperture. The  $\text{LiNbO}_3$  wafer was coated by spinning AZ4562 photoresist before transferring the pattern

using standard photolithography and developed using AZ400K. A 20 nm titanium adhesion layer was evaporated prior to deposition of 100 nm of gold and lift-off was then performed in acetone. For the observation of fluorescent beads, the electrodes were patterned on a transparent double side polished LiNbO<sub>3</sub> wafer.

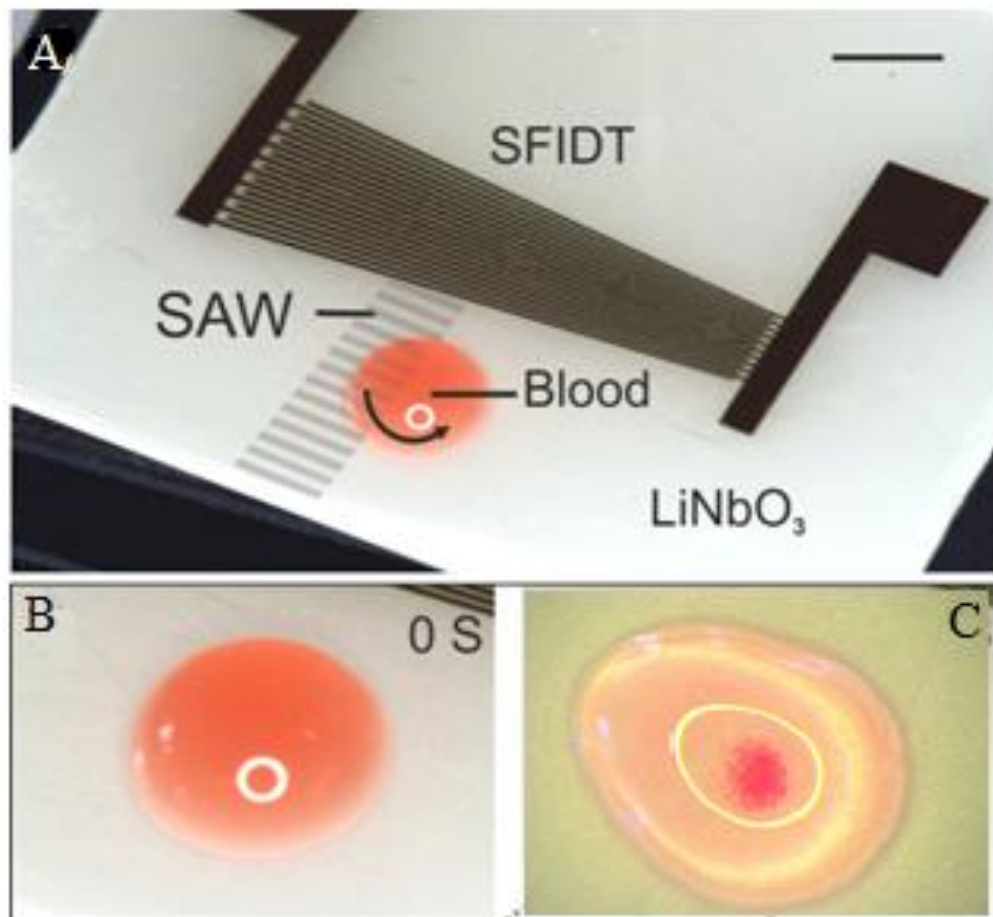


Figure 7.1: (A) Picture of the SAW device comprising a slanted finger interdigitated electrode (SFIDT) on LiNbO<sub>3</sub>. The surface acoustic wave (SAW) is generated at a defined position asymmetrically with respect to the drop of blood, only a fraction of which will lie in the acoustic pathway, thereby inducing a rotational motion within the drop. The scale bar is 3 mm; (B) Pictures of the concentration of red blood cells before and (C) after actuation with SAW. Red blood cells (RBCs) are concentrated in the middle of the drop, while trypanosomes are enriched at the periphery.

A hydrophilic spot was created in front of the IDT to reproducibly position the blood. The wafer was coated with AZ4562 photoresist, patterned using standard photolithography and developed using AZ400K. The pattern comprised a disk of 3 mm diameter. The wafer was then treated in O<sub>2</sub> Plasma for 2 min at 100 W before silanisation in a solution of 30 µl of trichloro(1H,1H,2H,2H-

perfluorooctyl)silane (Aldrich) in 50 ml of heptane for 10 min. The photoresist was removed in acetone and the glass was rinsed with methanol and blow dried. The SAW device was finally positioned on a heat sink.

The SAW device was characterized using a Network Analyzer (Agilent Technologies E5071C ENA series) and a vibrometer (Polytec). The SFIDT was connected to a TGR1040 - 1GHz Synthesised RF Generator (Thurlby Thandar Instruments) in conjunction with a Mini Circuits ZHL-5W-1, 5 - 500 MHz amplifier and a 3A, 24V dc power supply to generate the SAW.

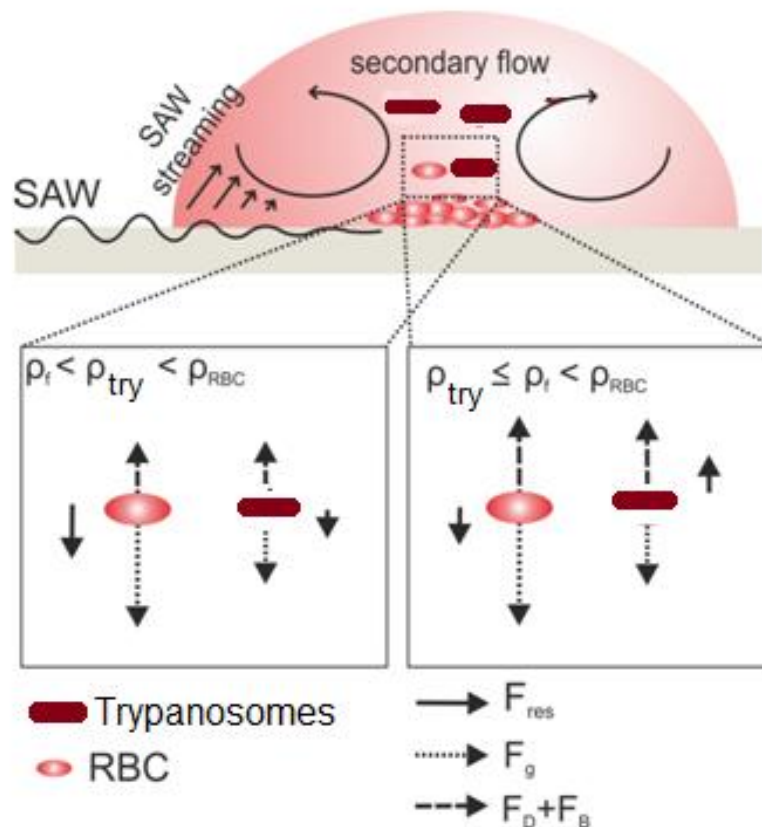


Figure 7.2: Schematic representation of the flow pattern in infected blood droplet. The SAW induced streaming in the drop and a secondary flow brings the particles at the centre of the drop. The two lower schematics show the forces acting on the RBCs and trypanosomes for different value of  $\rho_f$ . When  $\rho_{try} \leq \rho_f < \rho_{RBC}$ , the resultant force  $F_{res}$  is strong enough to lift the trypanosomes but not the RBCs.

### 7.3.1.2 SAW Transducer and Phononic Superstrate

The SAW device was fabricated as described above, with a pitch of 160  $\mu\text{m}$ , and an 80  $\mu\text{m}$  width. The phononic superstrates were fabricated using <100> silicon wafer with an approximate thickness of 470  $\mu\text{m}$  and standard photolithography. The phononic crystal was constructed using a square array (pitch 200  $\mu\text{m}$ ) of circular holes (radius 80  $\mu\text{m}$ ), dry-etched in the silicon (STS ICP) to a depth of 250 $\mu\text{m}$ . At a frequency within the bandgap of the structure, the lattice filters the wave that then propagates only on the side of the superstrate not containing the structures, as described in (Wilson et al., 2011, Reboud et al., 2012), enabling to break the symmetry of wave propagation, resulting in the rotational flows that lead to cell concentration. A hydrophilic spot was lithographically defined as described in the main text, to position the drop of blood reproducibly.

The superstrate was placed on top of the piezoelectric wafer and coupled with 2  $\mu\text{l}$  of water-based gel spread manually (KY jelly, Johnson and Johnson) in between, yielding a film approximately 50  $\mu\text{m}$  thick.

### 7.3.2 Density Solutions

For the experiments with *Trypanosoma* spiked blood, Histodenz (Sigma-Aldrich) was diluted in deionized water to a concentration of 30% in order to have a high density solution with osmolality of 300 mOsm. This solution was then further diluted in the culture medium before use in the experiments. The density of the solution was measured using DA-510 (Kyoto Electronics Manufacturing) and the osmolality was measured using an Advanced Model 3300 Osmometer (Advanced Instruments, Inc.). The densities of Histodenz 0%, 10%, 15%, 20% in Cunningham's medium were 1.006, 1.057, 1.083, 1.108  $\text{g cm}^{-3}$  respectively.

### 7.3.3 *Trypanosoma cyclops* preparation

*T. cyclops* were cultured in Cunningham's medium supplemented with 20% FBS and maintained at 27  $^{\circ}\text{C}$ . 1 mL of trypanosomes in culture medium was centrifuged at 1000 x g for 5 minutes and the pellet re-suspended in fresh medium. Human blood was spiked with 10,000 trypanosomes  $\text{mL}^{-1}$  to mimic the human parasitaemia levels (0.00237%). For  $4.4 \times 10^{-4}$  and  $4.32 \times 10^{-5}\%$ , the blood was spiked with 1000 and 100 trypanosomes respectively.

### 7.3.4 *Trypanosoma* Enrichment

The spiked blood was mixed with the density gradient solutions to a final percentage of RBCs of ~1 % in each experiment. The blood (10  $\mu\text{L}$ ) was then pipetted on to the SAW device. The SAW was actuated for 5 seconds for the separation and the outer part of the droplet was pipetted out. The samples were then analysed using haemocytometry.

## 7.4 Results and Discussion

The enrichment of *T. cyclops* was characterized by spiking human blood with different parasitaemia levels. A study of the optimal density was made by varying the concentration of gradient solution. The density of trypanosomes ( $> 1.077 \text{ g cm}^{-3}$ , Hirumi et al 1977) is lower than those of the RBCs (1.080 - 1.110  $\text{g cm}^{-3}$ , Leif and Vinogaurd, 1964). Histodenz, a common isopycnic gradient generating agent, was preferentially used for its low viscosity, non-toxicity and relatively low osmolality. A maximum of 30 % Histodenz maintained osmolality at around 300 mOsm and solutions with densities between 1.05 - 1.11  $\text{g cm}^{-3}$  were prepared with the osmolality set at 300 mOsm.

Figure 7.3 shows the increasing enrichment with the increasing density of the solution until an optimum density  $1.083 \text{ g cm}^{-3}$ , after which the enrichment decreases below a statistically significant difference with the control. This can be attributed to the fact that the density of the trypanosomes has been reported below around  $1.077 \text{ g cm}^{-3}$  (Hirumi et al., 1977). Consequently, above  $1.083 \text{ g cm}^{-3}$ , they behave similarly to the normal RBCs and are not separated from them.

In addition, trypanosomes have a very different shape, when compared RBCs. They are elongated and thin, while the red blood cell can be approximated as a disk. This results in their behaviour in flow being different and could lead to decrease in the drag force with respect to RBCs, making the separation more efficient.

The limit of detection for the system was investigated to judge its ability to detect low parasitaemia (down to  $4.32 \times 10^{-5}\%$ ). As the initial parasitaemia decreased, the enrichment increased up to 100-fold (Figure 7.4) for  $4.4 \times 10^{-4}\%$  parasitaemia and more than 1000 fold for  $4.32 \times 10^{-5}\%$ , allowing the detection of

as low as 100 trypanosomes mL<sup>-1</sup>, which is lower than the current limit of detection using a thin smear.

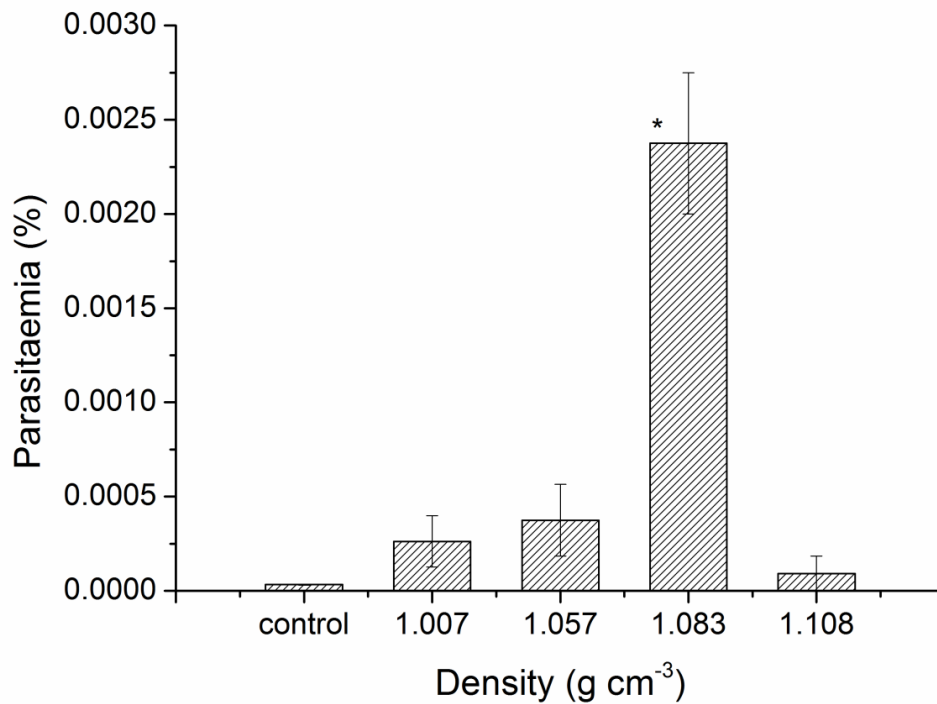


Figure 7.3: The concentration effect of SAW microseparation on *Trypanosoma cyclops* suspended in Histodenz as a function of the density of the solution for a frequency of 10.9 MHz and power of 2 W. Control indicates the parasitaemia in the sample used prior to SAW microseparation. Parasitaemias were determined by haemocytometry in samples taken from the periphery of the droplet following SAW microseparation. The data are means of 3 replicates and the error bars are standard errors of the mean deviations. Statistically significant enrichment is marked with \* (99%).

The experiments were repeated using phononic superstrate, which provide a low cost and disposable alternative to LiNbO<sub>3</sub> chips. The phononic chips are free of electrodes, channel and pumps making it user friendly as well. The disposable chips with phononic structures filter the acoustic waves generating asymmetric flows required for enrichment of cells in the microdroplet. Though the phononic superstrate is disposable and low cost, it requires more power to drive the flows compared to carrying out the enrichment directly on LiNo3 and also needs to be mechanically coupled to the piezoelectric surface. Figure 7.5 shows the separation efficiency of the superstrate. The phononic structure provides an excellent reflecting or scattering medium for the incoming acoustic waves without compromising the separation efficiency of the developed system.

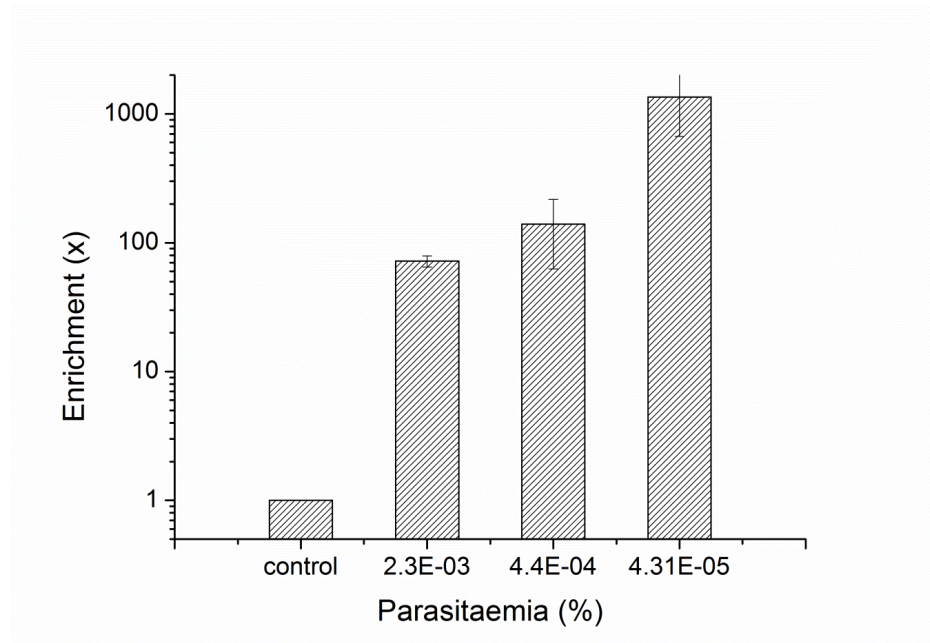


Figure 7.4: The fold enrichment achieved following SAW microseparation of samples containing trypanosomes at parasitaemia from 0.0023% to  $4.32 \times 10^{-5}\%$  in Histodenz at 15% ( $\rho=1.08326 \text{ g cm}^{-3}$ ), input frequency of 10.9 MHz and power of 2 W. The data are means of 3 replicates and the error bars are standard errors of the mean deviations.

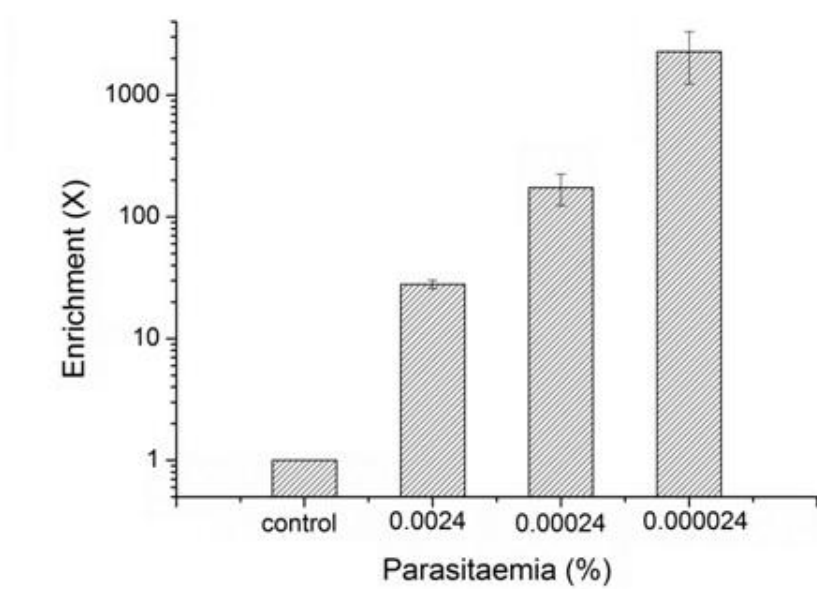


Figure 7.5: Enrichment of *Trypanosoma cyclops* suspended in 15% Histodenz as a function of the initial parasitaemia for a frequency of 8.8 MHz and input power of 1 W on a disposable superstrate. Parasitaemias were determined by haemocytometry in samples taken from the periphery of the droplet following SAW microseparation. The data are means of 3 replicates and the error bars are standard errors of the mean deviations.

Parasitaemias of  $2.3 \times 10^{-3}$ ,  $2.4 \times 10^{-4}$  and  $2.4 \times 10^{-5}\%$  were used in the experiment. The results were comparable to the ones obtained using  $\text{LiNbO}_3$  chips only. The enrichment for various parasitaemias varied from 50 to more than 1000 folds.

## 7.5 Conclusion

Cell separation based upon centrifugation requires relatively expensive instrumentation including fixed infrastructure and mains power - resulting in a high capital cost for those working in resource poor environments. This new method of enrichment of parasite-infected samples from fingerprick of blood relies on the different biophysical properties of the different species present in the sample. As such, it has the potential to be used for a wide range of diseases in addition to sleeping sickness. Here we illustrate enrichment in trypanosomes at parasitaemia of 0.002% and lower to mimic a human infection. A 72 fold enrichment of parasites was obtained in 5 seconds and allows detection of less than 100 trypanosomes  $\text{mL}^{-1}$  of infected blood.

The increasing availability of cheap and easy to use LED based fluorescence microscopes is also facilitating the diagnosis of numerous infectious diseases and the method described in this chapter would work alongside LED based field fluorescence microscopes and lensfree systems. This technique has the potential to improve the available diagnostic techniques for sleeping sickness. It is quicker, more reliable and more sensitive than the conventional techniques, and may provide an essential tool to identify patients with low level parasitaemia, as we move towards a goal of elimination of the disease.

## Chapter 8 - Conclusions

African trypanosomes cause the disease human African trypanosomiasis, a neglected tropical disease that has been targeted for elimination by 2020. A central tenet of the elimination programme will be the establishment of novel diagnostic tests that enable identification of cases of the disease. The fact that trypanosomes are frequently present in very low numbers (e.g.  $100 \text{ mL}^{-1}$ ) in blood adds difficulties to diagnosis. This work demonstrates novel techniques to enrich trypanosomes from blood cells to enable easy detection of the parasites in the field setting.

The first part of this thesis focuses on studying the behaviour of trypanosomes in vitro and how those findings can be exploited in improving the available diagnostic techniques. As trypanosomes are motile, the presence of chemotactic responses could serve as a means to separate parasites from blood cells. Trypanosomes use D-glucose as their primary source of the energy. Fructose and glycerol are other reported energy sources. The trypanosomes demonstrate selective chemotaxis towards D-glucose but not the other energy sources.

These findings could be integrated with a microfluidic system to separate or enrich the parasites from the whole blood for sensitive diagnosis of HAT. The limitation of this study has been to study the behaviour of trypanosomes towards glucose in real time. It would be interesting to further investigate the chemotaxis of *Trypanosoma brucei* using optical tweezers and optoelectronic tweezers. Further, after getting the results from the real-time chemotaxis study, a sheath flow microfluidic device could be designed to attract trypanosomes from the whole blood using glucose as an attractant.

The second part of this thesis focuses on development of microfluidic techniques to enrich trypanosomes. The field of microfluidics has been growing rapidly due to its diverse applications in the area biochemical analysis and diagnostics. Microfluidics and lab-on-a-chip techniques hold the prospect to change the face of the medical diagnostics in the developing world. With manipulation of small sample volumes, microfluidic technologies are enabling miniaturisation and integration of laboratory tests into low cost, low power, hand-held microchip

formats. This can allow complex medical diagnostic procedures to be carried out in remote locations where healthcare facilities are not adequate.

The microfluidic devices were fabricated using soft lithography and the designs were then replicated in PDMS. The first design developed in this work was based on PFF. In PFF, the separation process is entirely based on the particles sizes. The device was successfully used to separate a mixture of 10  $\mu\text{m}$  and 25  $\mu\text{m}$  polystyrene beads and 3  $\mu\text{m}$  and 10  $\mu\text{m}$  beads. The technique did not prove to be efficient to separate trypanosomes from blood cells. This could be due to the fact that trypanosomes are cylindrical compared to the blood cells that are spherical. Also, the initial testing was carried out on spherical particles only.

The second device developed during this work was five loop spiral microchannel. The design took advantage of Dean forces and inertial lift forces acting on the particles to achieve separation. The channels were 500  $\mu\text{m}$  wide and 40  $\mu\text{m}$  high and were used to show the separation of 5  $\mu\text{m}$  and 10  $\mu\text{m}$  beads and blood cells and plasma at  $De = 0.06$ .

The major drawback of this is that it does not work efficiently with concentrated cell solutions (whole blood). The device works better with low cell concentrations, which is a problem when enriching trypanosomes as there are not more than 10,000 trypanosomes  $\text{mL}^{-1}$  of infected blood at any given time.

The third device developed during this work exploited inertial migration of particles in rectangular microchannels to achieve separation. The device had one inlet and two outlets. The channel has 75 alternating pinched and expanded units. The length of each unit is 100  $\mu\text{m}$  and the width of the expanded units is 60  $\mu\text{m}$ . The total length of the channel is 1.5 cm. In microfluidics systems, the particles are generally expected to follow a laminar flow profile in absence of any external forces but inertial forces can cause the particles to migrate across the flow profile to attain specific equilibrium positions.

In experiments conducted with *T. cyclops* spiked blood, ~99% of the blood cells were removed enriching the trypanosomes thus facilitating the use of haemocytometry for the detection of the parasites. The advantages of this device include continuous processing of the sample, miniature size and low volume of reagents used and multiplexing of the design would facilitate high-

throughput analysis of large sample volumes. The disadvantages include the techniques reliance on external pumps for injecting sample that might be a problem in resource poor field settings. Also, the sample needs to be diluted 20X before analysis thus increasing the required sensitivity of the device and it might also lead to the loss of a fraction of parasites along with the cellular components.

The third part of this thesis focuses on density based separation of trypanosomes from blood cells. The first technique involved using Dextran-Ficoll Aqueous two-phase systems. The ATPS are generated from mixtures of immiscible solutions of solutes in water that separate spontaneously into two phases. The interface between phases of an ATPS discriminates species based on density. This capability was demonstrated by separating polystyrene microspheres ( $\rho = 1.05 \text{ g cm}^{-3}$ ) and Dynabeads ( $\rho = 1.14 \text{ g cm}^{-3}$ ), particles with equivalent sizes ( $2.8 \mu\text{m}$ ) but different densities, using a poly(ethylene glycol)-Ficoll ATPS.

A Dextran-Ficoll ATPS ( $\rho_{\text{top}} = 1.076 \text{ g cm}^{-3}$ ,  $\rho_{\text{bottom}} = 1.080 \text{ g cm}^{-3}$ ) was used to separate the cellular components of human blood based on density. For larger volumes ( $> 1 \text{ mL}$ ), after 100 minutes of centrifugation at  $2000 \text{ g}$ , the top and bottom phase of the ATPS are intact and separate different isolates of blood. An appropriately formulated ATPS is capable of enriching and concentrating blood cells into three fractions: a relatively pure sub-population of MNCs, a mixture of WBCs and young erythrocytes, and the vast majority of erythrocytes. For  $10 \mu\text{L}$  blood samples, a microhaematocrit centrifuge was used to speed up the separation. The samples were centrifuged for five minutes before extracting the isolates.

The trypanosomes were enriched using a Dextran-Ficoll ATPS ( $\rho_{\text{top}} = 1.076 \text{ g cm}^{-3}$ ,  $\rho_{\text{bottom}} = 1.082 \text{ g cm}^{-3}$ ). Trypanosomes being less dense than red blood cells were mainly collected from the top phase and the interphase. The system needs to be fine tuned so that all the parasites are collected from either one phase. Density-based separations through an ATPS provide a new method to separate sub-populations of interest. ATPSs combine the biocompatibility of aqueous media with the thermodynamic stability of separated phases.

The major drawback of this technique is that sample with large volumes need to be centrifuged for about an hour to enhance the separation and reach equilibrium. This technique for enrichment of parasites, if used in field settings, needs to be optimized for smaller volumes that can be coupled with simple centrifugation devices like the egg beater centrifuge.

The second technique is based on developing unique flow patterns generated by the interaction of ultrasonic surface acoustic waves (SAW) with blood, which, when coupled with an isopycnic density gradient, results in the separation of parasites from RBCs. The samples were spiked with trypanosomes at parasitaemia levels of 0.002% to mimic a human infection. The method produced an enrichment of trypanosomes by 72 fold in less than 5 seconds. This low cost technique has the potential to make diagnosis of sleeping sickness quicker, reliable and more sensitive.

The instrumentation potentially provides a low cost, low power technique which could find broad application in both point-of-care and field hospital settings. The phononic chips are free of electrodes, channel and pumps making it easier and cheaper to fabricate. Using the charge stored in a mobile phone, 30,000 enrichment assays can be carried out (the power consumption required for enrichment is 1 W for 5 seconds) on a LiNo<sub>3</sub> surface and 2000 on the disposable phononic superstrate.

The novel techniques developed in this work could be used in to develop rapid, low-cost diagnostic test for sleeping sickness allowing continuous separation and enrichment of trypanosomes in real-world samples. They may provide an essential tool to identify patients with low level parasitaemia, as we move towards the goal of elimination of the disease.

## 9 - References

- Adler, J. (1973). "A Method for Measuring Chemotaxis and Use of the Method to Determine Optimum Conditions for Chemotaxis by *Escherichia coli*." Journal of General Microbiology **74**(1): 77-91.
- Albertsson, P. A. (1958). "Particle fractionation in liquid two-phase systems; the composition of some phase systems and the behaviour of some model particles in them; application to the isolation of cell walls from microorganisms." Biochem Biophys Acta **27**(2): 378-395.
- Albertsson, P. Å. (1961). "Fractionation of particles and macromolecules in aqueous two-phase systems." Biochemical Pharmacology **5**(4): 351-358.
- Asmolov, E. S. (1999). "The inertial lift on a spherical particle in a plane Poiseuille flow at large channel Reynolds Number." J. Fluid Mech. **381**: 63-87.
- Barrett, M. P., Burchmore, R. J. S., Stich, A., Lazzari, J. O., Frasch, A. C., Cazzulo, J. J., and Krishna, S. (2003). "The Trypanosomiases." Lancet **362**: 1469-1480.
- Barrett, M. P., Boykin, D. W., and Tidwell, R. R. (2007). "Human African Trypanosomiasis: Pharmacological Re-engagement with a Neglected Disease." British Journal of Pharmacology **152**: 1155-1171.
- Bhagat, A. A. S., Kuntaegowdanahalli, S. S., and Papautsky, I. (2008). "Continuous particle separation in spiral microchannels using dean flows and differential migration." Lab on a Chip **8**: 1906-1914.
- Bhagat, A. A. S., Kuntaegowdanahalli, S. S., and Papautsky, I. (2009). "Inertial microfluidics for continuous particle filtration and extraction." Microfluid Nanofluid **7**: 217-226.
- Bhagat, A. A. S., Hou, H. W., Li, L. D., Lim, C. T., and Han, J. (2011). "Pinched flow coupled shear-modulated inertial microfluidics for high-throughput rare blood cell separation." Lab on a Chip **11**: 1870-1878.
- Blankenstrin, G., and Larsen, U. D. (1998). "Modular concept of a laboratory on a chip for chemical and biochemical analysis." Biosens. Bioelectron. **13**: 427-438.
- Blattert, C., Jurischka, R., Schoth, A., Kerth, P., and Menz, W. (2005). "Fabrication and testing of novel blood separation devices based on microchannel bend structures." Proc. SPIE **5651**.
- Bourquin, Y., Reboud, J., Wilson, R., and Cooper, J. M. (2010). "Tuneable surface acoustic waves for fluid and particle manipulations on disposable chips." Lab on a Chip **10**(15): 1898-1901.
- Bourquin, Y., Wilson, R., Zhang, Y., Reboud, J., and Cooper, J. M. (2011a). "Phononic Crystals for Shaping Fluids." Advanced Materials **23**(12): 1458-1462.

- Bourquin, Y., Reboud, J., Wilson, R., Zhang, Y., and Cooper, J. M. (2011b). "Integrated immunoassay using tuneable surface acoustic waves and lensfree detection." Lab on a Chip **11**(16): 2725-2730.
- Bøyum, A., Løvhaug, D., Tresland, L., and Nordlie, E. M. (1991). "Separation of leucocytes: improved cell purity by fine adjustments of gradient medium density and osmolality." Scand J Immunol **34**(6): 697-712.
- Bøyum, A., Brincker, F. H., Martinsen, I., Lea, T., and Løvhaug, D. (2002). "Separation of human lymphocytes from citrated blood by density gradient (Nycoprep) centrifugation: Monocyte depletion depending upon activation of membrane potassium channels." Scand J Immunol **56**(1): 76-84.
- Bray, R. S. (1983). "Leishmania: Chemotactic Responses of Promastigotes and Macrophages in Vitro." Journal of Eukaryotic Microbiology **30**(2): 322-329.
- Brakke, M. K., and Daly, J. M. (1965). "Density-Gradient Centrifugation: Non-Ideal Sedimentation and the Interaction of Major and Minor Components." Science **148**(3668): 387-389.
- Brown, J., Theis, L., Kerr, L., Zakhidova, N., O'Connor, K., Uthman, M., Oden, Z. M., and Richards-Kortum, R. (2011). "A hand-powered, portable, low-cost centrifuge for diagnosing anemia in low-resource settings." The American journal of tropical medicine and hygiene **85**(2): 327-332.
- Brugnara, C. (2003). "Iron deficiency and erythropoiesis: New diagnostic approaches." Clinical Chemistry **49**: 1571-1578.
- Bunn, H. F., and Aster, J. C. (2011). Pathophysiology of Blood Disorders. New York, Mc Graw Hill.
- Chin, C. D., Laksanasopin, T., Cheung, Y. K., Steinmiller, D., Linder, V., Parsa, H., et al (2011). "Microfluidics-based diagnostics of infectious diseases in the developing world." Nature Medicine **17**(8): 1015-1019.
- CDC (2012). "Trypanosomiasis, African." Retrieved 27-12-2012, from <http://www.dpd.cdc.gov/dpdx/HTML/TrypanosomiasisAfrican.htm>.
- Chappuis, F., Loutan, L., Simarro, P., Lejon, V., and Buscher, P. (2005). "Options for Field Diagnostics of Human African Trypanosomiasis." Clinical Microbiology Reviews **18**(1): 133-146.
- Chun, B., and Ladd, A. J. C (2006). "Inertial migration of neutrally buoyant particles in a square duct: An investigation of multiple equilibrium positions." Phys. Fluids **18**(3): 031704.
- Corash, L., Tan, H., and Gralnick, H. R. (1977). "Heterogeneity of human whole blood platelet subpopulations. I. Relationship between buoyant density, cell volume, and ultrastructure." Blood **49**(1): 71-87.

- Cross, G. A. M. and J. C. Manning (1973). "Cultivation of *Trypanosoma brucei* spp. in semi -defined and defined media." Parasitology **67**: 315-331.
- Dean, W. R. (1927). "Note on the motion of fluid in a curved pipe." Phil. Mag. (Ser. 7) **4**: 208-223.
- Cutnell, J. D., and Johnson, K. W. (2009). Physics 8e, Pearson (Prentice Hall).
- Dean, W. R. (1928). "The stream-line motion of fluid in a curved pipe." Phil. Mag. (Ser. 7) **5**: 673-695.
- D'Hondt, J., and Kondo, M. (1980). "Carbohydrate alters the trypanocidal activity of normal human serum with *Trypanosoma brucei*." Molecular and Biochemical Parasitology **2**(2): 113-121.
- Di Carlo, D., Irimia, D., Tompkins, R., and Toner, M. (2007). "Continuous inertial focusing, ordering, and separation of particles in microchannels." Proceedings of the National Academy of Sciences **104**(48): 18892-18897.
- Di Carlo, D., Edd, J. F., Irimia, D., Tompkins, R. G. and Toner, M. (2008). "Equilibrium Separation and Filtration of Particles Using Differential Inertial Focusing." Analytical Chemistry **80**(6): 2204-2211.
- Di Carlo, D. (2009). "Inertial microfluidics." Lab on a Chip **9**(21): 3038-3046.
- Dittrich, P., and Manz, A. (2006) "Lab-on-a-chip: microfluidics in drug discovery," Nat. Rev. Drug Discovery **5**(3): 210-218.
- Dürr, M., Kentsch, J., Müller, T., Schnelle, T., and Stelzle, M. (2003). "Microdevices for manipulation and accumulation of micro- and nanoparticles by dielectrophoresis." Electrophoresis **24**(4): 722-731
- Fairlamb, A. H., Carter, N. S., Cunningham, M., and Smith, K. (1992). "Characterisation of melarsen-resistant *Trypanosoma brucei brucei* with respect to cross-resistance to other drugs and trypanothione metabolism." Molecular and Biochemical Parasitology **53**(1-2): 213-222.
- Fèvre, E. M., Wissmann, B-v., Welburn, S. C., and Lutumba, P. (2008). "The Burden of Human African Trypanosomiasis." PLoS Negl Trop Dis **2**(12): e333.
- FIND (2012). "Sleeping Sickness." Retrieved 20-10-2012, from [http://www.finddiagnostics.org/programs/hat/about\\_hat.html](http://www.finddiagnostics.org/programs/hat/about_hat.html).
- Fisher, D. (1981). "The separation of cells and organelles by partitioning in two-polymer aqueous phases." Biochem J **196**: 1-10.
- Frampton, J. P., Lai, D., Sriram, H., and Takayama, S. (2011). "Precisely targeted delivery of cells and biomolecules within microchannels using aqueous two-phase systems." Biomedical Microdevices **13**(6): 1043-1051.
- Friend, J. a. Y. L. Y. (2011). "Microscale acoustofluidics: Microfluidics driven via acoustics and ultrasonics." Reviews of Modern Physics **83**: 647-704.

Geha, R. S., Rosen, F. S., and Merler, E. (1973). "Identification and characterization of subpopulations of lymphocytes in human peripheral blood after fractionation on discontinuous gradients of albumin. The cellular defect in X-linked agammaglobulinemia. ." J Clin Invest **52**(7): 1726-1734.

Giddings, J. C., Yang, F. J. and Myers, M. N. (1976). "Flow-field-flow fractionation: a versatile new separation method." Science**193**(4259): 1244-1245.

Giddings, J. C. (1993) "Field-flow fractionation: analysis of macromolecular, colloidal, and particulate materials," Science **260**(5113): 1456-1465.

Glass, N. R., Shilton, R. J., Chan, P. P. Y., Friend, J. R., Yeo, L. Y. (2012). "Lab-on-a-Disc: Miniaturized Lab-on-a-Disc (miniLOAD) (Small 12/2012)." Small **8**(12): 1880-1880.

Glinski, W., Gershwin, M. E., Budman, D. R., and Steinberg, A. D. (1976). "Study of lymphocyte subpopulations in normal humans and patients with systemic lupus erythematosus by fractionation of peripheral blood lymphocytes on a discontinuous Ficoll gradient." Clin Exp Immunol **26**(2): 228-238.

Gregoratto, I., McNeil, C. J., and Reeks, M. W. (2007). "Micro-devices for rapid and continuous separation of suspensions for use in micro-total-analysis-systems ( $\mu$ TAS)." Proc. SPIE **6465**: 646503.

Grover, W. H., Bryan, A. K., Diez-Silva, M., Suresh, S., Higgins, J. M., and Manalis, S. R. (2011). "Measuring single-cell density." Proceedings of the National Academy of Sciences **108**(27): 10992-10996.

Hatti-Kaul, R. (2001). "Aqueous two-phase systems." Molecular Biotechnology **19**(3): 269-277.

Heron, S. R., Wilson, R., Shaffer, S. A., Goodlett, D. R., and Cooper, J. M. (2010). "Surface Acoustic Wave Nebulization of Peptides as a Microfluidic Interface for Mass Spectrometry." Analytical Chemistry **82**(10): 3985-3989.

Hirumi, H., Doyle, J. J., and Hirumi, K (1977). "Cultivation of bloodstream *Trypanosoma brucei*." Bulletin of the World Health Organization **55**(2-3): 405-409.

Hirumi, H., and Hirumi, K. (1989). "Continuous cultivation of *Trypanosoma brucei* blood stream forms in a medium containing a low concentration of serum protein without feeder cell layers." The Journal of Parasitology **75**(6):985-989.

Ho, J., Tan, M. K., Go, D. B., Yeo, L. Y., Friend, J. R., and Chang, H-C (2011). "Paper-Based Microfluidic Surface Acoustic Wave Sample Delivery and Ionization Source for Rapid and Sensitive Ambient Mass Spectrometry." Analytical Chemistry **83**(9): 3260-3266.

- Holm, S. H., Beech, J. P., Barrett, M. P., and Tegenfeldt, J. O. (2011). "Separation of parasites from human blood using deterministic lateral displacement." Lab on a Chip **11**(7): 1326-1332.
- Howell, J. P. B., Mott, D. R., Golden, J. P., and Ligler, F. S. (2004). "Design and evaluation of a Dean vortex-based micromixer." Lab on a Chip **4**(6): 663-669.
- Huang, L. R., Cox, E. C., Austin, R. H., and Sturm, J. C. (2004). "Continuous particle separation through Deterministic Lateral Displacement." Science **304**(5673): 987-990.
- Huh, D., Bahng, J. H., Ling, Y., Wei, H-H., Kripfgans, O. D., Fowlkes, J. B., Grotberg, J. B., and Takayama, S. (2007). "Gravity-Driven Microfluidic Particle Sorting Device with Hydrodynamic Separation Amplification." Analytical Chemistry **79**(4): 1369-1376.
- Inglis, D. W., Davis, J. A., Austin, R. H., and Sturm, J. C. (2006). "Critical particle size for fractionation by deterministic lateral displacement." Lab on a Chip **6**(5): 655-658.
- Jain, A., and Posner, J. D. (2008). "Particle Dispersion and Separation Resolution of Pinched Flow Fractionation." Analytical Chemistry **80**: 1641-1648.
- Kalmar, J. R., Arnold, R. R., Warbington, M. L., and Gardner, M. K. (1988). "Superior leukocyte separation with a discontinuous one-step Ficoll-Hypaque gradient for the isolation of human neutrophils." J Immunol Methods **110**(2): 275.
- Kinetoplastids. (2012) Retrieved 27-12-2012, from <http://www.tulane.edu/~wiser/protozoology/notes/kinet.html>
- Kratz, A., Ferraro, M., Sluss, P. M. and Lewandrowski, K. B. (2004). "Normal Reference Laboratory Values." New England Journal of Medicine **351**(15): 1548-1563.
- Kuntaegowdanahalli, S. S., Bhagat, A. A. S., Kumar, G., and Papautsky, I. (2009). "Inertial microfluidics for continuous particle separation in spiral microchannels." Lab on a Chip **9**: 2973-2980.
- Kurosawa, M., Watanabe, T., Futami, A., and Higuchi, T. (1995). "Surface acoustic wave atomizer." Sensors and Actuators A: Physical **50**(1-2): 69-74.
- Kushwaha, M. S., Halevi, P., Dobrzynski, L., and Djafari-Rouhani, B. (1993). "Acoustic band structure of periodic elastic composites." Physical Review Letters **71**(13): 2022.
- Landau, L. D., and Lifshitz, E. M. (1966). Fluid Mechanics [3<sup>rd</sup> Ed.], Pergamon Press. Pp 219-227.

Leif, R. C., and Vinograd, J. (1964). "The distribution of buoyant density of human erythrocytes in bovine albumin solutions." Proceedings of the National Academy of Sciences **51**(3): 520-528.

Lejon, V., Legros, D., Richer, M., Ruiz, J. A., Jamonneau, V., Truc, P., Doua, F., et al. (2002). "IgM quantification in the cerebrospinal fluid of sleeping sickness patients by a latex card agglutination test." Tropical Medicine and International Health **7**(8): 685-692.

Leslie, G., Barrett, M. P., and Burchmore, R. (2002). "*Leishmania mexicana*: Promastigotes Migrate Through Osmotic Gradients." Experimental Parasitology **102**: 117-120.

Martinez, A. W., Phillips, S. T., Butte, M. J., and Whitesides, G. M. (2007). "Patterned Paper as a Platform for Inexpensive, Low-Volume, Portable Bioassays." Angew. Chem. Int. Ed. **46**: 1318 -1320.

Matovu, E., Kazibwe, A., Boobo, A., Biéler, S., and Ndung'u, J. (2010). Revisiting Red Blood Cell Lysis as a Critical Step in Demonstrating Trypanosomes in Patient Blood, Foundation for Innovative New Diagnostics (FIND), Switzerland.

Menachery, A. Kremer, C., Wong, P. E., Carlsson, A., Neale, S. L., Barrett, M. P., and Cooper, J. M. (2012). "Counterflow Dielectrophoresis for Trypanosome Enrichment and Detection in Blood." Scientific Reports **2**.

Nilsson, A., Petersson, F., Jonsson, H., and Laurell, T. (2004). "Acoustic control of suspended particles in micro fluidic chips." Lab on a Chip **4**(2): 131-135.

Ogbunude, P. O. J., and Magaji, Y. (1982). "A silicone centrifugation technique for the detection of low parasitaemias of salivarian trypanosomes." Transactions of the Royal Society of Tropical Medicine and Hygiene **76**(3): 317-318.

Olgac, U., Kurtcuoglu, V., and Poulidakos, D. (2008). "Computational modeling of coupled blood-wall mass transport of LDL: effects of local wall shear stress." American Journal of Physiology - Heart and Circulatory Physiology **294**(2): H909-H919.

Oliveira, J. S., Melo, M. N., and Gontijo, N. F. (2000). "A Sensitive Method for Assaying Chemotactic Responses of *Leishmania* Promastigotes." Experimental Parasitology **96**: 187-189.

Ookawara, S., Higashi, R., Street, D., and Ogawa, K. (2004). "Feasibility study on concentration of slurry and classification of contained particles by microchannel." Chem. Eng. J **101**: 171-178.

Pai, M., Riley, L. W., and Colford, J. M. (2004). "Systematic review: T-cell-based assays for the diagnosis of latent tuberculosis infection: an update." Lancet Infect Dis **4**(12): 761-776.

Pamme, N. (2007). "Continuous flow separations in microfluidic devices." Lab on a Chip **7**: 1644 - 1659.

Park, J.-S., Song, S.-H., and Jung, H.-I (2009). "Continuous focusing of microparticles using inertial lift force and vorticity via multi-orifice microfluidic channels." Lab on a Chip **9**(7): 939-948.

Pozzo, L. Y., Fontes, A., de Thomaz, A. A., Barbosa, L. C., Ayres, D. C., Giorgio, S. and Cesar, C. L. (2007). "*Leishmania amazonensis* chemotaxis under glucose gradient studied by the strength and directionality of forces measured with optical tweezers." Proc. of SPIE **6441**: 64411R-64411-64417.

Raghavan, R. V., Friend, J. R., and Yeo, L. Y. (2010). "Particle concentration via acoustically driven microcentrifugation: microPIV flow visualization and numerical modelling studies." Microfluidics and Nanofluidics **8**(1): 73-84.

Reboud, J., Bourquin, Y., Wilson, R., Pall, G. S., Jiwaji, M., Pitt, A. R., Graham, A., Waters, A. P., and Cooper, J. M. (2012). "Shaping acoustic fields as a toolset for microfluidic manipulations in diagnostic technologies." Proceedings of the National Academy of Sciences **109**(38): 15162-15167.

Sai, Y., Yamada, M., Yasuda, M., and Seki, M. (2006). "Continuous separation of particles using a microfluidic device equipped with flow rate control valves." Journal of Chromatography A **1127**(1-2): 214-220

Seo, J., Lean M. H., and Kole, A. (2007a). "Membraneless microseparation by asymmetry in curvilinear laminar flows." J. Chromatogr. A **1162**: 121-131.

Seo, J., Lean M. H., and Kole, A. (2007b). "Membrane-free microfiltration by asymmetric inertial migration." Applied Physics Letters **91**: 033901-033903.

Segré, G., and Silberberg, A. (1962a). "Behaviour of macroscopic rigid spheres in Poiseuille flow Part 1. Determination of local concentration by statistical analysis of particle passages through crossed light beams." J. Fluid Mech. **14**: 115-135.

Segré, G., and Silberberg, A. (1962b). "Behaviour of macroscopic rigid spheres in Poiseuille flow Part 2. Experimental results and interpretation." J. Fluid Mech. **14**: 136-157.

Shiokawa, S., Matsui, Y., and Ueda, T. (1989) "Liquid streaming and droplet formation caused by leaky Rayleigh waves." Proceedings of IEEE 1989 Ultrasonics Symposium **1**: p. 643-646.

Shortman, K., Haskill, J. S., Szenberg, A., and Legge, D. G. (1967). "Density distribution analysis of lymphocyte populations." Nature **216**(5121): 1227-1228.

Sigalas, M., and Economou, E. N. (1993). "Band structure of elastic waves in two dimensional systems." Solid State Communications **86**(3): 141-143.

SooHoo, J. R., and Walker, G. M (2009). "Microfluidic aqueous two phase system for leukocyte concentration from whole blood." Biomedical Microdevices **11**(2): 323-329.

Sritharan, K., Strobl, C. J., Schneider, M. F., Wixforth, A., and Guttenberg, Z. (2006). "Acoustic mixing at low Reynold's numbers." Applied Physics Letters **88**(5): 054102-054103.

Stein, W. D. (1990). Channels, carriers and pumps: An introduction to membrane transport. USA, Academic Press, Inc. pp 32.

Stone, H. A., and Kim, S. (2001). "Microfluidics: Basic issues, applications, and challenges," AICHE J **47**: 1250-1254.

Takagi, J., Yamada, M., Yasuda, M., and Seki, M. (2005). "Continuous particle separation in a microchannel having asymmetrically arranged multiple branches." Lab on a Chip **5**(7): 778-784.

Tan, M. K., Friend, J. R., and Yeo, L. Y. (2007). "Microparticle collection and concentration via a miniature surface acoustic wave device." Lab on a Chip **7**(5): 618-625.

Tan, M. K., Friend, J. R., and Yeo, L. Y. (2009). "Interfacial Jetting Phenomena Induced by Focused Surface Vibrations." Physical Review Letters **103**(2): 024501.

Ter Kuile, B. H., and Opperdoes, F. R. (1991). "Glucose uptake by *Trypanosoma brucei*. Rate-limiting steps in glycolysis and regulation of the glycolytic flux." Journal of Biological Chemistry **266**(2): 857-862.

Tetaud, E., Barrett, M. P., Bringaud, F., and Baltz, T. (1997). "Kinetoplastid glucose transporters." Biochem. J. **325**(3): 569-580.

Thomas, K. (2011). Running and tumbling. Soft Matter Blog, RSC Publishing. 2012.

Toner, M., and Irimia, D. (2005). "Blood-on-a-Chip." Annu. Rev. Biomed. Eng. **7**: 77-103.

Tseng, E-K., Lin, J-L., Sung, W-C., Chen, S-H., and Lee G-W (2006). "Active micro-mixers using surface acoustic waves on Y-cut 128° LiNbO<sub>3</sub>." Micromechanics and Microengineering **16**(3): 539-548.

Urdea, M., Penny, L. A., Olmsted, S. S., Giovanni, M. Y., Kaspar, P., Shepherd, A., et al (2006). "Requirements for high impact diagnostics in the developing world." Nature **444**(Suppl 1): 73-79.

Visser, B. (2012). "Human African Trypanosomiasis." Retrieved 27-12-2012, from <http://gm.stijlfabriek.com/issues/issue-7/human-african-trypanosomiasis-a-neglected-disease/>.

Vona, G., Sabile, A., Louha, M., Sitruk, V., et al. (2000). "Isolation by Size of Epithelial Tumor Cells: A New Method for the Immunomorphological and

- Molecular Characterization of Circulating Tumor Cells." The American Journal of Pathology **156**(1): 57-63.
- Whitesides, G. M. (2006). "The origins and the future of microfluidics." Nature **442**(7101): 368-373.
- WHO (2002). "WHO programme to eliminate sleeping sickness: Building a global alliance." Retrieved 10-10-2012, from [http://whqlibdoc.who.int/hq/2002/WHO\\_CDS\\_CSR\\_EPH\\_2002.13.pdf](http://whqlibdoc.who.int/hq/2002/WHO_CDS_CSR_EPH_2002.13.pdf).
- WHO (2010). "Working to overcome the global impact of neglected tropical diseases - First WHO report on neglected tropical diseases." Retrieved 10-10-2012, from [http://whqlibdoc.who.int/publications/2010/9789241564090\\_eng.pdf](http://whqlibdoc.who.int/publications/2010/9789241564090_eng.pdf).
- WHO. (2012). "Human African Trypanosomiasis - Control and Surveillance." Retrieved 27-12-2012 from [http://www.who.int/trypanosomiasis\\_african/surveillance/en/](http://www.who.int/trypanosomiasis_african/surveillance/en/).
- Wilson, R., Reboud, J., Bourquin, Y., Neale, S. L., Zhang, Y., and Cooper, J. M. (2011). "Phononic crystal structures for acoustically driven microfluidic manipulations." Lab on a Chip **11**(2): 323-328.
- Wiser, M. F. (1999). "Kinetoplastids." Retrieved 12-10-2012, from <http://www.tulane.edu/~wiser/protozoology/notes/kinet.html>.
- Wong, A. P., Gupta, M., Shevkoplyas, S. S., and Whitesides, G. M. (2008). "Egg beater as centrifuge: isolating human blood plasma from whole blood in resource-poor settings." Lab on a Chip **8**(12): 2032-2037.
- Wu, T.-T., Huang, Z.-G., and Lin, S. (2004). "Surface and bulk acoustic waves in two dimensional phononic crystal consisting of materials with general anisotropy." Phys. Rev. B **69**: 094301.
- Wu, Z., Willing, B., Bjerketorp, J., Jansson, J. K., and Hjort, K. (2009). "Soft inertial microfluidics for high throughput separation of bacteria from human blood cells." Lab on a Chip **9**(9): 1193-1199.
- Yager, P., Edwards, T., Fu, E., Helton, K., Nelson, K., Tam, M.R., and Weigl, B. H. (2006). "Microfluidic diagnostic technologies for global public health." Nature **442**(7101): 412-418.
- Yager, P., G. J. Domingo, et al. (2008). "Point-of-Care Diagnostics for Global Health." Annual Review of Biomedical Engineering **10**(1): 107-144.
- Yamada, M., Nakashima, M., and Seki, M. (2004). "Pinched Flow Fractionation: Continuous Size Separation of Particles Using Laminar Flow Profile in a Pinched Microchannel." Analytical Chemistry **76**: 5465-5471.

Yamada, M., Kano, K., Tsuda, Y., Kobayashi, J., Yamato, M., Seki, M., and Okano, T. (2007). "Microfluidic devices for size-dependent separation of liver cells." Biomedical Microdevices **9**(5): 637-645

Yang, S., Undar, A., and Zahn, J. D. (2006). "A microfluidic device for continuous, real time blood plasma separation." Lab on a Chip **6**: 871-880.

Yapici, K., Powell, R. L., and Phillips, R. J. (2009). "Particle migration and suspension structure in steady and oscillatory plane Poiseuille flow." Physics of Fluids **21**(5): 053302-053316.

Zhang, C.-X. and A. Manz (2003). "High-Speed Free-Flow Electrophoresis on Chip." Analytical Chemistry **75**(21): 5759-5766.

Zhang, X., Cooper, J. M., Monaghan, P. B., and Haswell, S. J. (2006). "Continuous flow separation of particles within an asymmetric microfluidic device." Lab on a Chip **6**: 561-566.

## 10 - Appendices

### 10.1 HM1 - 9 Medium Recipe

Components		g/L	
Salts, etc.	CaCl <sub>2</sub>	0.165	
	KCl	0.33	
	KNO <sub>3</sub>	0.000076	
	MgSO <sub>4</sub>	0.098	
	NaCl	4.5	
	NaHCO <sub>3</sub>	3.020	
	NaH <sub>2</sub> PO <sub>4</sub> .H <sub>2</sub> O	0.125	
	Na <sub>2</sub> SeO <sub>3</sub> .5H <sub>2</sub> O	0.000017	
	Glucose	4.5	
	Phenol Red	0.015	
	HEPES	5.960	
	Mercaptoethanol	0.015	
	Bathocuproine disulfonate.Na <sub>2</sub>	0.028	
	Amino Acids	DL-alanine	0.025
L-arginine.HCl		0.084	
L-asparagine. H <sub>2</sub> O		0.025	
L-aspartic acid		0.030	
L-cysteine		0.182	
L-cystine		0.091	
L-glutamic acid		0.075	
L-glutamine		0.584	
glycine		0.030	
L-histidine.HCl.H <sub>2</sub> O		0.042	
DL-isoleucine		0.105	
L-leucine		0.105	
L-lysine.HCl		0.146	
DL-methionine		0.030	
L-phenylalanine		0.066	
L-proline		0.040	
DL-serine		0.042	
DL-threonine		0.095	
L-tryptophane		0.016	
L-tyrosine		0.104	
DL-valine	0.094		
Vitamins, etc.	B <sub>12</sub>	0.000013	
	Biotin	0.000013	
	D-Ca pantothenate	0.004	
	Choline chloride	0.004	
	Folic acid	0.004	
	i-Inositol	0.0072	
	Niacinamide	0.004	
	Pyridoxal HCl	0.004	
Riboflavin	0.0004		

	Thiamine HCl	0.004
<b>Organic acids</b>	Pyruvate Na	0.114
<b>Purines, etc.</b>	Hypoxanthine	0.136
	Uracil	0.010
	Cytosine	0.010

### 10.2 Carter's Balances Salt Solution (CBSS) Recipe

Components	Molarity (mM)	g/L
HEPES	25	5.95
NaCl	120	7.0
KCl	5.4	0.4
CaCl <sub>2</sub> .6H <sub>2</sub> O	0.55	0.08
MgSO <sub>4</sub> .7H <sub>2</sub> O	0.4	0.098
Na <sub>2</sub> HPO <sub>4</sub> .2H <sub>2</sub> O	5.6	0.79
D-glucose	5.5	0.995

### 10.3 Cunninghams Medium Recipe

Components		g/L
<b>Salts, Sugars, etc.</b>	CaCl <sub>2</sub> .2 H <sub>2</sub> O	0.15
	KCl	2.98
	NaH <sub>2</sub> PO <sub>4</sub> .H <sub>2</sub> O	0.53
	MgSO <sub>4</sub> .7 H <sub>2</sub> O	3.7
	MgCl <sub>2</sub> .6 H <sub>2</sub> O	3.04
	Glucose	0.7
	D-Fructose	0.4
	Sucrose	0.4
	Phenol Red	0.015
<b>Amino Acids</b>	B-alanine	2
	DL-alanine	1.09
	L-arginine.HCl	0.44
	L-asparagine. H <sub>2</sub> O	0.024
	L-aspartic acid	0.11
	L-cysteine	0.08
	L-cystine	0.03

	L-glutamic acid	0.25
	L-glutamine	1.64
	glycine	0.12
	L-histidine	0.16
	DL-isoleucine	0.09
	L-leucine	0.09
	L-lysine	0.15
	DL-methionine	0.20
	L-phenylalanine	0.20
	L-proline	6.90
	DL-serine	0.20
	DL-threonine	0.10
	L-tryptophane	0.10
	L-tyrosine	0.20
	DL-valine	0.21
<b>Vitamins, etc.</b>	BME vitamins (100X)	2 mL
<b>Organic acids</b>	Pyruvate Na	0.114
	L-malic	0.67
	$\alpha$ -ketoglutaric	0.37
	Fumaric	0.055
	Succinic	0.06
	Cis-aconitic acid	0.522